Targeted Drug Delivery Using Electromagnetic Actuation System

A
thesis submitted
in partial fulfillment of the requirements
for the degree of

DOCTOR OF PHILOSOPHY

by

PRALAY CHAKRABARTY

DEPARTMENT OF ELECTRONICS AND ELECTRICAL ENGINEERING
INDIAN INSTITUTE OF TECHNOLOGY GUWAHATI
GUWAHATI - 781039, ASSAM, INDIA

March, 2022

DECLARATION

This is to certify that the thesis entitled ***"Targeted Drug Delivery using Electromagnetic Actuation System"****, submitted by me to the Indian Institute of Technology Guwahati for the award of the degree of* ***Doctor of Philosophy*** *is a bonafide work carried out by me under the supervision of* ***Prof. Roy P Paily****. The content of this thesis, in full or in parts, have not been submitted to any other Institute or University for the award of any degree or diploma.*

Signed:

Pralay Chakrabarty
Department of Electronics and Electrical Engineering,
Indian Institute of Technology Guwahati,
Guwahati-781039, Assam, India.

Date:

CERTIFICATE

This is to certify that the thesis entitled ***"Targeted Drug Delivery using Electromagnetic Actuation System"****, submitted by* ***Pralay Chakrabarty*** *(156102004), a research scholar in the Department of Electronics & Electrical Engineering, Indian Institute of Technology, for the award of the degree of* ***Doctor of Philosophy****, is a record of an original research work carried out by him under my supervision and guidance. The thesis has fulfilled all requirements as per the regulations of the Institute and in my opinion has reached the standard needed for submission. The results embodied in this thesis have not been submitted to any other University or Institute for the award of any degree or diploma.*

Signed:

Supervisor: Prof. Roy P Paily
Professor,
Department of Electronics and Electrical Engineering,
Indian Institute of Technology Guwahati,
Guwahati-781039, Assam, India.

Date:

Dedicated

to

my beloved parents

Late Pranay Kanti Chakrabarty

&

Mrs. Rakhi Chakrabarty

ACKNOWLEDGEMENTS

My heart is filled with immense pleasure as I take this opportunity to thank those who have instilled the confidence in me to fulfill this thesis. First and foremost, I express my deep sense of gratitude and indebtedness to my supervisor Prof. Roy P Paily, for providing constant support and guidance throughout my Ph.D. journey. His continuous encouragement to explore different domains led to developing my personal and professional skills over these years. I am also indebted to him for providing me with all kinds of logistic support during this period.

I am thankful to my doctoral committee members Prof. Harshal B. Nemade, Dr. Arun Tej Mallajosyula and Dr. Nelson Muthu for spending their precious time evaluating my progress and providing constructive criticism on my work. I wish to remember Late Dr. A. Narayana Reddy for his suggestions to my work during which he was a part of my doctoral committee. I would like to thank Prof. Dipankar Bandyopadhyay, Dr. D. Pamu, and Dr. Sidananda Sarma for their valuable suggestions and help in carrying out this work. My sincere thanks to the Head of the Department and staff members of Electronics and Electrical Engineering, IIT Guwahati, for providing all the necessary facilities for carrying out my research work. I extend my sincere regards to all the department faculty members for their generous help and kind cooperation during this course. I also thank the technical staff of the department for their helpfulness in teaching assistantship duties and other experimental assignments. My special thanks to Mrs. Josphene S for providing all the necessary support in handling laboratory resources.

I would also like to extend my gratitude to the Head of Centre of Nanotechnology, IIT Guwahati and the faculty members associated with this center for providing the opportunity to utilize the high-end instruments for fabrication and characterization of our devices. My sincere thanks to Central Instruments Facility, IIT Guwahati, for permitting me to perform material characterization using Vibrating Sample Magnetometer (VSM) and Field Emission Scanning Electron Microscope (FESEM). I am also thankful to the Department of Chemical Engineering for allowing me to utilize DELSA Nano for particle size analysis. Finally, I express my thankfulness to the Ministry of Electronics and IT, Government of

India, for granting me a research fellowship under the Visvesvaraya Ph.D. scheme, the absence of which would have made this work impossible.

I feel delighted to express my heartfelt thanks to all my colleagues and friends at IIT Guwahati. I would like to thank my seniors, friends and lab mates Dr. Saroj Mondal, Dr. Pavan K Manchi, Dr. Brajesh Rawat, Dr. Ujjwol Barman, Dr. Mohd. Tasleem Khan, Dr. Indrajit Das, Dr. Vimal K S Yadav, Dr. Thomas T Daniel, Mr. Rajan Singh, Mr. Mridul Goswami and Mr. Pallab Das for their selfless support, guidance and companionship. I also find myself privileged to gain knowledge from exchanging ideas with my enthusiastic juniors Mr. Chintak K Parashar, Mr. Himangshu Gogoi, Dr. Monica Naorem and Mr. Eedara Prabhakara Rao. I have been blessed with friends and colleagues, Dr. Kamlesh Badiyari, Dr. Satyajit Bora, Dr. Siddhanta Roy, Mr. Rahul Sharma, Dr. Prateek Sharma and Dr. Himakshi Choudhury, who made my Ph.D. journey nothing less than an adventure. I wish to express my gratitude to all the workforce staff of the Institute for making my stay at IIT Guwahati an unforgettable and rewarding experience.

I shall be eternally grateful to Mr. Rupam Roy Choudhury for believing in me since my childhood and for his words of encouragement. My heartfelt gratitude goes to Satyajit Nandy, Sudip Paul, Abhijit Purkayastha, Ibadur Rahman Laskar, Monojyoti Bhattacharjee, Monodeep Bhattacharjee and last but not least, my younger cousin Pratik Chakrabarty for always lending a helping hand.

It would remain incomplete without expressing my love and respect to my parents for giving me the best possible education and teachings which has made me the person that I am today. No words are enough to express my gratitude to my parents and younger sister, Barnalee Chakrabarty, for being a constant pillar of support in my life and for their sacrifice to accomplish the work. This work belongs to my mother, Mrs. Rakhi Chakrabarty, as much as it is mine. I am extremely thankful to my wife, Sangeeta Bhattacharjee, for her constant motivation, unconditional support and love through the ups and downs of my Ph.D. journey. It is impossible for me to acknowledge her contribution in words.

Sincerely

Pralay Chakrabarty

ABSTRACT

This thesis addresses the stiction issue of magnetic nanoparticles (MNPs) in a targeted drug delivery system (TDDS). In a magnetically actuated TDDS, the MNPs are guided to the desired blood vessel by steering them from the bifurcation points, using an external electromagnetic actuation (EMA) system. Meanwhile, some MNPs get stuck to the vessel wall during the steering process. To overcome this problem, an EMA system is designed using four coils and the coil parameters are optimized for efficiently steering the MNPs in a Y-shaped microchannel. The system operates by applying a time-varying magnetic field (TVMF) to navigate the MNPs in the channel efficiently. The TVMF alternately switches between two modes of operation described as follows. The TVMF is applied for a specific duration to generate the magnetic force required to steer the MNPs to the desired outlet in the first mode of operation. The second mode of operation facilitates mitigation of the stiction and aggregation of MNPs by modulating the TVMF and time duration of operation to yield a lower magnetic force in the reverse direction to that in the first mode. The MNPs separated from the sidewalls move ahead with the fluid flow to the desired channel and this guidance mechanism is repeated until the MNPs reach the target point. Extensive simulations are performed to analyse the switching time for effective steering of the MNPs using COMSOL Multiphysics. Furthermore, the experimental validation of the proposed EMA system highlights its practical feasibility to mitigate the stiction issue. Results demonstrate that the magnetophoretic force produced to release the adhered particles in our system is around 99.5% lower than that of an existing EMA system, which aims to address the same issue. Moreover, the duration between the two modes of operation should be set using a ratio of $3:1$ for effective guidance of the MNPs to the correct outlet. Thus, our system provides enhanced efficacy in mitigating the stiction issue by alleviating the detrimental effect of the MNPs getting steered to the undesired outlet.

Contents

List of Figures xix

List of Tables xxi

List of Abbreviations xxiii

List of Symbols xxv

1 Introduction 1

1.1 Background . . . 2
1.2 Need for Targeted Drug Delivery . . . 4
1.3 Methods of Targeted Drug Delivery . . . 5
1.3.1 Passive Targeting . . . 5
1.3.2 Active targeting . . . 6
1.4 Targeted Drug Delivery System . . . 6
1.4.1 Nanoparticles for TDD . . . 8
1.4.2 Guidance System for TDD . . . 9
1.5 State-of-the-art . . . 10
1.6 Motivation . . . 12
1.7 Problem Definition . . . 13
1.8 Thesis Contribution and Organization . . . 14

2 Analysis of Electromagnetic Actuation Systems for TDD 17

2.1 Introduction . . . 18
2.2 Theoretical Model . . . 20
2.3 Methodology . . . 22
2.3.1 Simulation Framework . . . 23
2.3.2 Experimental Framework . . . 24
2.4 Results & Discussion . . . 24
2.4.1 Single Coil . . . 25
2.4.2 Helmholtz Coil . . . 25

2.4.3 Maxwell Coil . . . 26
2.4.4 Differential Current Coil . . . 26
2.5 Chapter Summary . . . 28

3 Design and Optimization of EMA Systems 29
3.1 Introduction . . . 30
3.2 Classification of Materials . . . 31
3.2.1 Diamagnetic . . . 31
3.2.2 Paramagnetic . . . 31
3.2.3 Ferromagnetic . . . 31
3.2.4 Antiferromagnetic . . . 32
3.2.5 Ferrimagnetic . . . 32
3.3 Theoretical Concepts . . . 33
3.3.1 Electromagnet . . . 33
3.3.2 Magnetic Phenomena . . . 34
3.4 Actuation System . . . 35
3.4.1 Mathematical Model . . . 35
3.4.2 Proposed Design . . . 40
3.5 Optimization of EMA System . . . 45
3.6 Results and Discussions . . . 48
3.7 Chapter Summary . . . 50

4 Stiction Mitigation and Disaggregation of Magnetic Particles in TDDS 51
4.1 Introduction . . . 52
4.2 System Model . . . 54
4.2.1 Stiction Issue and Aggregation . . . 55
4.2.2 Working Principle . . . 56
4.3 Simulation Framework . . . 58
4.4 Results and Discussions . . . 58
4.5 Chapter Summary . . . 63

5 Experimental Validation of TDDS 65
5.1 Introduction . . . 66
5.2 Magnetic Nanoparticles . . . 66
5.2.1 Synthesis . . . 66
5.2.2 Characterization . . . 67
5.3 Experimental Setup . . . 68
5.3.1 3D Printing of Mold . . . 69

5.3.2 Fabrication of Y-shaped Microchannel 70
5.3.3 Electromagnetic Actuation System 71
5.4 Results and Discussions 72
5.5 Chapter Summary 75

6 Conclusions and Future Scope **77**
6.1 Conclusion 78
6.2 Future Scope 80

Bibliography **81**

Author's Statements **93**

List of Figures

1.1 Carrier based drug delivery 3
1.2 Ideal characteristics of TDD 4
1.3 Targeted drug delivery: (a) drug and carrier, (b) functionalization, (c) injection, (d) steering. 7

2.1 a) Single coil of radius R and b) Cross-sectional view of the single coil. 19
2.2 a) Two coils of radius R, separated by a distance d and b) Cross-sectional view of the two coils. 20
2.3 a) Helmholtz coil and b) Maxwell coil. 20
2.4 Experimental set-up using single coil and two coils. 23
2.5 Magnetic field generated by single coil. 24
2.6 Magnetic field generated by Helmholtz coil. 25
2.7 Magnetic field generated by Maxwell coil. 26
2.8 Magnetic flux density generated by Helmholtz, Maxwell, Helmholtz-Maxwell pair and DCC configuration. 27
2.9 Surface plot of (a) Helmholtz coil, (b) Maxwell coil, (c) Helmholtz-Maxwell pair and (d) DCC configuration 27

3.1 Paramagnetic material 31
3.2 Ferromagnetic material 32
3.3 Antiferromagnetic material 32
3.4 Ferrimagnetic material 32
3.5 Electromagnet 33
3.6 A 3D Y-shaped fluidic channel 36
3.7 3D view of the proposed EMA system 40
3.8 XY cross-sectional view of the proposed EMA system 41
3.9 XY cross-sectional view of EMA system for steering both in X and Y direction. 41

3.10 Qualitative illustration of nature of magnetic field strength with respect to coil parameters (H and ∇H positive in the region of interest for steering the MNPs): (a) XY cross-sectional view of EMA system with a region of interest represented by a square of side length S_l, (b) magnetic field strength produced by each coil without superposition, (c) resultant magnetic field strength produced by EMA after superposition and (d) resultant magnetic field strength produced by only outer two coils. 42
3.11 Qualitative illustration of nature of magnetic field strength with respect to coil parameters (H and ∇H negative in the region of interest for steering the MNPs): (a) XY cross-sectional view of EMA system with a region of interest represented by a square of side length S_l, (b) magnetic field strength produced by each coil without superposition, (c) resultant magnetic field strength produced by EMA after superposition and (d) resultant magnetic field strength produced by only outer two coils. 44
3.12 Variation of H vs following coil design parameters: (a) w_i and h_i, (b) I_{iL} and I_{iR}, (c) w_o and h_o, (b) I_{oL} and I_{oR}. 47
3.13 Variation of (a) magnetic field and (b) magnetic gradient, in the region of interest along the x-axis. 49
3.14 Variation of magnetophoretic force in the region of interest along the x-axis 49

4.1 3D view of the electromagnetic actuation system and Y-shaped fluidic channel. 53
4.2 XY cross-sectional view of proposed EMA system and Y-shaped channel. 54
4.3 XY cross-sectional view of Y-shaped channel in Mode 1 and Mode 2. 54
4.4 Qualitative illustration of the nature of magnetophoretic force vs time. 57
4.5 (a) Magnetic field intensity with respect to position and time along the space available in between the symmetrical coils, and (b) magnetic field intensity along the channel diameter for Mode 1 and Mode 2 respectively. 59
4.6 Magnetic field intensity with respect to time. 60
4.7 (a) Magnetic field intensity, (b) Magnetic field gradient along the x-axis for both Mode 1 and Mode 2. 60
4.8 Magnetophoretic force for both Mode 1 and Mode 2. 61
4.9 MNP trajectory inside the channel. 62

5.1 FESEM image of Fe_3O_4 67
5.2 Size distribution of Fe_3O_4 using particle size analyzer (Beckman Coulter Delsa Nano). 67
5.3 Vibrating Sample Magnetometer (VSM) magnetization curve showing saturation. 68
5.4 Y-shaped microchannel fabricated on the PDMS substrate by replica molding from the master mold. 69
5.5 PDMS based Y-shaped microfluidic channel. 70
5.6 Microscopic view of the Y-shaped channel. 70
5.7 Experimental Setup. Coil 1 & Coil 4 represent the outer coils and Coil 2 & Coil 3 represent the inner coils. (a) Keithley 2230G-30-1, (b) PASCO 850 Universal Interface (UI-5000), (c) Aplab LQ6324S, (d) PASCO Capstone Control Panel, (e) PASPORT 2-Axis Magnetic Field Sensor (PS-2162) and (f) PASPORT Rotary Motion Sensor (PS-2120A). 71
5.8 Magnetic field produced by Mode 1 72
5.9 Magnetic field produced by Mode 2. 73
5.10 Timing Analysis 73
5.11 Video image analysis of the steering experimets. (a) Before applying magnetic field and (b) after applying magnetic field around the bifurcation point. 74
5.12 Experimental validation of MNP steering to outlet 1 due to magnetophoretic force. 75

List of Tables

2.1 Coil Parameters 23

3.1 Modeling parameters of MNP, microchannel and suspension fluid . 35
3.2 Optimal values of coil parameters using positive H and ∇H constraint 48
3.3 Optimal values of coil parameters using negative H and ∇H constraint 48

4.1 Coil parameters of the proposed EMA system 53

List of Abbreviations

EMA	Electromagnetic Actuation System
DDS	Drug Delivery
DDS	Drug Delivery System
NDDS	Novel Drug Delivery System
TDD	Targeted Drug Delivery
TDDS	Targeted Drug Delivery System
NP	Nanoparticle
MP	Microparticle
MNP	Magnetic Nanoparticle
MMP	Magnetic Microparticle
MRI	Magnetic Resonance Imaging
SPION	Superparamagnetic Iron Oxide Nanoparticle
EPR	Enhanced Permeation and Retention
DCC	Differential Current Coil
TVMF	Time-Varying Magnetic Field
FEA	Finite Element Analysis
PDE	Partial Differential Equation
CFD	Computational Fluid Dynamics
CAD	Computer-Aided Design

List of Symbols

B	Magnetic field (T)
H	Magnetic field strength ($\mathrm{A\,m^{-1}}$)
M	Magnetization ($\mathrm{A\,m^{-1}}$)
M_{eff}	Effective magnetic dipole moment ($\mathrm{Am^2}$)
R	Radius of the Y-shaped microchannel (m)
μ_f	Relative permeability of the fluid in the microchannel
μ_p	Relative permeability of Fe_3O_4 nanoparticles
F_{MAP}	Magnetophoretic force (N)
F_D	Drag force (N)
F	Total force acting on the MNPs (N)
η	Viscosity of the fluid (Pa s)
v_f	Velocity of the fluid ($\mathrm{m\,s^{-1}}$)
v_p	Velocity of the nanoparticles ($\mathrm{m\,s^{-1}}$)
w_i	Width of the inner coils (m)
h_i	Height of the inner coils (m)
w_o	Width of the outer coils (m)
h_o	Height of the outer coils (m)
d_w	Diameter of winding wire (m)
k_w	Coil winding factor
N_i	Number of wire turns in the inner coils

N_o Number of wire turns in the outer coils

R_i Radius of the inner coils (m)

R_o Radius of the outer coils (m)

d_i Inner diameter of the inner coils (m)

d_o Inner diameter of the outer coils (m)

I_{oL} Current flowing in Coil 1 (A)

I_{iL} Current flowing in Coil 2 (A)

I_{iR} Current flowing in Coil 3 (A)

I_{oR} Current flowing in Coil 4 (A)

x_i Distance of inner coils from origin (m)

x_o Distance of outer coils from origin (m)

Chapter 1

Introduction

Contents

1.1 Background 2
1.2 Need for Targeted Drug Delivery 4
1.3 Methods of Targeted Drug Delivery 5
1.4 Targeted Drug Delivery System 6
1.5 State-of-the-art 10
1.6 Motivation 12
1.7 Problem Definition 13
1.8 Thesis Contribution and Organization 14

1.1 Background

In recent years, the dramatic progress in the pharmaceutical industry has paved the way to cure critical diseases like diabetes, cancer, atherosclerosis, asthma, pulmonary tuberculosis, Parkinson's disease, and Alzheimer's disease [1]. Some of the medications used for treating these diseases are highly toxic, thus inducing off-target side effects [2]. Cancer is a leading cause of death worldwide, accounting for almost 10,000,000 cancer deaths in 2020 [3]. The number of cancer patients in India was nearly 1,392,179 for the year 2020 [4]. Cancer refers to any one of many diseases characterized by the development of uncontrolled cellular growth and can multiply much more quickly than most cells in the body. Cancer often has the ability to spread throughout the body. Chemotherapy is one of the most common treatments for cancer and it can be used alone or in combination such as surgery with chemotherapy to treat a wide variety of cancers. It uses certain drugs to kill the fast-growing cells or stop them from growing and spreading to other parts of the body. In this process of targeting fast-growing cancer cells, chemotherapy drugs can also damage other fast-growing healthy cells, such as those in the hair follicles, bone marrow and digestive tract. Chemotherapy drugs fail to distinguish between the normal and cancerous fast-growing cells and kill both during the treatment process. This leads to common side effects such as fatigue, nausea, diarrhea, mouth sores, hair loss, anemia and immune system disorder [5–7]. Conventional drug delivery possess serious side effects due to nonspecific targeting resulting in impaired treatment with reduced dose and unsuccessful in improving patients' quality of life. Therefore, the systemic administration of conventional chemotherapy reduces therapeutic efficacy.

A century ago, *Paul Ehrlich*, the father of chemotherapy, proposed a concept of smart medicine "magic bullet" that selectively eliminates the diseased cells without damaging the surrounding normal cells. Drug delivery (DD) refers to an extensive field of research on the advancement of novel materials or carrier systems for the effective delivery of drugs. Advances in medicine and biotechnology have led to the development of numerous drugs, which are being administered through various conventional DD dosage forms such as lotions, creams, powders, solutions, pastes, mixtures, ointments, pills, suspensions, suppositories, injectables, immediate release capsules and tablets, etc., and so on to achieve the desired therapeutic effect. Examples of novel devices with enhanced therapeutic potential include oral controlled release systems, liposomes, taste-masking systems, transdermal patches, aerosols, and site-specific delivery systems [8]. Drug delivery systems (DDS) are extensively studied and developed to improve the methods, formulations, tech-

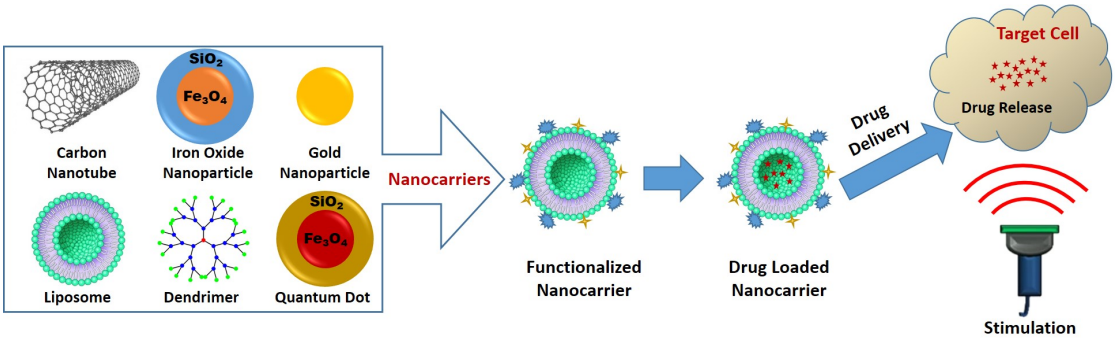

Figure 1.1: Carrier based drug delivery

nologies, and processes involved in delivering a therapeutic substance in the body to safely achieve its desired pharmacological effects [9]. The development of Novel DDS (NDDS), such as nanoparticles (NPs) and microparticles (MPs), transdermal patches, inhalers, drug reservoir implants, and antibody-drug conjugate fulfilled the state of the art therapeutic demands e.g., controlled release, solubility enhancement, on-demand activation, targeted delivery and new administration routes [10]. The potential of NDSS has resulted in a growing interest among researchers and this leads to improved efficacy of the therapeutic using site-specific delivery of the drug [11].

The promise shown by controlled drug delivery technology has led to several clinical formulations towards the improvement of patient compliance and convenience [12]. One such area is targeted drug delivery (TDD) to sites of infection. The clinically significant impact of TDD lies in the ability to specifically target a drug or drug carrier to minimize drug-originated systemic toxic effects [13]. Carrier-based drug delivery is an engineered technique for targeted delivery of the drug to the specific location as depicted in Fig. 1.1. Metal nano- and microparticles as drug carriers have made tremendous progress in the field of therapeutics by boosting therapeutic efficacy through site-specific drug delivery [14–16]. Recently, there have been immense advancements in the area of delivery systems to supply therapeutic agents to their target location for the treatment of numerous diseases [17, 18]. Targeted delivery to sites of infection is a rapidly advancing science where nanocarriers are utilized to restrict the distribution of therapeutic agents to targeted sites in a controlled manner [10, 19]. Nanocarrier-based TDD paved the way for a controllable rate of drug release at the specific location, at the right concentration for an appropriate period of time [20]. For more than two decades, advancements in drug delivery systems have been an active area of interdisciplinary research, leading to successful improvements in therapies for various pathologies.

Figure 1.2: Ideal characteristics of TDD

1.2 Need for Targeted Drug Delivery

Traditional DDS, such as oral ingestion or intravascular injection, transmits medication throughout the body via systemic blood circulation. For most therapeutic agents, only a small percentage of the therapeutic agent reaches the organ to be impacted, where most of the medications administered do not reach the target site. The need for TDD over conventional DD is crucial to improve the therapeutic effectiveness and minimize the toxicity associated with a small therapeutic index and high doses. Targeting is required to find answers to these limits and inherent shortcomings of traditional DDs. Ideally, TDD strives to improve therapeutic efficacy, achieve controlled distribution, improve drug localization, reduce therapeutic toxicity, reduce dose, and improve patient compliance as depicted in Fig 1.2. The fundamental premise of drug targeting is to deliver a high concentration of medication to the targeted site while limiting its concentration in the non-targeted region. Targeting also reduces undesirable drug interactions with bio-environmental variables that affect drug access to specific areas in the body. Drug targeting entails coordinating drug behavior, targeting site, and a pharmaceutical carrier. The target is the particular organ, cell, or group of cells in a chronic or acute illness that requires treatment and with which the medicine will interact.

The carrier is a specially designed system that is needed for the safe transportation of the loaded medicine to its destination [21]. Drug carriers are expected to be non-toxic, non-immunogenic, biochemically inert, biodegradable, biocompatible, and physicochemically stable *in vivo* and *in vitro*. In addition, predictable and controlled drug release patterns, sufficiently simple, reproducible and economical preparation, should be easily and quickly excreted from the body and drug leakage during transport should be minimized [22]. The benefits of the targeted release system include a reduction in the frequency of the patient's doses, a more uniform action of the medication, a reduction in drug side effects, and a reduction in volatility in circulating drug levels. The system's downside is its expensive cost, which makes productivity difficult and its limited capacity to change doses.

1.3 Methods of Targeted Drug Delivery

Drug targeting strategies are broadly classified into two categories, namely passive and active targeting.

1.3.1 Passive Targeting

Passive targeting is a type of DD that focuses on systemic circulation. Drug targeting occurs in this technique as a result of the body's natural response to the physicochemical properties of the drug or drug-carrier system [23]. This is based on drug accumulation at the site of interest, such as tumor tissue. Drugs administered intravenously tend to spread uniformly throughout the body. On the other hand, tumor cells tend to take up particles of a specific size to a more significant extent than healthy cells due to a combination of leaky tumor blood arteries and defective particle screening. This is known as the enhanced permeation and retention (EPR) effect, and it is the mechanism underpinning passive targeting. For example, NPs are used as carriers in passive targeting, and they are directed to enter blood vessels more at the disease site, allowing for significant drug accumulation at the target. The EPR effect aids in this process [24]. The EPR effect is regulated by NP parameters such as particle size, shape, and surface charge, which affects circulation duration, penetration speed, and intracellular internalization [25]. Despite the effectiveness of EPR, more than 95% of NPs with passive targeting do not reach the tumor upon intravenous injection [13]. Targeting can be substantially enhanced by limiting medication release at the tumor location and this can be induced by changes in the microenvironment e.g., pH, temperature, or enzymatic, or by external stimuli e.g., light, electric fields, magnetic fields, or

ultrasound.

1.3.2 Active targeting

Active targeting is a ligand-receptor interaction that happens following blood circulation and extravasation. It is primarily dependent on the biological interaction formed between target cells and the ligands associated with drug or drug carriers e.g., NPs [26]. Proteins, polysaccharides, nucleic acids, peptides, and tiny molecules are used extensively as ligands in this application. Active targeting employs ligands attached to the NP surface to increase uptake selectivity. These ligands can interact with target cells and frequently shield NPs from enzyme degradation. Ligands having a high binding affinity for the target cell will significantly improve delivery efficiency. The most fundamental method of active targeting includes functionalizing an NP with a ligand that binds to target cells. The problem with this is that healthy cells still express the same cells, and because healthy cells outnumber target cells, most NPs miss their target. This problem can be alleviated by utilizing numerous ligands or ligands of various kinds.

Active targeting modifies a carrier's normal distribution patterns, directing it to a particular cell. On the other hand, passive targeting is based on the drug's natural distribution and the EPR effect. Both of these mechanisms are dependent on blood circulation and the original site of medication administration. Drug-loaded nanoparticle outperforms conventional drug by utilizing both passive and active targeting. It has the ability to circulate throughout the body for an extended length of time until it is successfully attracted to its target using cell-specific ligands, magnetic placement, or pH-responsive materials.

1.4 Targeted Drug Delivery System

A targeted drug delivery system (TDDS) is a promising technique, which aims at overcoming the off-target side effects by navigating the toxic drugs to the affected locations such as tumors or infected areas [27]. Effective TDDS necessitates formulations designed for intravenous administration, which means efficient drug loading into some sort of delivery vehicle, sufficient circulation time to reach intended sites of the body, retention by specific characteristics within intended sites and drug release at the intended site within a time that allows for the drug's effective function [28]. Carriers for TDD should ideally be nontoxic, stable, nonimmunogenic, biocompatible, and biodegradable, easily expelled from the body, and unidentifiable by the host's defensive mechanisms [29, 30]. Furthermore, they must adequately

carry the medication to the target location, overcome barriers and tumor vasculatures as needed, and have optimum release qualities at the target site with no or little drug leakage before that spot. Carriers should also have preparation methods that are simple, reproducible, and cost-effective [31,32]. The DDS should have excellent target selectivity and specificity, which may be achieved by regulating the drug and carrier material's biodistribution patterns. The biodistribution profile is determined by combining both parties' physicochemical and biological features. However, an emerging area known as nanotoxicology is concerned that the nanoparticles themselves may harm both the environment and human health, with their side effects.

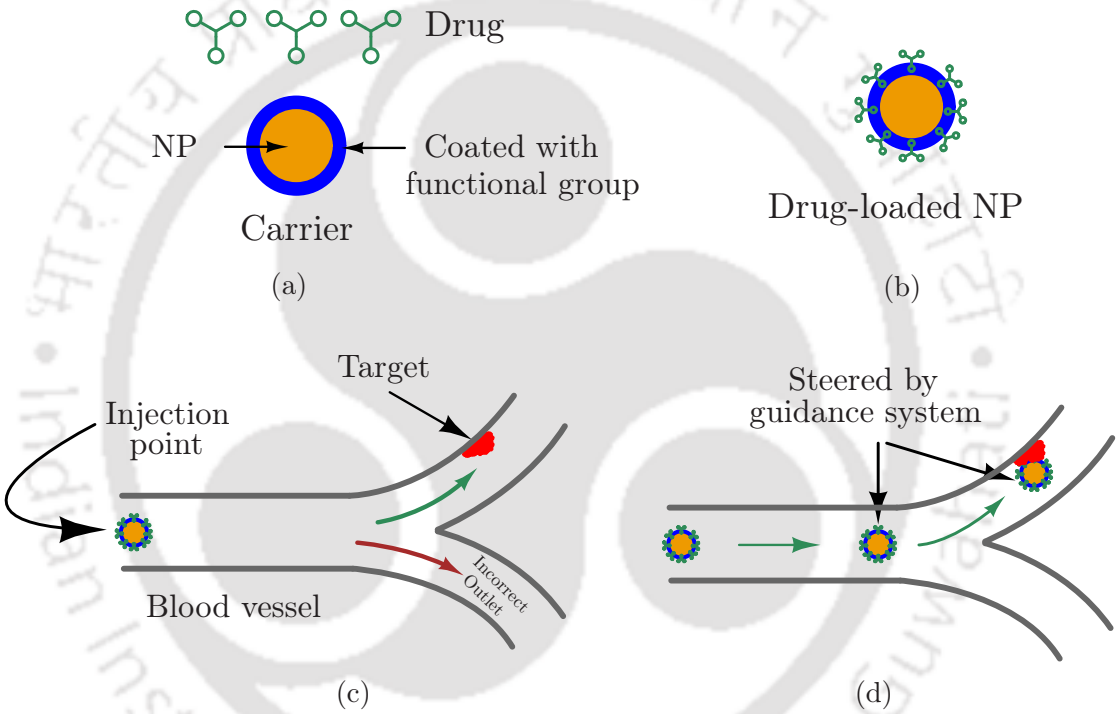

Figure 1.3: Targeted drug delivery: (a) drug and carrier, (b) functionalization, (c) injection, (d) steering.

The basic constituents of TDD are: (i) drug, (ii) carrier and (iii) guidance system, as shown in Fig. 1.3. A pictorial representation of the drug and NP based carrier are shown in Fig. 1.3a. The drug used for treatment is loaded in the surface functionalized NPs [33–35] and followed by the injection into the vasculature of a patient's body, as shown in Fig. 1.3b and Fig. 1.3c, respectively. While the flow of blood in the vessel propels the carrier automatically, a guidance system is used at the bifurcation region to guide the NP based drug carriers into the targeted vessel as represented in Fig. 1.3d. The most crucial entity necessary for successful transport of the drug to the intended target is drug carriers and guidance system to navigate the drug carriers *in vivo*. Therefore, TDDS can be broadly classified

into two main areas: (a) synthesis, characterization and functionalization of drug carriers (b) design of a guidance system to navigate the carriers from the point of injection to the target location in the vasculature.

1.4.1 Nanoparticles for TDD

NPs have shown promise as drug delivery vehicles, but they must be properly tailored to improve effectiveness. Because of their large surface area and limited quantum mechanical effects, NPs usually display a wide range of magnetic, thermal, optical, and electrical properties [36]. Nanoparticles (NPs) are nanoscale materials capable of encapsulating medicines, imaging agents, and genes [37]. NPs have the ability to deliver large quantities of therapeutic substances into tumor cells while bypassing normal cells. While the scaffold structure of NPs allows medications and contrast agents to be attached, their surface allows for biodistribution and targeted delivery by conjugation with ligands that bind to tumor biomarkers [38]. NPs have eliminated the difficulties associated with traditional chemotherapy, such as non-specific biodistribution, drug resistance, and undesired side effects. Several NP-based therapies have entered the clinical trial stage in the recent two decades due to their intriguing properties [39]. The ability to modulate numerous properties of NPs has made them robust therapeutic vectors for cancer treatment. Nanocarriers extend the half-life of treatments in the body and improve their accumulation in the target site. Among the various kinds of drug carriers, such as polymeric micelles, liposomes, lipoprotein-based drug carriers, nanoparticle-based carriers and dendrimers, the magnetic nanoparticles (MNPs) are most effective owing to their unique magnetic properties [40]. MNPs are made comprised of a metal or metallic oxide core encased in an inorganic or polymeric covering that makes the particles biocompatible and stable and serves as a support for biomolecules. Because of their magnetic characteristics, these particles, which belong to one or more of the following classes, can be employed in a wide range of applications.

- Magnetic contrast agents in magnetic resonance imaging (MRI) [41].
- Hyperthermia agents [42].
- Magnetic nanocarrier [43].

Iron oxide NPs are one of the most effective forms of inorganic MNPs. Because these particles can be viewed using Magnetic Resonance Imaging (MRI), they have been employed for imaging purposes in various malignancies. Regarding the magnetic properties of iron oxide NPs, they can be exploited for medicinal purposes

via hyperthermia, in which MNPs are selectively heated by applying a high frequency magnetic field. Since, these NPs are biodegradable and degraded iron may be absorbed by hemoglobin in the body, they can also be used for *in vivo* studies [44]. Superparamagnetic iron oxide nanoparticles (SPIONs) are extremely valuable nanomaterials that may be used for both imaging and therapeutic purposes [45]. The magnetic properties enable these MNPs to be utilized as nanocarriers that may be guided to a specific location *in vivo* by a magnetic field gradient.

1.4.2 Guidance System for TDD

Over the past few decades, nanomaterials have been developed for cancer diagnostics and imaging by manipulating their shape, size, and composition. Nanocarriers have received increased attention in the field of drug delivery systems because they can be stimulated by external elements such as magnetic fields, cell membrane coating, or internal elements such as pH gradients, glutathione and enzymes to improve drug retention and penetration during tumour therapy [46]. The therapeutic effectiveness of multifunctional nanocarriers has been hampered by complicated biological/physiological aspects due to the heterogeneity of tumor tissues. However, certain multifunctional nanocarriers, such as transducers, can transform environmental impulses, including magnetic fields, cell membrane coating, and phototherapy, into physical quantities such as light irradiation, converting the energy to heat. In recent years, combining external stimulation with a multifunctional nanocarrier has been shown to be a potential technique for achieving tumor-specific accumulation of therapeutic drugs, improving therapeutic benefits, and lowering the necessary dosage and systemic toxicity.

Since conventional approaches have major side effects and low EPR results for targeted delivery, several nanocarriers have been designed for delivering therapeutic chemicals to diseased regions using passive or active targeting methods [47]. Magnetic nanocarriers are made up of a magnetic core and a coated shell; therapeutic medications loaded into the shell and targeting molecules can affect the shell's surface [48]. When subjected to a magnetic field, multifunctional magnetic nanocarriers incorporate diagnostics and treatment into delivery systems with good tissue penetration. Magnetic nanocarriers can efficiently induce thermal or mechanical effects in hyperthermia theranostics based on the intensity of the magnetic field [49]. Magnetic field-induced treatment is a novel approach in clinical site-specific therapy that minimizes medication dosage and related systemic toxicity. Magnetic particles are integrated into the therapeutic agent in this magnetic targeting technique, and the agent is concentrated at the targeted spot using gradient fields created by magnets. A magnet can be used to direct a bolus

of magnetized medicines through a vascular bifurcation as an alternative to the systemic circulation.

Many actuation techniques, including chemical propulsion, magnetic propulsion, acoustic propulsion, and biological propulsion, have been explored and developed to improve targeting efficacy [50]. Due to the penetrability of the magnetic field, magnetic drug delivery systems have the benefit of remote controllability. By adjusting the magnetic field remotely as the magnetic field penetrates the human body, NPs carrying medications may be given to the target [51]. Permanent magnets were utilized to produce a magnetic field as an early magnetic actuation device for a drug delivery system due to its simplicity and convenience of usage [52, 53]. However, permanent magnet drive systems cannot easily control the magnetic field because they have to physically move to change the magnetic field. Furthermore, they cannot be switched off during an emergency [54, 55]. As a result of these considerations, electromagnetic actuation (EMA) systems have been offered as an alternative to permanent magnets. As opposed to permanent magnet actuation systems, EMA systems may rapidly change the magnetic field by altering the current. Because of its benefits, numerous EMA methods have been studied to date. Although researchers have proposed various electromagnet-based actuation systems, these systems still have some difficulties controlling magnetic particles.

1.5 State-of-the-art

Microrobotic devices have sparked a lot of attention in recent years, owing to their enormous potential to improve the functionality of micromanipulation in medical, biological, chemical, and industrial environments. Microrobots, since they are tiny and untethered, have the potential to significantly increase the effectiveness of a variety of activities, including TDD, particle separation, mixing, pumping, assembly, manipulation, microsurgery, and chemical analysis [56, 57]. Wireless management of micro/nanostructures in fluids across long distances is critical in medicine, particularly in cancer treatment [58]. Only 0.1% of the medication dosage administered during chemotherapy reaches the intended target; the remaining 99.9% is absorbed by healthy tissue [59]. As a result, a strategy that allows for TDD for maximum efficacy is necessary. The goal of TDD is to increase drug absorption in tumor tissues while reducing side effects such as harm to healthy cells and reducing the needed drug dose. The transmission of power for mobility is a critical barrier for wireless management of micro/nanostructures. One method is to use wireless magnetic control. Magnetic fields penetrate human tissue and are biocompatible

up to several Tesla field strengths widely employed in MRI scanners. Magnetic carriers containing pharmaceuticals might be navigated through physiological fluids and steered to the location of interest using magnetic fields and field gradients [60]. The manipulation and transportation of MNPs using external magnetic fields are finding widespread applications in biotechnology, biomedical engineering and environmental applications [61–64]. Magnetic separation is a process used to segregate magnetic and non-magnetic materials. Materials with different magnetic permeability, under the exposure of magnetic field gradient, experience various magnetic forces which lead to the isolation of the target entity [65]. In this regard, magnetic actuation systems play a vital role in controlling the locomotion of MNPs. The magnitude and direction of magnetophoretic force produced by such an actuation system are responsible for the navigation of MNPs. Different actuation systems are used to control the movement of MNPs. Permanent magnet [66] based actuation systems are simple to use but they are not effective for the propulsion of MNPs in a fluidic suspension. However, EMA systems in [67] and [68] are more effective in producing desired magnetophoretic force for the propulsion of MNPs. This type of actuation system can also be used in water and wastewater treatment [69]. DDS [70] also utilizes a similar kind of electromagnet for the transportation of MNPs to a specific location. Magnetic resonance imaging (MRI) [71] is a popular imaging technique used in biomedical applications, which uses a combination of strong magnetic fields and magnetic field gradients to generate images of body organs.

In the context of guidance mechanism design, recent studies show the explicit application of magnetic field in many biomedical applications [72, 73]. A wireless capsule endoscope system uses magnetic actuators to control the movement of the camera-equipped capsule to capture the internal images of the digestive organs for use in medical diagnosis[74]. Likewise, magnetically assisted TDDS is adopted to control the movement of MNPs in the blood vessel [75]. In this regard, much attention is devoted to usage of magnetic actuation system for targeted delivery of MNPs *in vivo*[76–78]. The magnetic field produced by such an actuation system exerts a magnetic force on the MNPs, navigating them in the blood vessel. Magnetically actuated TDDS are potentially effective in navigating the MNPs inside the blood vessels. Superconductors and permanent magnets based actuators are proposed as viable means to guide the MNPs in the vasculature [79, 80]. However, the magnetic fields produced by these systems are inadequate to penetrate deep into the target region inside the human body. A two coils electromagnetic actuator is proposed to enhance the penetration and to define the trajectory of MNPs inside the blood vessel [70]. This system produces a gradient magnetic field

responsible for exerting a force on the MNPs. A further improved electromagnetic actuation (EMA) system using Maxwell coil, comprising of two electromagnetic coils with equal but opposite currents, is proposed in [81] to produce a gradient magnetic field for steering the MNPs. However, in this system, the movement of MNPs would depend on their position with reference to the center of the coil separation. Furthermore, [71] highlights that concurrent use of two coils generates a higher magnetic field gradient for navigation of MNPs. Until now, traditional MRI systems were used just for imaging, but their range of possible medical and scientific uses can be broadened beyond imaging by using MRI scanners to provide propulsion for minimally invasive devices [82,83]. The MRI systems can overcome organ depth, gradient linearity, and imaging feedback restrictions. An electromagnetic guidance system composed of one Helmholtz coil and two racetrack coils is proposed in [67], to steer the MNPs irrespective of their position by exerting a unidirectional magnetic force on the MNPs. The authors in [84] propose a combination of Helmholtz and Maxwell coils to produce a gradient magnetic field along the desired direction with lesser geometrical complexities as compared to that in [67]. Their work is further extended in [85] to attain a higher gradient magnetic field with reduced structural complexity by adopting Differential Current Coil (DCC) approach.

1.6 Motivation

The MNPs in a blood vessel are propelled by the laminar flow of blood, which shows a parabolic profile of flow velocity. Consequently, the hydrodynamic drag force experienced by the MNPs in the blood vessel is maximum at the center of the vessel and lower at the sidewalls [85]. Therefore, the orthogonal magnetic force applied by an EMA system is much higher than the drag force at the sidewalls. This causes a fairly large number of MNPs to adhere to the vessel walls and thus, the *stiction issue* is induced. The aggregation of MNPs in the presence of a continuous magnetic field has been investigated experimentally [86]. The accumulation of aggregates at the bifurcation occurs from the steering of aggregated microparticles in a Y-shaped channel under magnetic field [71]. To address this concern, different actuation schemes are proposed [87–89]. More precisely, the concept of a functionalized magnetic field is proposed in [87], whereby a unitless time-varying multiplier function is used to vary the direction of magnetic force for steering and to detach the MNPs alternately over time. However, the magnitudes of force applied to steer and detach the MNPs remain the same in this scheme, which may result in the steering of the MNPs to an incorrect outlet. To further improve the

efficiency of the guidance system in [87], a modified version of the field function is introduced in [88]. It is noteworthy that the scheme uses a much lower magnetic force for stiction removal than that for steering, while the duration of application of both these forces remains the same. An alternate scheme that generates discontinuous asymmetrical field function is proposed to mitigate the stiction issue along with disaggregation of stuck MNPs [89]. In this scheme, a time-slotted approach is used to steer and detach the MNPs respectively, with the applied magnetic field being much lesser in the latter case than the former, which is further followed by a null magnetic field time slot for particle disaggregation. This scheme alternates between two coils for steering and detaching operations (only one coil is active in each slot). Specifically, the scheme uses three different time slots. The first two are used for steering and stiction removal, while the third time slot comprises a null magnetic field intended for disaggregation of the MNPs. However, it may be noted that during the null slot, there will be no control of the actuation system over the MNPs. This may lead to the random propulsion of MNPs to the undesired outlet along with the fluid flow. This motivates us to adopt a different approach using two coils simultaneously for both steering and stiction mitigation, thus allowing better control over MNPs in a bifurcated channel.

1.7 Problem Definition

Motivated by the above works, we present a time-varying magnetic field (TVMF) for effective steering of MNPs to the correct outlet of the bifurcated channel while taking into account the stiction and aggregation of MNPs during navigation operation. Specifically, we emphasize the fact that in contrast to [89], the stiction removal and disaggregation of MNPs can be achieved in a single time slot by adjusting both the magnetic force as well as the slot duration. The TVMF operates by switching between two modes of operation viz, (i) Mode 1 and (ii) Mode 2. In Mode 1, the TVMF is applied for a particular duration so as to facilitate steering of the MNPs towards the target outlet. During this process, some MNPs that aggregate and get stuck to the side-walls are released by applying the TVMF in the reverse direction to Mode 1. The magnetic force resulting from the TVMF in Mode 2 has a small magnitude, releasing the stuck MNPs at side-walls but not steering them into the incorrect outlet. Furthermore, the fluidic force dominates over this small magnetic force as the MNPs are pulled back from the side walls (due to the former's parabolic nature), thereby minimizing the aggregation of MNPs. However, the influence of fluid force could result in the random flow of MNPs in the channel. Hence, the duration for applying TVMF in Mode 2 has to be adjusted

so that the MNPs are confined within the desired region of interest. Therefore, this thesis aims to address the specific aspects of a magnetically targeted drug delivery system.

- Design and analysis of an EMA system using a novel coil topology to navigate the MNPs to the target location.
- Optimization of the system design parameters to enhance the guidance efficacy.
- Effect of TVMF on the mitigation of stiction and aggregation of MNPs during their navigation towards the desired outlet.
- Analyse the coupling of applied magnetic field and switching time for effective navigation of MNPs in the channel.
- Experimental validation of the novel EMA system by tracking the trajectory of the synthesized MNPs into the fabricated Y-shaped channel.

1.8 Thesis Contribution and Organization

An EMA system is designed using a particular arrangement of four circular electromagnetic coils to navigate the MNPs from the inlet to the target outlet in the Y-shaped microchannel. The coils are used to produce a magnetic force for steering of MNPs to the correct outlet. The proposed work is done in the following two stages: (i) design, analysis and optimization of the coil topology for guiding the MNPs, (ii) removal of stiction and aggregation issue while ensuring that the MNPs are always administered to the desired outlet. Simulation results are presented to highlight the optimal switching time for the applied magnetic field, which is required to obtain the desired particle trajectory.

The thesis begins with an analysis of the EMA system for different coil topologies. Based on this analysis, a novel coil topology is proposed to navigate the MNPs to the target location. Furthermore, the system design is optimized to enhance the guidance efficacy through stiction mitigation and disaggregation of magnetic particles. The proposed system design is experimentally validated. Lastly, a summary and future prospects are presented. The outcome of the thesis exhibits superior guidance efficiency compared to another TDDS design reported. The main contributions of this thesis are summarized below:

- Design and analysis of EMA system using different coil topologies, to steer the MNPs in the bifurcated microchannel.

- Optimization of the geometry and supply currents for each coil in the four coils arrangement, to produce a magnetic force along the desired steering direction. In this process, a few MNPs get stuck to sidewalls.
- To overcome the stiction and aggregation issue, a switching mechanism is adopted. A pair of coils in the actuation system operates exclusively for a certain time period to release the stuck MNPs with a reverse magnetic force, while the other pair of coils is switched OFF during this period.
- The navigation of MNPs in a Y-shaped channel is experimentally validated due to the gradient magnetic field produced by the proposed EMA system.

The thesis is organized into six chapters. An overview of the thesis is presented as follows.

Chapter 1

This introductory chapter presents a brief history of the development of the EMA system as a guidance system and MNPs as drug carriers. This chapter also discusses the need for TDDS followed by the methods and processes that have been developed in the existing literature for guiding the MNPs to the target location. The chapter ends by summarizing the overview of its content and the contributions of the thesis.

Chapter 2

In this chapter, we present a comparative performance analysis of actuation systems, consisting of coils having the following five different topologies: single coil, Helmholtz coil, Maxwell coil, Helmholtz-Maxwell pair and differential current coil (DCC). The experiments are performed using PASCO EX-5540A setup while the numerical analyses are done using COMSOL Multiphysics software.

Chapter 3

This chapter proposes an EMA system using four circular current-carrying coils to navigate the MNPs in the Y-shaped channel. The design parameters are further optimized to enhance the performance of EMA-based TDDS.

Chapter 4

In this chapter, we propose a time-varying magnetic field (TVMF), which switches between two modes of operation. Our proposed TVMF can be utilized to mitigate

the stiction and aggregation of the MNPs, whereas effectively navigating them towards the desired outlet.

Chapter 5

This chapter deals with the methods involved in synthesizing the MNPs as drug carriers, fabricating the Y-shaped channel to mimic the vasculature and designing the electromagnetic coils as a guidance system. The complete system is experimentally validated and the results indicate that the system is practically realizable for TDDS.

Chapter 6

This chapter covers the conclusion and future prospects of the thesis. A summary of all the research works is presented in this chapter. The future scope of development on actuation systems towards other applications such as magnetic water treatment and magnetic separation for biomedical diagnostic are also presented in this chapter.

Chapter 2

Analysis of Electromagnetic Actuation Systems for TDD

Contents

2.1 Introduction 18
2.2 Theoretical Model 20
2.3 Methodology 22
2.4 Results & Discussion 24
2.5 Chapter Summary 28

2.1 Introduction

As medical science evolved, more and more medications were effectively produced and used to treat human ailments. Medications are often given orally or injected in the traditional method of illness treatment, ensuring that the drugs are spread widely throughout the human body. Such a condition would harm the body's regular cells and tissues, resulting in undesired side effects and potentially significant complications for the sufferers. TDD is an effective way to solve this issue since it not only cures the disease efficiently but also reduces dose and adverse effects. This is especially significant in the treatment of diseases such as cancer, nervous system ailments, and acute hearing impairment, among others. Drug targeting tries to deliver the medications to the target location, which can increase effectiveness, reduce drug doses, and lessen adverse effects. At the moment, numerous methods for drug targeting have been researched or proposed, including the use of physical surroundings such as light, electricity, ultrasonic, and magnetic fields. Among these physical contexts, magnetic drug targeting is an appealing technique. Magnetic drug targeting is a technique in which magnetic drug carriers within the body are controlled by external magnetic fields to reach the desired location. Magnetic drug carriers are made up of magnetic materials that interact with magnetic fields, often magnetic nanoparticles like ferric oxide particles. Magnetic fields, unlike other methods of medication targeting, may flow through the body safely, hence magnetic carriers can, in theory, be guided to deep tissue targets [90]. Since the advent of magnetic fields for drug targeting, many magnet designs for TDD have been researched. Existing magnet system designs are divided into two categories: static field magnet systems and variable field magnet systems.

Static Field Magnet System

Static field magnet systems have a magnetic field that remains constant over time. The systems are classified into two types based on the source of the field: permanent magnet systems and electromagnet systems.

Variable Field Magnet System

Varying field magnet systems are those in which the magnetic field varies over time. The relative movement of the sample and the magnet can produce such changing field magnet systems. The systems are classified into two types based on the source of the magnetic field: moving permanent magnet systems and variable field electromagnet systems.

Permanent magnets are inexpensive, easy to use, and efficient in terms of energy. Their magnetic field intensity (H) and magnetic field gradient (∇H) are, however, relatively modest, and they can occasionally present safety issues since they cannot be "turned off," even in an emergency. Electromagnets, on the other hand, may offer a reasonably strong magnetic field and field gradient with improved safety characteristics [91]. In the following sections, we present the popular coil topologies of electromagnet systems such as single coil, Helmholtz coil, Maxwell coil, Helmholtz-Maxwell pair and differential current coil (DCC)[85]. PASCO EX-5540A setup is used for experimental analysis. Also, COMSOL Multiphysics software is used for numerical analysis of the electromagnetic coils and the experimental results are validated with analytical and simulation results. Numerical, analytical and experimental results for single coil, Helmholtz coil and Maxwell coil are presented. Furthermore, a configuration of Helmholtz-Maxwell coil pair and DCC, based on MRI technique[81][76], is studied and analyzed for possible use in the guidance systems of TDD.

Amidst the growing concerns of adversities associated with magnetic stimulation to human body, regulatory bodies have standardized limits for exposure to radiation. Such limits are proposed taking into consideration the distribution of exposure among the population, time of exposure and other safety concerns. In this work we have followed the IEEE Std C95.1-2019, IEEE standard for safety levels with respect to human exposure to electric, magnetic, and electromagnetic fields [92]. The exposure reference limits of the magnetic field (B) and magnetic field strength (H) for head, torso and limbs are 353 mT and 2.81×10^5 kA/m, respectively.

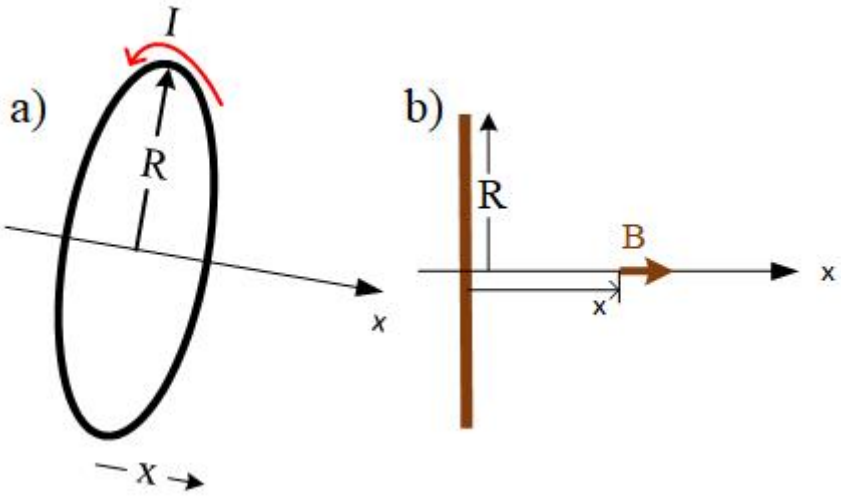

Figure 2.1: a) Single coil of radius R and b) Cross-sectional view of the single coil.

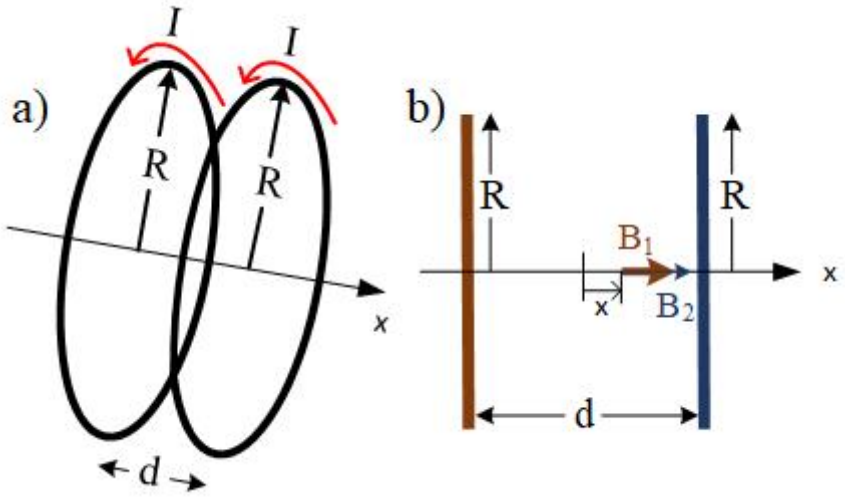

Figure 2.2: a) Two coils of radius R, separated by a distance d and b) Cross-sectional view of the two coils.

2.2 Theoretical Model

The basic building blocks of an EMA system, used for guiding the MNPs in a TDSS, are the circular coils carrying current. Fig. 2.1a shows a single coil configuration having N turns, carrying a current I, generates a magnetic field along the perpendicular axis. This configuration is not sufficient to penetrate deep into the desired region because the influence of the magnetic field decreases as the MNPs move away from the coil. Two identical coils are placed parallel to each other as shown in Fig. 2.2a, the magnetic field produced by each coil is superimposed to obtain the resultant magnetic field.

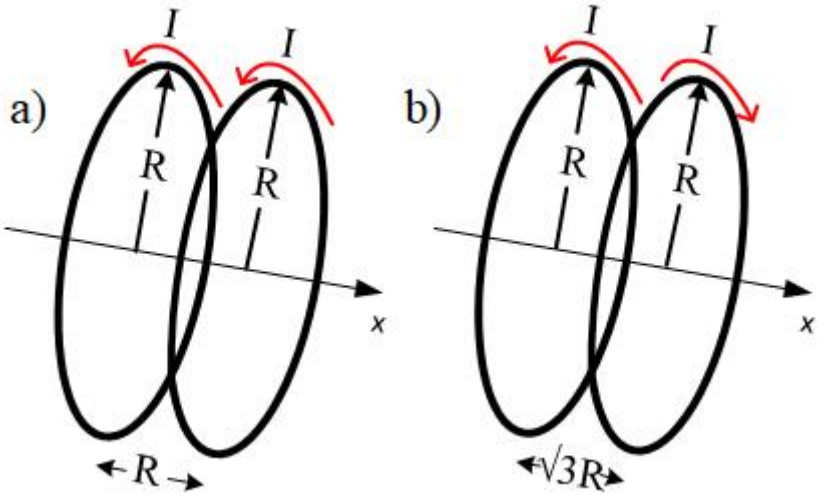

Figure 2.3: a) Helmholtz coil and b) Maxwell coil.

Helmholtz coil consists of a pair of circular coils having N turns, each carrying a current I in the same direction and are separated by a distance equal to the radius of the circular loops as depicted in Fig. 2.3a. It results in generation of uniform magnetic fields between the two coils. Maxwell coil is similar to Helmholtz coil with distance between the coils increased by a factor of $\sqrt{3}$ and the coils are fed with currents in opposite directions as shown in Fig. 2.3b. This configuration results in generating a gradient magnetic field in between the two coils. However, a Helmholtz coil or a Maxwell coil alone can not produce the desired magnetic field to propel the MNPs in fluidic suspension. To overcome this challenge, a combination of both Helmholtz coil and Maxwell coil is considered such that their magnetic fields can be superimposed to produce a uniform magnetic field gradient which can propel the MNPs. In such systems, one set of two Helmholtz coils is used to provide a uniform constant magnetic field in the desired direction for magnetic particle saturation, while another set of two Maxwell coils is used to generate the gradient magnetic field required to facilitate desired magnetophoretic force for the navigation of MNPs *in vivo*. But this benefit comes at the expense of increased geometrical complexities, which arises due to the use of four electromagnetic coils for designing the actuation system [84]. To this end, differential current coil (DCC) [85] arrangement is proposed as an efficient technique for controlling the MNPs with reduced complexity. DCC shows the characteristics of Helmholtz-Maxwell coil configuration using two coils only. The arrangement consists of a pair of circular coils having N turns, each carrying current in the same direction but the magnitude of currents are different in each coil.

Magnetic particles suspended in a viscous medium experience a force in response to the application of nonuniform magnetic field, which is known as magnetophoresis (MAP). The difference in permeability of magnetic particles and the surrounding medium results in the generation of MAP. The effective magnetic moment of the magnetic particle as a homogeneous sphere with radius R, suspended in a magnetically linear fluid of permeability μ_1 is calculated as[93]

$$M_{eff} = 4\pi R^3 \left[\frac{\mu_0 - \mu_1}{\mu_0 + 2\mu_1} H + \frac{\mu_0}{\mu_0 + 2\mu_1} M \right], \tag{2.1}$$

where $\mu_0 = 4\pi.10^{-7}$ H/m is the permeability of free space. H and M are the magnetic field intensity and net magnetic polarization respectively. For a magnetically linear particle of permeability μ_2, we have

$$M = \chi H, \tag{2.2}$$

where $\chi = \mu_2/\mu_0 - 1$ is the susceptibility of the particle. The magnetophoretic force for a magnetizable spherical particle in a nonuniform magnetic field may be expressed as

$$F_{MAP} = \mu_1 M_{eff}.\nabla H. \tag{2.3}$$

From (2.3), the MAP force depends on magnetic field intensity and gradient intensity. The relationship between magnetic field B and magnetic field intensity H is $B = \mu_0 H$.

For a single coil of wire having radius R and N turns of wire, the magnetic field along the perpendicular axis through the center of the coil (shown in Fig. 2.1b) is

$$B = \frac{\mu_0 N I R^2}{2(x^2 + R^2)^{\frac{3}{2}}}. \tag{2.4}$$

As shown in Fig. 5.9b, when two identical coils are placed parallel to each other, the magnetic field produced by each coil is superimposed to obtain the resultant magnetic field. For Helmholtz coil, the separation d between the two coils is equal to their radius R and each coil carries equal current in the same direction. This coil separation gives an uniform magnetic field between the coils and is given by

$$\begin{aligned} B &= B1 + B2 \\ &= \frac{\mu_0 N I R^2}{2} \left[\frac{1}{[(x-\frac{d}{2})^2+R^2]^{3/2}} + \frac{1}{[(x+\frac{d}{2})^2+R^2]^{3/2}} \right], \end{aligned} \tag{2.5}$$

where x is measured from the geometric center as shown in Fig. 5.9c.

Maxwell coil[94] pair consists of two circular coils of radius R, carrying currents circulating in opposite directions and the separation (d) between the two coils is equal to $\sqrt{3}$ of the coil radius, R. The flux gradient from the Maxwell coil is uniform in between the coils, which is given by

$$\begin{aligned} B &= B1 + B2 \\ &= \frac{\mu_0 N I R^2}{2} \left[\frac{1}{[(x-\frac{d}{2})^2+R^2]^{3/2}} - \frac{1}{[(x+\frac{d}{2})^2+R^2]^{3/2}} \right], \end{aligned} \tag{2.6}$$

2.3 Methodology

To realize the TDDS for in vivo applications, we require EMA system to remotely control the movement of MNPs used as drug carrier. The next step is to design and analyse the actuation system using electromagnets.

2.3.1 Simulation Framework

COMSOL Multiphysics employs finite element method (FEM) to numerically approximate solutions of partial differential equations (PDEs) with known boundary conditions. The Magnetic Fields interface from AC/DC module is used to compute magnetic field in and around the electromagnetic coils. The Magnetic Fields interface solves Maxwell's equations formulated using the magnetic vector potential. The variables that describe the current direction in coils is solved using Coil Geometry Analysis. The Magnetic Field interface used to compute the magnetic field may not be able to evaluate the spatial derivative of the magnetic field components, as the degrees of freedom correspond to components of the magnetic vector potential. Therefore, Coefficient Form PDE interface is used to evaluate the gradient of the magnetic field components using scalar basis functions.

Table 2.1: Coil Parameters

Parameter	**Value**	**Unit**
Number of turns	500	-
Height	2	cm
Width	2	cm
Outer diameter	23.4	cm
Inner diameter	19.4	cm
Wire diameter	1	mm
Current	1	A

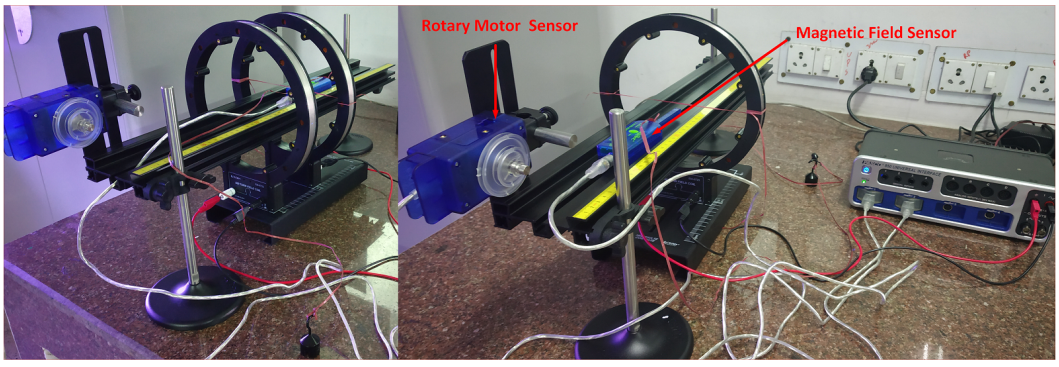

Figure 2.4: Experimental set-up using single coil and two coils.

2.3.2 Experimental Framework

PASCO EX-5540A setup as shown in Fig 2.4 along with PASCO Capstone software are used for experimental evaluation. Rotary motor sensor tracks the position and magnetic field sensor measures the magnetic field of the coil. The magnetic fields of the coils are plotted versus position as the magnetic field sensor is passed through the coils, guided by a track. The position is recorded by a string attached to the magnetic field sensor that passes over the rotary motion sensor pulley to a hanging mass.

2.4 Results & Discussion

The electromagnetic actuation systems presented in this paper are designed and modeled in COMSOL Multiphysics software. The experimental results are validated with analytical as well as simulation results considering three different coil configurations viz. single coil, Helmholtz coil and Maxwell coil. For comparison purpose identical coil geometry is used and the coil parameters are listed in Table 2.1. Also, the DCC coil is simulated considering 500 ampere-turn (500 turn coil with 1 A current through it) for one coil and 2500 ampere-turn (2500 turn coil with 1 A current through it) for the other one. The magnetic flux density gener-

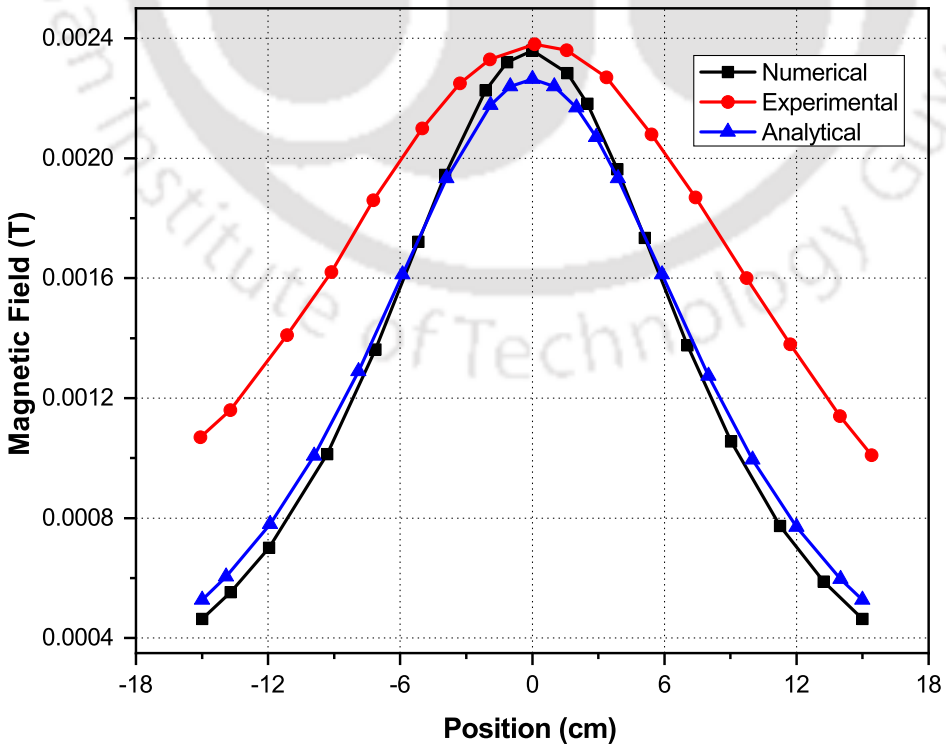

Figure 2.5: Magnetic field generated by single coil.

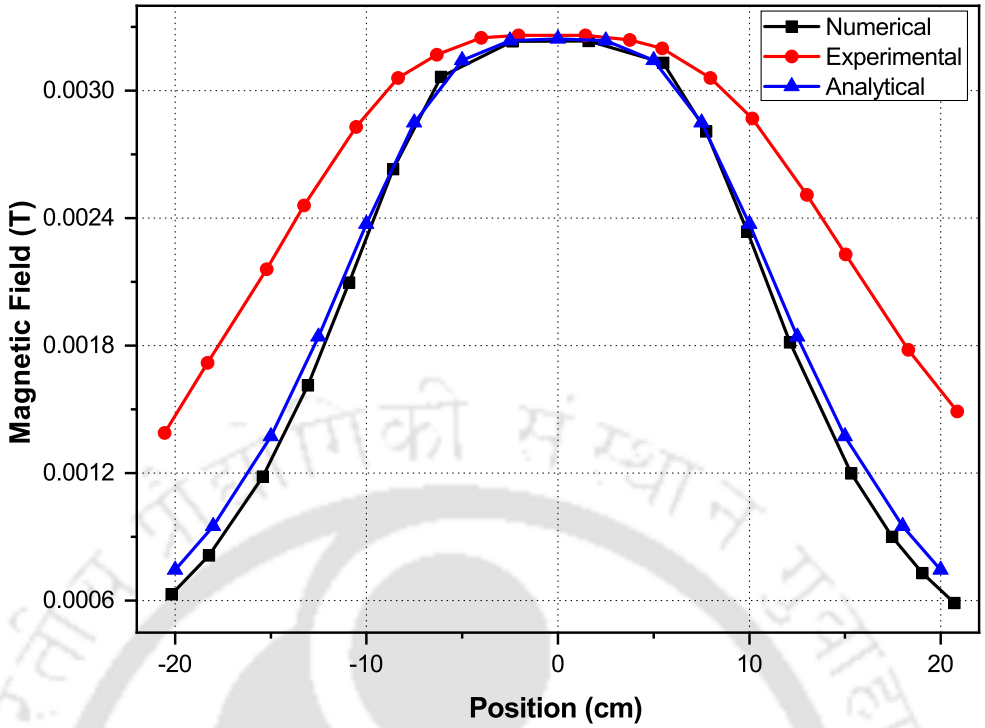

Figure 2.6: Magnetic field generated by Helmholtz coil.

ated by different coil topologies are calculated by AC/DC module of COMSOL in steady state.

2.4.1 Single Coil

Fig. 2.5 shows the variation of magnetic flux density along the perpendicular axis of the single coil. Clearly, it is observed that experimental result shows close match with the analytical as well as the simulation results. It is noted that the influence of magnetic flux density generated by the coil decreases on MNPs as they move farther on both side of the perpendicular axis of the coil. This is because of the fact that the magnetic flux density generated by the coil at any point is inversely proportional to the distance of the point from the coil (2.4). This actuation system is not useful since the magnetic flux generated by the single coil cannot penetrate into deep region, thereby failing to manipulate the MNPs.

2.4.2 Helmholtz Coil

Fig. 2.6 depicts the experimental validation of magnetic flux density along the perpendicular axis of the Helmholtz coil. It is seen that Helmholtz coil generates a uniform magnetic flux density for a range equal to the radius of the coil. This uniformity is due to the superposition of magnetic flux densities produced by

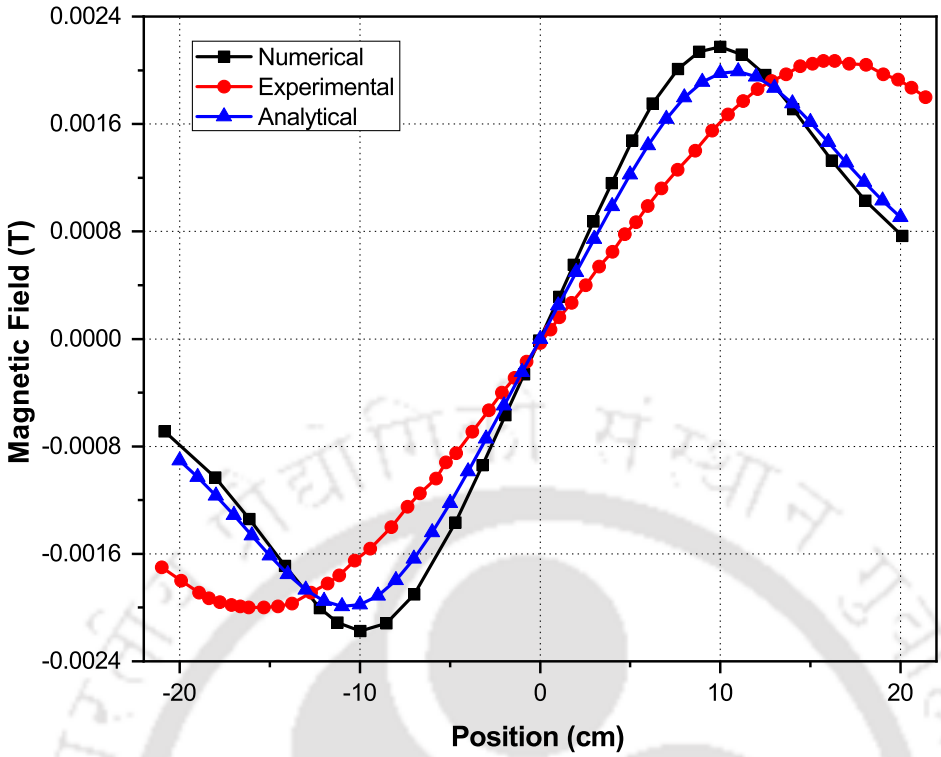

Figure 2.7: Magnetic field generated by Maxwell coil.

individual coil of the Helmholtz coil pair following (2.5). This actuation system is unable to move the MNPs as it produces zero magnetophoretic force.

2.4.3 Maxwell Coil

Fig. 2.7 depicts the experimental validation of magnetic flux density along the perpendicular axis of the Maxwell coil. It is seen that Maxwell coil generates a gradient magnetic flux density. This gradient nature is due to current flowing in opposite direction in both the coils of Maxwell coil. Although, the gradient flux density produced by the Maxwell coil results in a nonzero magnetophoretic force, this actuation system is not sufficient to magnetize the MNPs to saturation level due to low magnetic strength.

The experimental results show good agreement with both simulation and analytical results for the region of our interest. However, the experimental results deviate a little due to the considerable width and height of the coils, which is not included in our theoretical analysis.

2.4.4 Differential Current Coil

DCC configuration is considered where two coils are used in a such a manner that it shows the characteristics of Helmholtz-Maxwell coil pair [85]. Fig. 2.8 presents

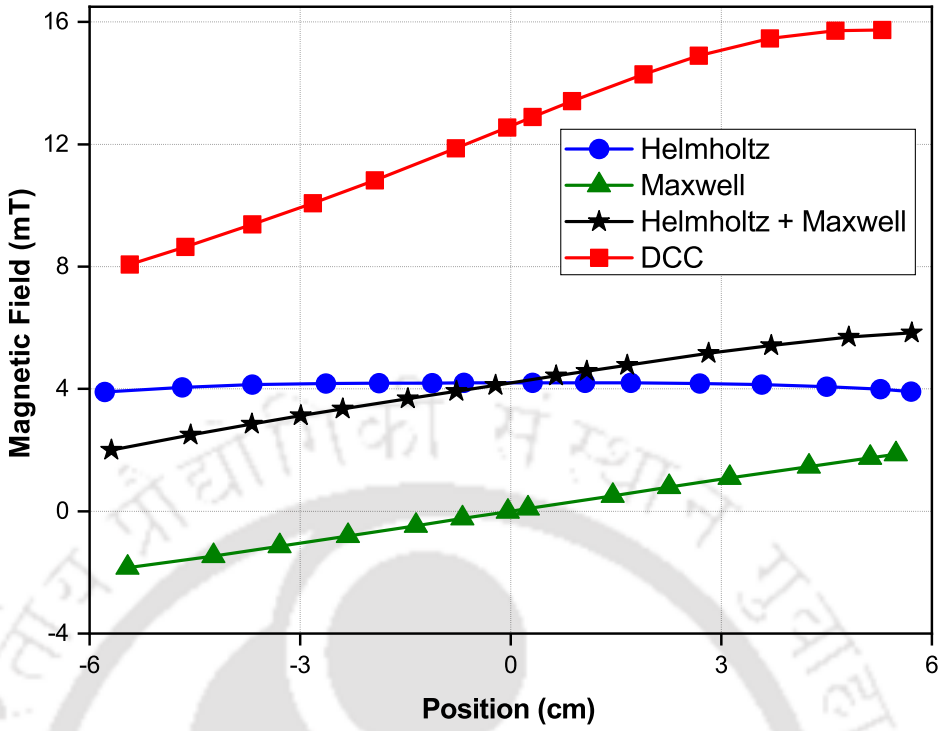

Figure 2.8: Magnetic flux density generated by Helmholtz, Maxwell, Helmholtz-Maxwell pair and DCC configuration.

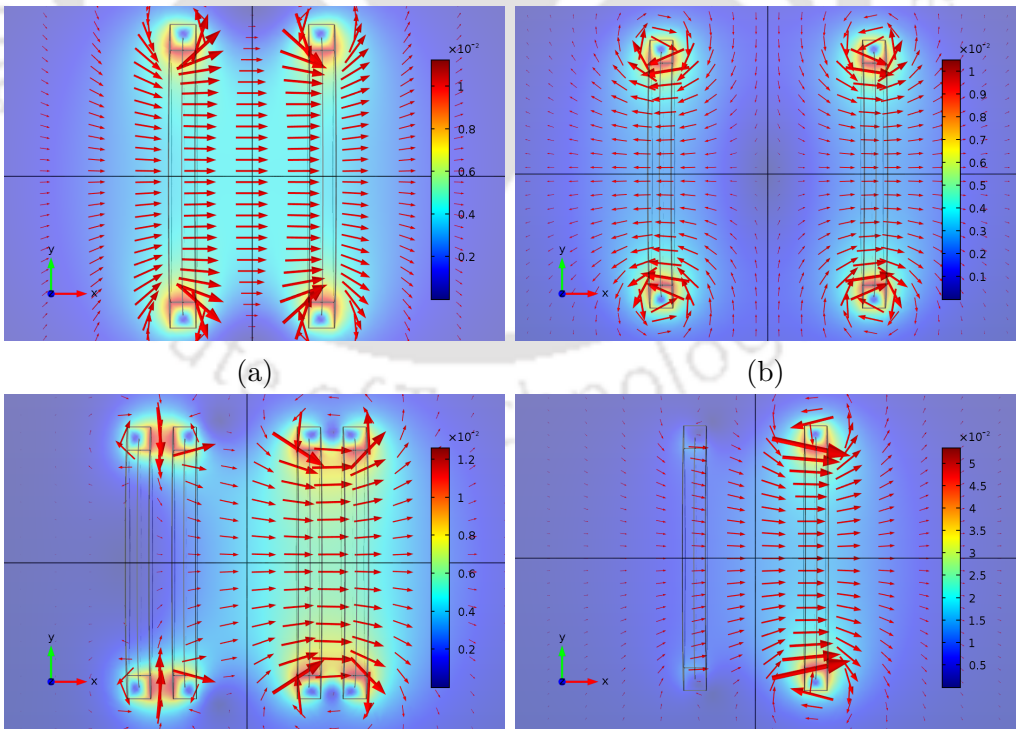

Figure 2.9: Surface plot of (a) Helmholtz coil, (b) Maxwell coil, (c) Helmholtz-Maxwell pair and (d) DCC configuration

numerical comparison of flux densities of Helmholtz, Maxwell and a combination of Helmholtz-Maxwell coils. Fig. 2.8 highlights that Helmholtz-Maxwell pair outperforms the individual performances of Helmholtz and Maxwell coil in terms of magnetic flux density. Moreover, DCC approach shows higher flux density gradient as compared to that of the other configurations presented here.

The surface plots for magnetic fields, corresponding to each coil configuration discussed above, are graphically represented in fig. 2.9. The arrows in the plot indicate the magnitude and direction of magnetic flux density on x-y plane. Thus, to summarize, DCC approach is more suitable as it has lower geometrical complexity than that of Helmholtz-Maxwell pair which uses four coils.

2.5 Chapter Summary

Electromagnetic actuation systems are used to generate magnetic forces for the manipulation of magnetic nanoparticles. In this work, we present a comparative performance analysis of actuation systems, consisting of coils having the following five different topologies: single coil, Helmholtz coil, Maxwell coil, Helmholtz-Maxwell pair and differential current coil (DCC). The experiments are performed using PASCO EX-5540A setup, while the numerical analyses are done using COMSOL Multiphysics software. It is observed that the experimental results conform to analytical results as well as simulation results. Furthermore, the results highlight that both Helmholtz-Maxwell pair and DCC topologies produce strong gradient magnetic flux density, thus leading to better manipulation of magnetic nanoparticles as compared to that of other topologies. Additionally, the DCC approach with two coils achieves better gradient flux density while having lesser geometrical complexity as compared to that of the Helmholtz-Maxwell pair consisting of four coils. To conclude, the DCC configuration is a promising approach for the future study of actuation systems as it has higher gradient flux density, lesser geometric complexity and is also cost effective.

Chapter 3

Design and Optimization of EMA Systems

Contents

3.1 Introduction 30
3.2 Classification of Materials 31
3.3 Theoretical Concepts 33
3.4 Actuation System 35
3.5 Optimization of EMA System 45
3.6 Results and Discussions 48
3.7 Chapter Summary 50

3.1 Introduction

TDD is a means of administering medication to a patient in such a way that the medication concentration in disease-affected areas of the body is higher than in others. MNPs have various benefits over standard DDSs, including regulated magnetic responsiveness, biocompatibility, longer circulation lifespan, surface recognition and surface stability. MNPs based therapeutics have been explored and developed for biomedical applications in the treatment of cancer and many other disorders over the past three decades. MNP-based drug delivery research is broadly divided into two areas. The first one focuses on the synthesis and characterization of MNPs for drug delivery. Another area of investigation is the development of actuation devices to regulate the movement of MNPs from the location of injection to a targeted diseased location in the vasculature. Several strategies have been offered in the literature to attain this goal. Magnetic particles were initially trapped by static magnetic fields generated by permanent magnets or superconducting magnets. However, the use of a static magnetic field was not shown to be successful in targeting magnetic particles deep within the body. Chapter 2 demonstrates that the influence of the magnetic field produced by a single coil decays significantly as the MNPs move away from the coil. Electromagnets are commonly utilized as actuators to reach deep regions within the body. A comparative analysis of Helmholtz, Maxwell, Helmholtz-Maxwell pair and DCC configuration presented in Chapter 2, highlights that the DCC approach produces the highest gradient magnetic flux density for navigating the MNPs.

In a magnetically actuated TDDS, the MNPs are guided to the desired blood vessel by steering them from the bifurcation points, using an external EMA system. To facilitate the steering process, the magnetic force exerted by the EMA system dominates over the hydrodynamic drag force induced by the blood flow. However, this dominance has an adverse effect of adhering some MNPs to the sidewalls of the channel. To overcome this problem, we propose an EMA system with a new approach for actuating the MNPs using electromagnets. An EMA system is designed using a particular arrangement of four circular electromagnetic coils. The coils are used to produce a magnetic force for steering of MNPs to the correct outlet. The coil parameters and currents in each coil are optimized to efficiently steer the MNPs in a Y-shaped microchannel. The goal of the proposed design is to enhance efficacy by alleviating the detrimental effect of the MNPs getting steered to the undesired outlet. The main contribution of this chapter is to optimize the geometrical parameters and supply current for each coil in the four coils arrangement to produce a magnetic force along the desired direction of steering.

3.2 Classification of Materials

Magnetic materials are considered to be magnetizable, which means that when a magnetic field is applied, the material itself becomes a source of the magnetic field. Magnetic materials are classified as diamagnetic, paramagnetic, ferromagnetic, antiferromagnetic and ferrimagnetic.

3.2.1 Diamagnetic

Diamagnetic materials have permeability that is just slightly different from that of free space, with little or no magnetism. It does not have a permanent magnetic field and when these materials are subjected to an applied field, atomic currents are generated, resulting in a bulk magnetization that resists the field.

3.2.2 Paramagnetic

At the atomic level, paramagnetic materials have a net magnetic moment, but the coupling between nearby moments is weak, as shown in Fig 3.1. These moments tend to align with an applied field, but the degree of alignment diminishes at increasing temperatures owing to thermal agitation's randomizing effects.

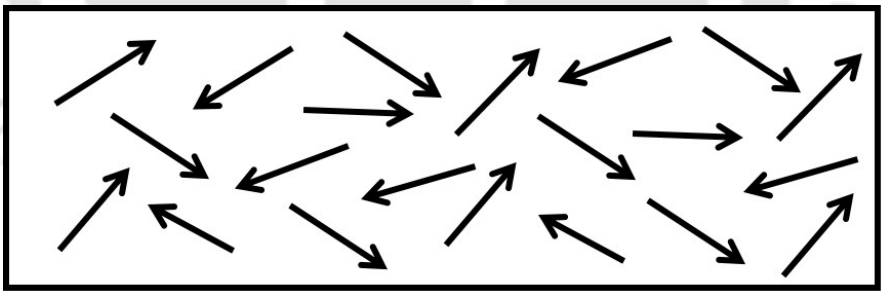

Figure 3.1: Paramagnetic material

3.2.3 Ferromagnetic

At the atomic level, ferromagnetic materials have a net magnetic moment, but unlike paramagnetic materials, there is a significant coupling between nearby moments, as shown in Fig 3.2. This connection causes a spontaneous alignment of moments over macroscopic areas known as domains. When the material is exposed to an applied field, the domains become even more aligned.

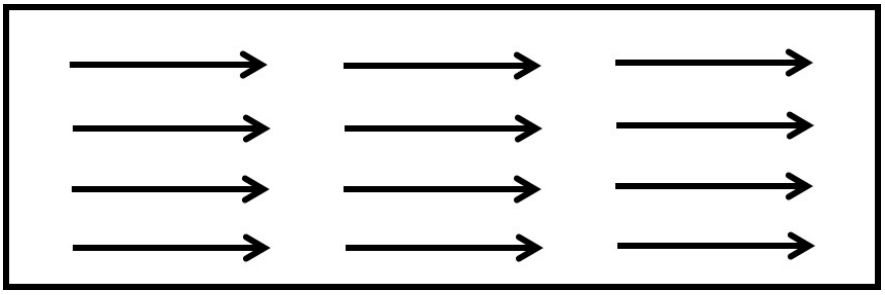

Figure 3.2: Ferromagnetic material

3.2.4 Antiferromagnetic

Antiferromagnetic materials have orientated atomic moments, with adjacent moments antiparallel to one another, as shown in Fig 3.3. There is no net magnetic moment in antiferromagnetic materials since the surrounding moments are equal.

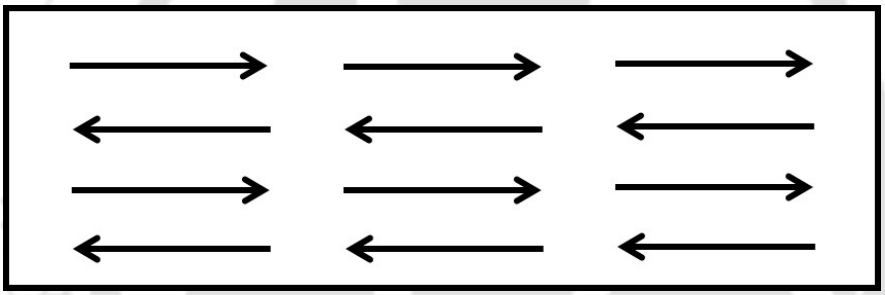

Figure 3.3: Antiferromagnetic material

3.2.5 Ferrimagnetic

Ferrimagnetic materials have orientated atomic moments, with adjacent moments antiparallel to one another. Unlike antiferromagnetic materials, ferrimagnetic materials have uneven adjacent moments and a net magnetic moment, as shown in Fig 3.4.

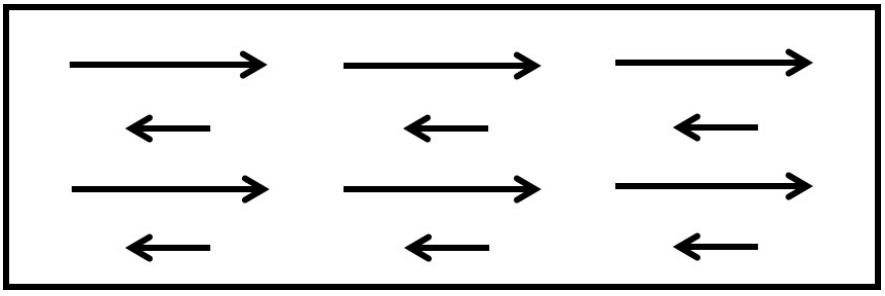

Figure 3.4: Ferrimagnetic material

3.3 Theoretical Concepts

3.3.1 Electromagnet

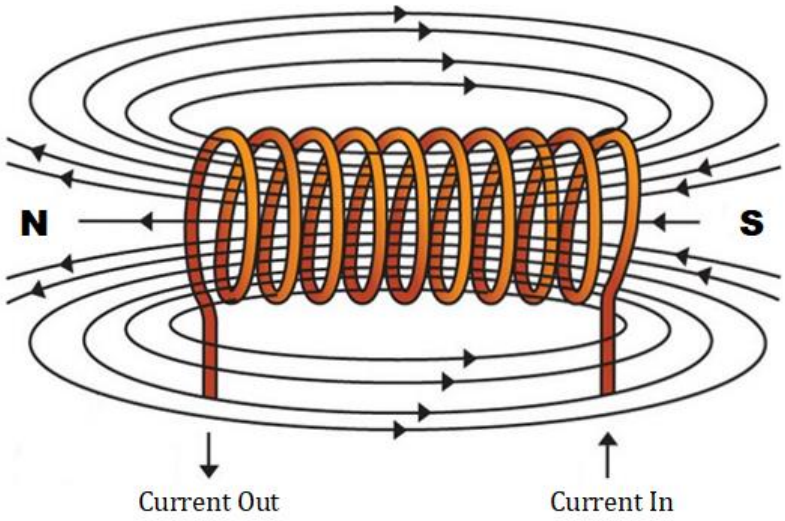

Figure 3.5: Electromagnet [95]

An electromagnet is a magnet that generates a magnetic field by using an electric current. When the current is switched off, the magnetic field vanishes. Electromagnets are typically made of wire twisted into a coil. A current flowing through the wire produces a magnetic field that is focused in the hole in the middle of the coil. The wire turns are frequently coiled around a magnetic core consisting of a ferromagnetic or ferrimagnetic material. The magnetic core concentrates the magnetic flux and creates a more powerful magnet. The north and south poles of an electromagnet are determined by the direction of current flow through the wires, as shown in Fig 3.5. The strength of an electromagnet may be increased by increasing the number of wire turns in the coil, increasing the current in the wire, and adding a magnetic material for the core.

The major benefit of an electromagnet over a permanent magnet is that the magnetic field may be altered quickly by varying the amount of electric current in the winding. In contrast to a permanent magnet, which does not require electricity, an electromagnet requires a constant source of current to sustain the magnetic field. Electromagnets are frequently utilized in different electrical devices such as loudspeakers, motors, electromechanical solenoids, generators, hard discs, relays, scientific instruments, MRI machines, and magnetic separation equipment. In industry, electromagnets are used to pick up and move heavy iron items such as scrap iron and steel.

3.3.2 Magnetic Phenomena

The magnetic field can be generated easily using a permanent magnet or a current-carrying electromagnetic coil. Magnetic behaviors are classified into three types based on their response to magnetic fields and the nature of the material: ferromagnetic, paramagnetic, and diamagnetic. Ferromagnetic materials are those that can be strongly attracted to and hold magnetization by a magnet. Paramagnetic materials are weakly attracted to magnets and can only be magnetized if an external magnetic field is introduced; if the field source is withdrawn, the magnetization is lost. Diamagnetic items are frequently repelled by both poles of a magnet because their susceptibility is typically negative or tiny enough to be regarded as insignificant. The susceptibility is a dimensionless quantity that quantifies the amount of magnetization that material has in response to a magnetic field.

Magnetophoresis

Magnetophoresis occurs when a combination of any two materials in an aqueous solution with varying susceptibilities is subjected to an external magnetic field. Because the two materials have varied abilities to retain magnetization, the material with higher susceptibility will experience stronger attraction and will align towards the magnetic field source. However, because of the relative attraction motion of the higher susceptibility material, the other material with lower susceptibility will be repelled in the displacement of the attracted material. As a result, depending on the apparent magnetic susceptibility of the target particle in its medium, the magnetic force might be either attractive or repulsive.

Positive Magnetophoresis

Positive magnetophoresis is the most widespread manipulation method and occurs when paramagnetic particles are suspended in a diamagnetic medium such as water. It enables paramagnetic particles to concentrate at magnetic field maxima, allowing for separation and mixing. Positive magnetophoresis can be used to manipulate and separate biological samples that have been labeled with magnetic beads as tags.

Negative Magnetophoresis

Negative magnetophoresis is a label-free method of dealing with diamagnetic particles using a paramagnetic carrier fluid. When diamagnetic particles are subjected to an external magnetic field gradient, the magnetic susceptibility mismatch between the diamagnetic particle and the paramagnetic medium produces a negative

magnetophoretic force that pushes the particles away from the magnet. In a paramagnetic medium, a diamagnetic particle flows towards the magnetic field minima. Diamagnetic particles can be manipulated, mixed, and separated in this manner.

3.4 Actuation System

3.4.1 Mathematical Model

The transport of magnetizable particles in a microfluidic system is governed by several factors including (a) the magnetic force, (b) hydrodynamic drag force, (c) particle/fluid interactions, (d) gravity, (e) buoyancy, (f) inertia, and (g) interparticle interactions. Considering Fe_3O_4 particles in a Y-shaped microchannel and the modeling parameters of MNP, microchannel and suspension fluid are shown in Table 3.1. The gravitational force on a Fe_3O_4 particle suspended in a fluid is given by

Table 3.1: Modeling parameters of MNP, microchannel and suspension fluid

Parameter	**Value**	**Unit**
Diameter of the channel	1	mm
Diameter of the MNP	250	nm
Fluid relative permeability	1	-
Fluid flow rate	.1	mL/min
Fluid viscosity	.001	$Pa.s$
Fluid density	1000	kgm^{-3}
Particle density	5000	kgm^{-3}

$$F_g = \rho_p V_p g, \tag{3.1}$$

where ρ_p is the density of Fe_3O_4, $V_p = \frac{4\pi}{3} R_p^3$ is the volume of Fe_3O_4 particle, R_p is the radius of the particle and g is the acceleration due to gravity. The buoyant force on a Fe_3O_4 particle suspended in fluid is given by

$$F_b = \rho_f V_f g, \tag{3.2}$$

where ρ_f is the density of fluid , $V_f = V_p$ is the volume of displaced fluid which is equal to the volume of Fe_3O_4 particle. The forces due to gravity and buoyancy are significantly smaller than the magnetic and fluidic forces. Thus, these forces can be neglected in our analysis. Similarly, the inertial force is also a second-order term and could be neglected. As for the other forces, we assume that we are dealing with dilute particle suspensions, for which inter-particle effects and particle-fluid interactions can also be neglected [96]. We further restrict the analysis to particles that are sufficiently large (diameter $\approx 250\,\text{nm}$) so that Brownian motion can be ignored. For example, Brownian motion of Fe_3O_4 particles in fluid is negligible when the particle diameter is greater than 40 nm [97]. However, the details of these computations are complicated and beyond the scope of this thesis work. To simplify the analysis, we consider particles in low concentration and neglect particle/fluid and interparticle interactions [98]. Also, we take into account only the dominant forces, viz. magnetic force and drag force and ignore all other forces, which are second order. All other forces are ignored, as they are much weaker than the dominant forces [75]. We consider that the MNPs flow in a Y-shaped bifurcating microfluidic channel, which mimics the *in vivo* blood vessel [99, 100], as shown in Fig. 3.6. The MNPs injected into the inlet channel are propelled by the hydrodynamic drag force (F_D), resulted due to the fluid flow in the channel. The drag force on the MNPs with radius R_p is given by Stokes drag force [101], [102],

$$\vec{F}_D = 6\pi\eta R_p(\vec{v}_f - \vec{v}_p), \tag{3.3}$$

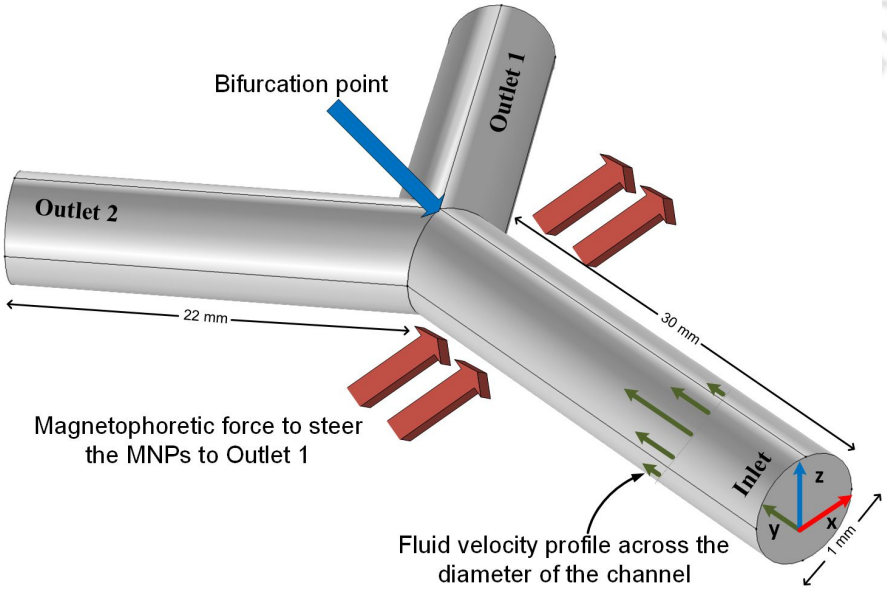

Figure 3.6: A 3D Y-shaped fluidic channel. Green arrows and red arrows represent the fluid velocity profile and applied magnetic field respectively.

where η is the fluid viscosity, v_f and v_p are fluid and particle velocity respectively. The MNPs injected into the inlet channel are propelled by the laminar flow, which shows a parabolic profile of fluid flow velocity. The fluidic force depends on the fluid velocity in the microchannel. The variation of a fully developed laminar flow along the x-axis with the flow velocity parallel to the y-axis, as represented in Fig. 3.6, is given by

$$v_f = 2\bar{v}_f \left(1 - \frac{x^2}{R_v^2}\right), \tag{3.4}$$

where $\bar{v}_f$ is the average fluid velocity and R_v is the radius of the microchannel. Considering the x-y plane and substituting (3.4) into (3.3), we obtain the fluidic force components

$$\begin{aligned} \vec{F}_{Dx} &= -6\pi\eta R_p \vec{v}_{px}, \\ \vec{F}_{Dy} &= -6\pi\eta R_p \left[\vec{v}_{py} - 2\bar{v}_f \left(1 - \frac{x^2}{R_v^2}\right)\right]. \end{aligned} \tag{3.5}$$

Due to this fluidic force, the MNPs are dragged along the direction of the fluid. In this analysis, we consider stabilized iron oxide (Fe_3O_4) as MNPs [103]. Meanwhile, at bifurcation points of the channel, the fluid flow will drag the MNPs to a random outlet. Therefore, an external guidance system is required to direct the MNPs, from the bifurcation point to the correct outlet. It is important to note that, while the hydrodynamic drag force drives the MNPs from the inlet to the target location, the guidance system is explicitly used at the bifurcation points to ensure that the MNPs are delivered through the desired outlet. We consider an EMA system, which produces magnetic force to steer the MNPs to a specific outlet. The basic building blocks of the EMA system, used for guiding the MNPs in a TDDS, are the circular coils carrying current. The wire turns and the current in the coils generate a magnetic field. This magnetic field along with its gradient produce a force, known as magnetophoretic force (F_{MAP}). The MNPs suspended in a viscous medium experience this force, F_{MAP}, as shown in Fig. 3.6, for guiding the MNPs to Outlet 1.

A first order approximated linear magnetization model with saturation is used to predict the magnetic force on MNP [104]. In free space, $m_{eff} = V_p M_p$, where M_p is the magnetization of the MMP with radius R_p and volume $V_p = \frac{4}{3}\pi R_p^3$. Note that M_p is a linear function of the field intensity ($M_p = \chi_p H_{in}$) up to a saturation value, beyond which it is constant. $H_{in} = H - H_{demag}$ is the field intensity inside the MMP, where $H_{demag} = \frac{M_p}{3}$ is the self demagnetization field intensity that opposes H [105]. The effective magnetic dipole moment, M_{eff}, of a spherical MNP, with radius R_p and permeability μ_p, suspended in a linear magnetizable

fluid of permeability μ_f is [93] given by

$$\begin{aligned} \vec{M}_{eff} &= 4\pi R_p^3 K(\mu_p, \mu_f)\vec{H}, \\ \text{where } K(\mu_p, \mu_f) &= \frac{\mu_p - \mu_f}{\mu_p + 2\mu_f}, \end{aligned} \tag{3.6}$$

such that K represents the strength of effective polarization of the MNPs and H is the strength of magnetic field produced by the EMA system. The magnetophoretic force exerted by a nonuniform magnetic field on an MNP is given by [93]

$$\begin{aligned} \vec{F}_{MAP} &= \mu_f(\vec{M}_{eff} \cdot \vec{\nabla})\vec{H} \\ &= 2\pi\mu_f R_p^3 \frac{\mu_p - \mu_f}{\mu_p + 2\mu_f}\vec{\nabla}\vec{H}^2, \\ \text{where } \vec{\nabla}\vec{H}^2 &= 2(\vec{H} \cdot \vec{\nabla})\vec{H}. \end{aligned} \tag{3.7}$$

Simplifying equation (3.7) in terms of magnetic susceptibility, we get

$$\vec{F}_{MAP} = 4\pi\mu_f R_p^3 \frac{(\chi_p - \chi_f)}{(\chi_p - \chi_f) + 3(\chi_f + 1)}(\vec{H} \cdot \nabla)\vec{H}. \tag{3.8}$$

Here, $\chi_p = \frac{\mu_p}{\mu_0} - 1$ and μ_p are the magnetic susceptibility and permeability of the particles, respectively. $\chi_f = \frac{\mu_f}{\mu_0} - 1$ and μ_f are the susceptibility and permeability of the carrier liquid, respectively. Considering $\chi_f << 1(\mu_f = \mu_0)$, equation (3.8) reduces to

$$\vec{F}_{MAP} = 4\pi\mu_f R_p^3 \frac{(\chi_p - \chi_f)}{(\chi_p - \chi_f) + 3}(\vec{H} \cdot \nabla)\vec{H}. \tag{3.9}$$

Therefore, equation (3.9) clearly shows the dependency of magnetophoretic force on radius of the particles.

The movement of the MNPs depends on the direction and magnitude of F_{MAP} and the direction of F_{MAP} depends on the direction of the magnetic field gradient. From the above discussion, it may be noted that the major forces experienced by the MNPs injected in a fluidic channel are hydrodynamic drag force and magnetic force [106]. Hence, to steer the MNPs to a specific outlet in the channel, F_{MAP}, generated by electromagnetic coils, is applied orthogonal to the direction of F_D, as shown in Fig. 3.6. Therefore, the total force, F, acting on the MNPs can be expressed as

$$\vec{F} = \vec{F}_{MAP} + \vec{F}_D. \tag{3.10}$$

The transport of MNPs in a microfluidic system can be predicted using Newton's

second law of motion,

$$m_p \frac{d\vec{v}_p}{dt} = \vec{F}_{MAP} + \vec{F}_D. \tag{3.11}$$

Where, m_p and v_p are the mass and velocity of the MNPs. Although the inertial term $m_p \frac{d\vec{v}_p}{dt}$ could be ignored due to its small value, we still consider its effect in our analysis to obtain more accurate MNP trajectories.

The equations of MNPs trajectory under the influence of both magnetic and fluidic force can be written in component form by substituting (3.5) and (3.9)) into (3.11) as follows:

$$v_{px}(t) = \frac{dx}{dt}, \tag{3.12}$$

$$m_p \frac{d\vec{v}_{px}}{dt} = \mu_0 V_p \frac{3(\chi_p - \chi_f)}{(\chi_p - \chi_f) + 3} \vec{H} \frac{d\vec{H}}{dx} - 6\pi\eta R_p \vec{v}_{px}, \tag{3.13}$$

$$v_{py}(t) = \frac{dy}{dt}, \tag{3.14}$$

$$m_p \frac{d\vec{v}_{py}}{dt} = -6\pi\eta R_p \left[\vec{v}_{py} - 2\bar{v}_f \left(1 - \frac{x^2}{R_v^2} \right) \right]. \tag{3.15}$$

Equations (3.12) - (3.15) represent a coupled system of first order differential equations, which are solved subject to initial conditions for $x(0)$, $y(0)$, $v_{px}(0)$ and $v_{py}(0)$. These equations can be solved numerically using various techniques such as the Runge-Kutta method [97]. Precisely, by solving equations (3.12) and (3.13) with initial condition $x(0) = 0$ and $v_{px}(0) = 0$, we obtain the solution of t at $x(t) = 1$ ($\hat{t}$, say). Now, we solve (3.14) and (3.15) using $\hat{t}$ with $y(0) = 0$ and $v_{py}(0) = 0$, to obtain the solution $y(\hat{t})$.

The fluid flow in a channel shows the parabolic velocity profile [87] with a maximum value at the center of the channel and F_D is proportional to the fluid flow velocity (3.3). Precisely, F_D decreases when traversed from the center to the sidewalls along a line segment in the channel. Thus, the minimum value of F_{MAP} must be greater than the maximum value of F_D for steering the MNPs to the desired channel. Therefore, $F_{MAP} >> F_D$ near the sidewalls as compared to the center of the channel. Due to this, the MNPs adhere to the channel walls at the bifurcation points. This problem is known as *Stiction Issue* of MNPs in this type of TDDS [87]. This sticking phenomenon reduces the efficiency of the actuation system for navigating the particles to the desired outlet. Therefore, we need a mechanism to free the particles from the channel walls.

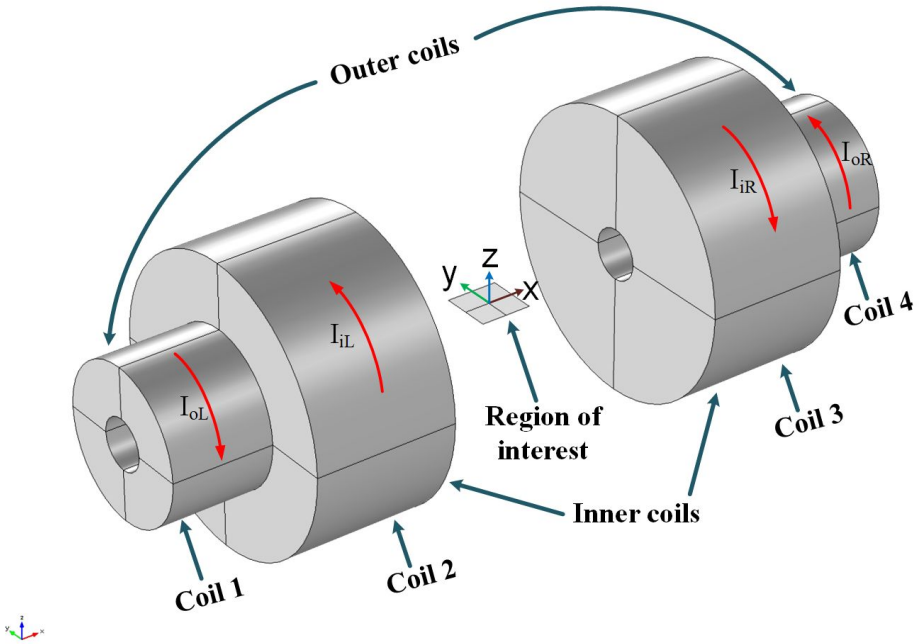

Figure 3.7: 3D view of the proposed EMA system

3.4.2 Proposed Design

In view of a simpler simulation and experimental framework, we design an EMA system considering the guidance of MNPs along a single axis (x axis) of the channel. The system comprises of four circular current carrying coils, as illustrated using 3D view in Fig. 3.7. The position and structural parameters of the two outer and two inner coils are identical and symmetric about the y-axis, as shown using XY cross-sectional view in Fig. 3.8. We consider a square cross-section of length S_l, symmetric about the origin in the $x-y$ plane, as the region of interest. The width and height of inner and outer coils are w_i, h_i, w_o and h_o respectively. The current flowing in Coil 1, Coil 2, Coil 3 and Coil 4 are represented as I_{oL}, I_{iL}, I_{iR} and I_{oR} respectively. The direction of current in each coil depicted using red arrows in Fig. 3.7 and Fig. 3.8, are such that it produces a positive magnetic field gradient along the x-axis. Fig 3.8 shows an actuation system for the line segment along the x-axis. To reduce structural complexities and for ease of data analysis, we consider one-dimensional steering of MNPs along the x-axis in the proposed work. Hence, the arrangement of electromagnetic coils is done in such a way that it can exert magnetic force only along the direction of x-axis. However, a real-time TDDS requires a three dimensional steering mechanism. Hence, a real-time system will require an arrangement of another 8 coils (4 along y-axis and 4 along z-axis), which are symmetric to the 4 coils considered in this work. Thus, to accommodate

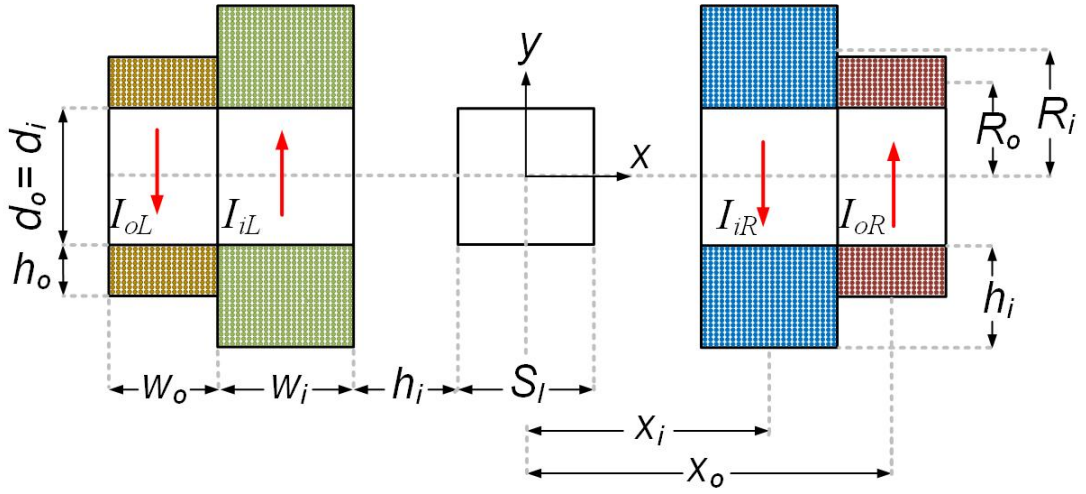

Figure 3.8: XY cross-sectional view of the proposed EMA system

the remaining coils in a symmetric fashion along the other two dimensions, while avoiding the overlapping of the coils, we need to have a minimum gap of inner coil height h_i in between the inner coil and the region of interest. For the sake of clarity, two dimensional system for two line segments along the x-axis and y-axis is shown in Fig. 3.9.

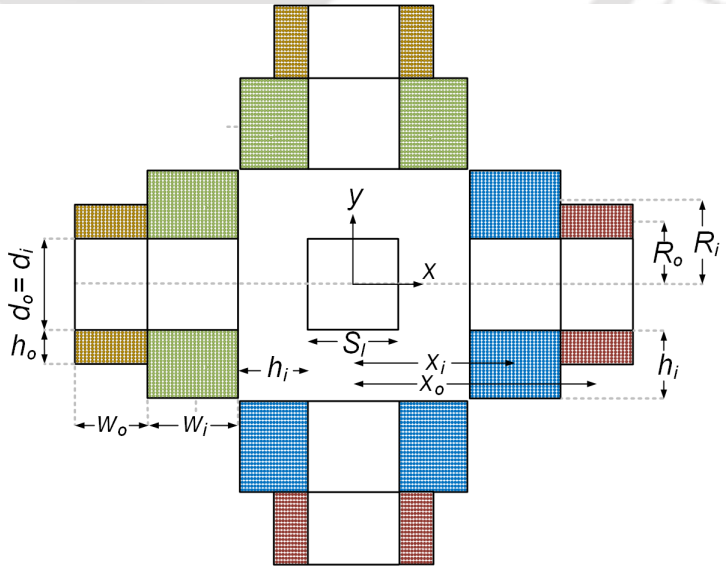

Figure 3.9: XY cross-sectional view of EMA system for steering both in X and Y direction.

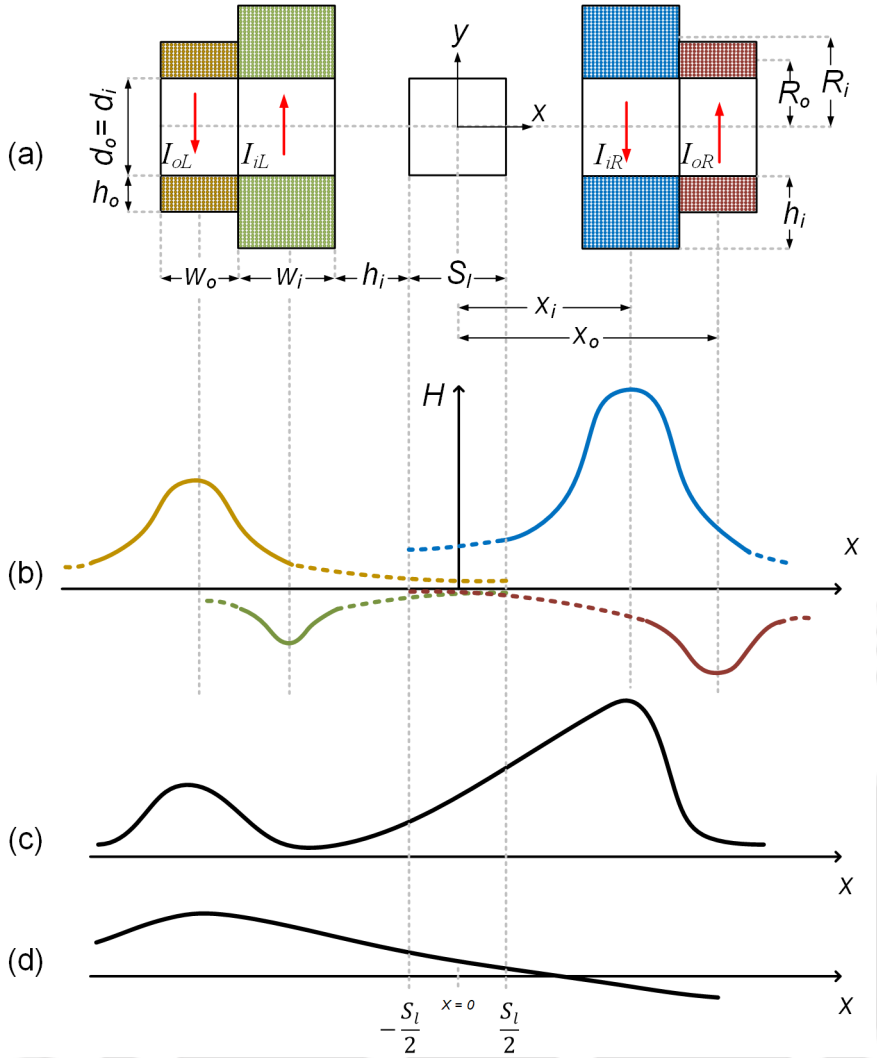

Figure 3.10: Qualitative illustration of nature of magnetic field strength with respect to coil parameters (H and ∇H positive in the region of interest for steering the MNPs): (a) XY cross-sectional view of EMA system with a region of interest represented by a square of side length S_l, (b) magnetic field strength produced by each coil without superposition, (c) resultant magnetic field strength produced by EMA after superposition and (d) resultant magnetic field strength produced by only outer two coils.

Fig. 3.10 plot represent a qualitative analysis of the desired magnetic field, required to be produced by the proposed system for steering, while overcoming the sticking phenomenon of MNPs. The direction of current in each coil depicted using red arrows in Fig. 3.7. This implies that Coil 1 and Coil 3 produce a positive magnetic field strength, while Coil 2 and Coil 4 produce a negative magnetic field strength, as shown in Fig. 3.10b. Now, for steering the MNPs along the positive x-axis, the resultant magnetic field strength and its gradient should be positive along the region of interest, as shown in Fig. 3.10c. Also, to mitigate the stiction issue of MNPs, it is desirable to have a positive magnetic field strength and negative

gradient, as shown in Fig. 3.10d. To achieve these objectives, we design the coil parameters elaborated as follows. The magnetic field strength produced by each coil as shown in Fig. 3.10b is expressed as:

$$\begin{aligned} H_{Coil\ 1} &= \frac{N_o I_{oL} R_o^2}{2[(x+x_o)^2 + R_o^2]^{3/2}}, \\ H_{Coil\ 2} &= -\frac{N_i I_{iL} R_i^2}{2[(x+x_i)^2 + R_i^2]^{3/2}}, \\ H_{Coil\ 3} &= \frac{N_i I_{iR} R_i^2}{2[(x-x_i)^2 + R_i^2]^{3/2}}, \\ H_{Coil\ 4} &= -\frac{N_o I_{oR} R_o^2}{2[(x-x_o)^2 + R_o^2]^{3/2}}, \end{aligned} \tag{3.16}$$

where, x_i & x_o, R_i & R_o are the mean distance from the origin and the effective radius of the inner & outer coils respectively. The number of wire turns for the coils are expressed as

$$\begin{aligned} N_i &= \frac{k_w w_i h_i}{{d_w}^2}, \\ N_o &= \frac{k_w w_o h_o}{{d_w}^2}, \end{aligned} \tag{3.17}$$

where k_w is the coil winding factor of the round wires of diameter $d_w = 1.02\,\text{mm}$ and $k_w = \frac{\pi}{4}$. The distance of the coils from the origin are given by

$$\begin{aligned} x_i &= \frac{S_l}{2} + h_i + \frac{w_i}{2}, \\ x_o &= \frac{S_l}{2} + h_i + w_i + \frac{w_o}{2}, \end{aligned} \tag{3.18}$$

The radius of the coils are defined as

$$\begin{aligned} R_i &= \frac{d_i + h_i}{2}, \\ R_o &= \frac{d_o + h_o}{2}. \end{aligned} \tag{3.19}$$

Fig. 3.10c shows the resultant magnetic field strength produced by the proposed EMA system, which is the vector sum of the fields due to each circular coil and is

expressed as

$$H = \frac{N_o I_{oL} R_o^2}{2[(x+x_o)^2 + R_o^2]^{3/2}} - \frac{N_i I_{iL} R_i^2}{2[(x+x_i)^2 + R_i^2]^{3/2}} + \frac{N_i I_{iR} R_i^2}{2[(x-x_i)^2 + R_i^2]^{3/2}} - \frac{N_o I_{oR} R_o^2}{2[(x-x_o)^2 + R_o^2]^{3/2}}. \tag{3.20}$$

Fig. 3.10d shows the resultant magnetic field strength produced by only outer two coils (Coil 1 and Coil 4) and is expressed as

$$H = \frac{N_o I_{oL} R_o^2}{2[(x+x_o)^2 + R_o^2]^{3/2}} - \frac{N_o I_{oR} R_o^2}{2[(x-x_o)^2 + R_o^2]^{3/2}}. \tag{3.21}$$

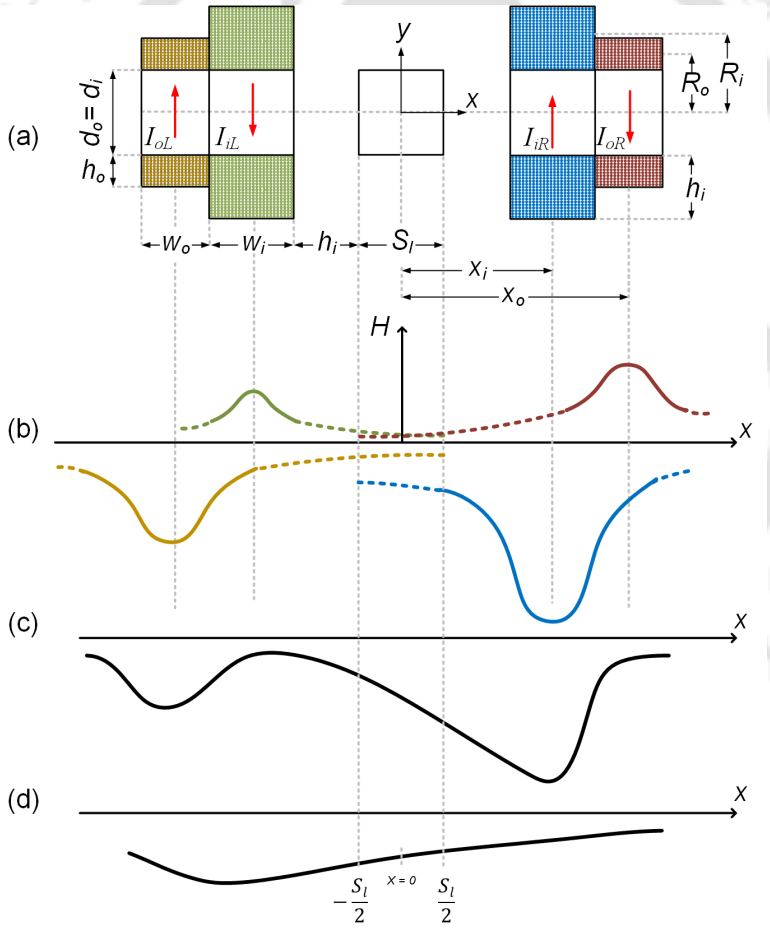

Figure 3.11: Qualitative illustration of nature of magnetic field strength with respect to coil parameters (H and ∇H negative in the region of interest for steering the MNPs): (a) XY cross-sectional view of EMA system with a region of interest represented by a square of side length S_l, (b) magnetic field strength produced by each coil without superposition, (c) resultant magnetic field strength produced by EMA after superposition and (d) resultant magnetic field strength produced by only outer two coils.

The F_{MAP} applied for steering the MNPs to Outlet 1 should be directed along the positive x axis. Therefore, from (3.9), it is clear that the actuation system should be designed in such a way that it generates a positive gradient magnetic field along the x-axis. In the subsequent section, we consider optimizing the coil parameters of our proposed design, such that the desired magnetic field is obtained.

3.5 Optimization of EMA System

In the proposed EMA system, a 2-D square area of length S_l in xy plane with center at the origin is considered as a region of interest for manipulating magnetic particles, as shown in Fig. 3.8. To reduce the geometrical complexities, we consider that the inner diameters of the inner and outer coils are the same, i.e., $d_i = d_o = 40$ mm. Now, the geometry of the coils, i.e., w_i, h_i, w_o, h_o and the magnitude of supply currents, i.e., I_{iL}, I_{iR}, I_{oL} and I_{oR} should be chosen such that the resultant field follows the same trajectory in the region of interest, as shown in Fig. 3.10c. Keeping this in mind, the coil parameters are optimized such that H has the maximum value at $\frac{S_l}{2}$, provided both the magnitude and the gradient of H are positive $\forall x \in [-\frac{S_l}{2}, \frac{S_l}{2}]$. Furthermore, for practical feasibility, the physical parameters of the coil and the power supply are limited by upper and lower bounds. The optimization framework with coil parameters as design variables is described in **P1** (3.23) and the range of the design variables are as follows:

$$\begin{aligned}
20 \leqslant w_i \leqslant 100\,\text{mm} \\
20 \leqslant h_i \leqslant 100\,\text{mm} \\
20 \leqslant w_o \leqslant 100\,\text{mm} \\
20 \leqslant h_o \leqslant 100\,\text{mm} \\
0 \leqslant I_{iL} \leqslant 15\,\text{A} \\
0 \leqslant I_{iR} \leqslant 15\,\text{A} \\
0 \leqslant I_{oL} \leqslant 15\,\text{A} \\
0 \leqslant I_{oR} \leqslant 15\,\text{A}.
\end{aligned} \tag{3.22}$$

$$\mathbf{P1}: \max_{\substack{w_i,h_i,w_o,h_o \\ I_{iL},I_{iR},I_{oL},I_{oR}}} H = \Bigg[\frac{N_o I_{oL} R_o^2}{2[(x+x_o)^2+R_o^2]^{3/2}} - \frac{N_i I_{iL} R_i^2}{2[(x+x_i)^2+R_i^2]^{3/2}} + \frac{N_i I_{iR} R_i^2}{2[(x-x_i)^2+R_i^2]^{3/2}} - \frac{N_o I_{oR} R_o^2}{2[(x-x_o)^2+R_o^2]^{3/2}}\Bigg]_{x=\frac{S_l}{2}}$$
$$\text{subject to:} H > 0$$
$$\nabla H > 0 for -S_l/2 \leq x \leq S_l/2$$
$$20\,\text{mm} \leq [w_i, w_o, h_i, h_o] \leq 100\,\text{mm}$$
$$0 \leq [I_{iL}, I_{iR}, I_{oL}, I_{oR}] \leq 15\,\text{A} \tag{3.23}$$

Furthermore, the optimization problem **P1** can also be solved by considering both H and ∇H are negative, which would require the coil current to be in the reverse direction as compared to that in our proposed coil arrangement with H and ∇H as positive, as shown in Fig. 3.11 (a). Note that our optimization problem is designed based on the nature of the resultant magnetic field produced by the four coils as shown in Fig. 3.11c. The coil parameters are optimized such that H has the minimum value at $\frac{S_l}{2}$, provided both the magnitude and the gradient of H are negative $\forall x \in [-\frac{S_l}{2}, \frac{S_l}{2}]$. Clearly, the optimization framework with negative H and

Algorithm 1 Steps for Solving **P1**

1: **Initialization**: Choose w_i^0, h_i^0, w_i^0, h_o^0, I_{iL}^0, I_{iR}^0, I_{oL}^0 and I_{oR}^0, such that they lie in the feasible range as specified in (3.23); Iteration index $q = 0$, Error tolerance $\zeta = 10^{-5}$
2: **repeat**
3: **Input**: w_i^q, h_i^q, w_i^q, h_o^q, I_{iL}^q, I_{iR}^q, I_{oL}^q and I_{oR}^q
4: Solve H^q using coordinate search method [107]
5: **if** $H^q - H^{q-1} < \zeta$ **then**
6: Convergence = **TRUE**;
7: **else**
8: Convergence = **FALSE**, q=q+1;
9: **end if**
10: **until** Convergence = **TRUE**
11: **Output**: $w_i^* = w_i^q$, $h_i^* = h_i^q$, $w_i^* = w_i^q$, $h_o^* = h_o^q$, $I_{iL}^* = I_{iL}^q$, $I_{iR}^* = I_{iR}^q$, $I_{oL}^* = I_{oL}^q$ and $I_{oR}^* = I_{oR}^q$

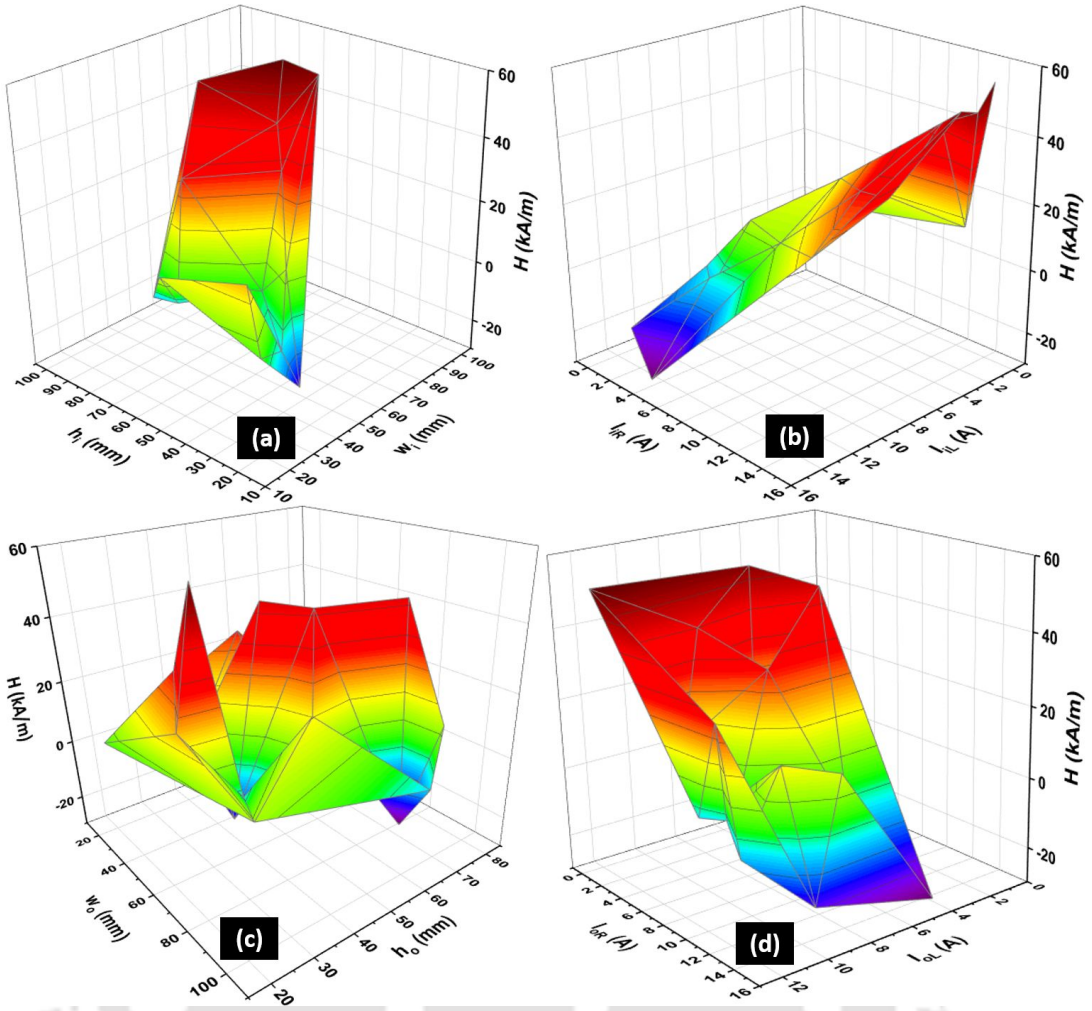

Figure 3.12: Variation of H vs following coil design parameters: (a) w_i and h_i, (b) I_{iL} and I_{iR}, (c) w_o and h_o, (b) I_{oL} and I_{oR}.

∇H would require changing the current constraints in reverse direction. In this work, we consider $H > 0$ and $\nabla H > 0$ as design constraint, which would steer the MNPs to correct outlet. To satisfy the above constraint, we design the coil arrangement and current directions of each coil in such a way that the nature of magnetic field strength H of each coil yields a positive resultant magnetic field in the region of interest ($H > 0$), as shown in Fig.3.10c. Now, the requirement for optimization of the coil parameters in the proposed arrangement arises so as to yield adequate F_{MAP} required for steering the MNPs. Since, H is monotonically increasing from $-S_l/2$ to $S_l/2$, it is obvious that maximizing the value of H at $S_l/2$ would also yield maximum ∇H, thus result in a high F_{MAP}. Hence, the constrained optimization problem **P1** is mathematically designed so as to attain the maximum value of H at $S_l/2$, which in turn, maximizes the slope of H, i.e. ∇H in the region of interest. Although a quick glance at **P1** conveys that the objective is to maximize H, we would like to reiterate that our entire optimization

Table 3.2: Optimal values of coil parameters using positive H and ∇H constraint

w_i (mm)	h_i (mm)	w_o (mm)	h_o (mm)	I_{oL} (A)	I_{iL} (A)	I_{iR} (A)	I_{oR} (A)
84.54	68.64	59.7	30.1	13.88	0.523	14.38	3.7

Table 3.3: Optimal values of coil parameters using negative H and ∇H constraint

w_i (mm)	h_i (mm)	w_o (mm)	h_o (mm)	I_{oL} (A)	I_{iL} (A)	I_{iR} (A)	I_{oR} (A)
84.54	68.64	59.7	30.1	-13.88	-0.523	-14.38	-3.7

framework is directly dependent on the nature of H obtained from the predefined coil arrangement as shown in Fig. 3.10 and the end goal is to obtain maximum ∇H in Mode 1. The solution of the problem **P1** is obtained using the co-ordinate search method [107], whereby the coil parameter values are iteratively updated till convergence using Algorithm 1. The coil parameters obtained at the convergence of Algorithm 1, denoted by z_j^*, where $z = \{w, h, I\}$ and $j = \{i, o, iR, iL, oR, oL\}$, are chosen for designing our proposed actuation system. The optimization problem **P1** is described in (3.23).

Fig 3.12 shows variation of H with respect to the design variables in **P1**, obtained from the intermediate steps of Algorithm 1. Clearly, the maximum value of H for the given framework **P1** is attained and the corresponding values of the design parameters are presented in Table 3.2. A comparison of optimization problems solved using H and ∇H as positive and H and ∇H as negative are presented in Table 3.2 and Table 3.3 respectively.

3.6 Results and Discussions

In this section, we verify the optimized coil properties using finite element analysis (FEA) simulation. The Simulation analyses are done using AC/DC and Partial Differential Equation (PDE) interfaces module of COMSOL in steady state, to evaluate the magnetic field, magnetic gradient and magnetophoretic force produced by the proposed coil topology. Here, we use the optimized values of coil parametrs, as shown in Table 3.2. In Fig. 3.13, the variation of magnetic field (B) and field gradient (∇B) are plotted. It may be observed from Fig. 3.13a & 3.13b that the

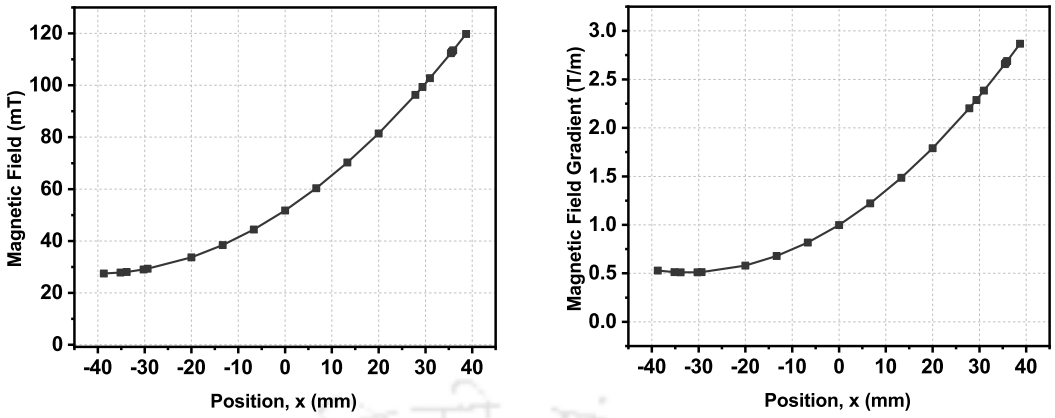

(a) (b)

Figure 3.13: Variation of (a) magnetic field and (b) magnetic gradient, in the region of interest along the x-axis.

magnetic field, B and its gradient ∇B is positive. Acute static magnetic field effects, such as nausea, vertigo, a metallic taste, and phosphenes can be induced in magnetic fields greater than 2 T. Adverse critical responses do not occur at magnetic fields less than 2 T [108].

It may be noted that F_{MAP} experienced by the MNPs in a fluidic channel is proportional to the particle volume [93]. Considering the diameter (R_p) of the MNP is 250 nm. Now, by using the values of B and ∇B as well as the value of R_p, it is clear from (3.9) that a positive F_{MAP} is produced to steer the MNPs. Fig. 3.14 shows the simulation result of our proposed system. It can be clearly seen that the positive B and ∇B produces a positive F_{MAP} for steering the MNPs.

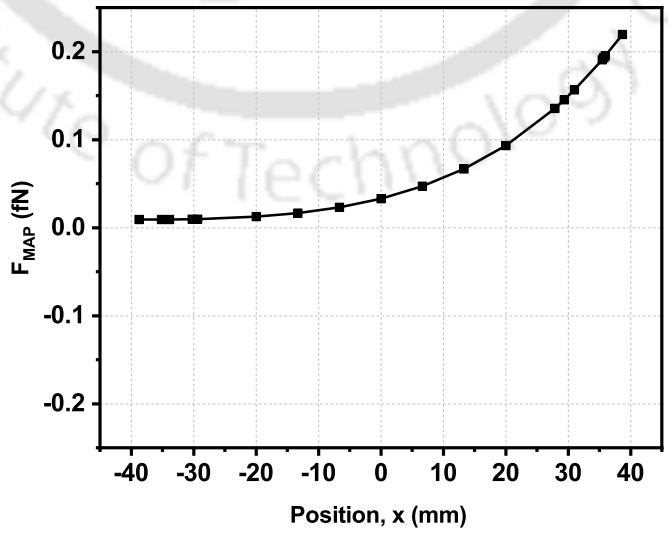

Figure 3.14: Variation of magnetophoretic force in the region of interest along the x-axis

This force F_{MAP} is mainly responsible to steer the MNPs to the desired location.

3.7 Chapter Summary

In TDDS, it is critical to focus MNPs deep into the body. The proposed concept was optimized within the constraints of the available resources by employing an optimum approach and commercially accessible software. The proposed design's theory, modeling descriptions, and simulation results were provided. The findings show that the suggested EMA system is capable of steering MNPs. Because of the basic coil construction and simple guidance system, this technique has a high practical application. This chapter investigates the design of an electromagnetic system to steer the magnetic nanoparticles in the desired direction for targeted drug delivery. We have also optimized the coil parameters. The system comprises of four coils, where all the four coils are operated simultaneously to produce a sufficient magnetophoretic force, which steers the MNPs. In conclusion, we propose a new design of an electromagnetic actuator for navigating the MNPs in a targeted drug delivery system with enhanced accuracy of steering the drug to the desired location.

Chapter 4

Stiction Mitigation and Disaggregation of Magnetic Particles in TDDS

Contents

4.1 Introduction 52
4.2 System Model 54
4.3 Simulation Framework 58
4.4 Results and Discussions 58
4.5 Chapter Summary 63

4.1 Introduction

Targeted Drug Delivery is a technique whereby drug loaded MNPs in the microfluidic channel are navigated to the target location under the influence of an external magnetic field [90, 100]. More precisely, the MNPs are injected into the inlet of a Y-shaped bifurcating microfluidic channel. From the injection point, the MNPs are propelled by the fluidic force, resulting from the laminar flow of fluid in the microchannel. To steer the MNPs to the target outlet, an external magnetic field is applied, which produces a magnetic force orthogonal to the direction of the fluidic force. The parabolic profile of fluid flow velocity results in the dominance of magnetic force over fluidic force at side-walls of the channel. This results in aggregation and stiction of MNPs to the inner walls of the channel.

Several actuation methodologies are proposed in the open literature to mitigate the stiction and aggregation problem of MNPs [87, 89, 109]. The concept of a functionalized magnetic field is proposed in [87, 109], whereby a time-varying multiplier function reverses the direction of magnetic force in alternate time slots for steering and detaching the MNPs, respectively. In these works, it is observed that the magnitude of the force exerted for steering the MNPs is the same as that during pull back operation of the stuck MNPs. However, pulling back the MNPs with such high force may cause some MNPs to cross over to the wrong direction, thus leading to a reduction of navigation efficiency. To address this issue, a discontinuous asymmetrical field function is applied in [89], whereby the stuck MNPs are detached with a much lower magnetic force, as compared to that for steering. Specifically, the scheme uses three different time slots, the first two being used for steering and stiction removal, while the third time slot comprises of a null magnetic field intended for disaggregation of the MNPs. However, it may be noted that during the null slot, there will be no control of the actuation system over the MNPs. This may lead to the random propulsion of MNPs to the undesired outlet along with the fluid flow.

Motivated by the above works, we present a time-varying magnetic field (TVMF) for effective steering of MNPs to the correct outlet of the bifurcated channel, while taking into account the stiction and aggregation of MNPs during navigation operation. Specifically, we emphasize on the fact that, in contrast to [89], the stiction removal and disaggregation of MNPs can be achieved in a single time slot by adjusting both the magnetic force as well as the slot duration. The TVMF operates by switching between two modes of operation viz, (i) Mode 1 and (ii) Mode 2. In Mode 1, the TVMF is applied for a certain duration so as to facilitate steering of the MNPs towards the target outlet. During this process, some MNPs which

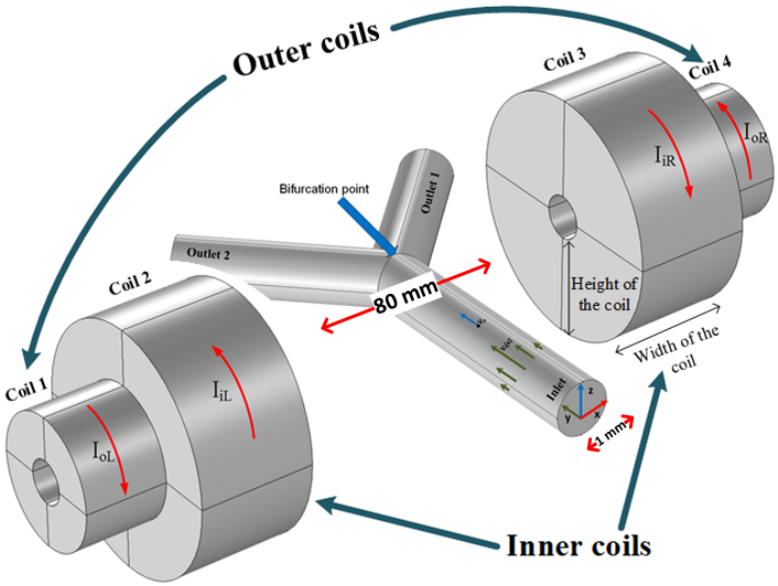

Figure 4.1: 3D view of the electromagnetic actuation system and Y-shaped fluidic channel.

aggregate and get stuck to the side-walls are released by applying the TVMF in the reverse direction to that in Mode 1. The magnetic force resulting from the TVMF in Mode 2 has a small magnitude, which can release the stuck MNPs at side-walls but cannot steer them into the incorrect outlet. Furthermore, the fluidic force dominates over this small magnetic force as the MNPs are pulled back from the side walls (due to the former's parabolic nature), thereby minimizing the aggregation of MNPs. However, the influence of fluid force could result in a random flow of MNPs in the channel. Hence, the duration for applying TVMF in Mode 2 has to be adjusted in such a way that the MNPs are confined within the desired region of interest. This work aims to analyze the coupling of applied magnetic field and switching time for effective navigation of MNPs in the channel. Simulation results are presented to highlight the optimal switching time with respect to the applied magnetic field, which is required to obtain the desired particle trajectory.

Table 4.1: Coil parameters of the proposed EMA system

w_i (mm)	h_i (mm)	w_o (mm)	h_o (mm)	I_{oL} (A)	I_{iL} (A)	I_{iR} (A)	I_{oR} (A)
84.54	68.64	59.7	30.1	13.88	0.523	14.38	3.7

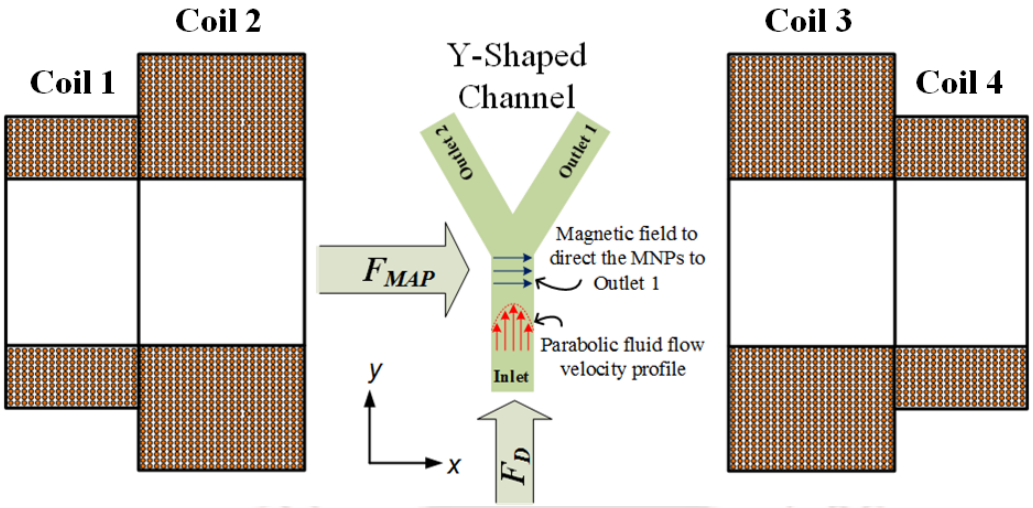

Figure 4.2: XY cross-sectional view of proposed EMA system and Y-shaped channel.

4.2 System Model

We consider a four coils electromagnetic actuation system as shown in the 3D view Fig. 4.1, for navigating the MNPs in a Y-shaped fluidic channel. The position and structural parameters of the two outer and two inner coils are identical and symmetric about the y-axis and the current flowing in Coil 1, Coil 2, Coil 3 and Coil 4 are represented as I_{oL}, I_{iL}, I_{iR} and I_{oR} respectively, as shown in Fig. 4.1. The XY cross-sectional view of the EMA system producing F_{MAP} perpendicular to F_D acting in the fluid flowing in the Y-shaped microchannel as shown in Fig 4.2.

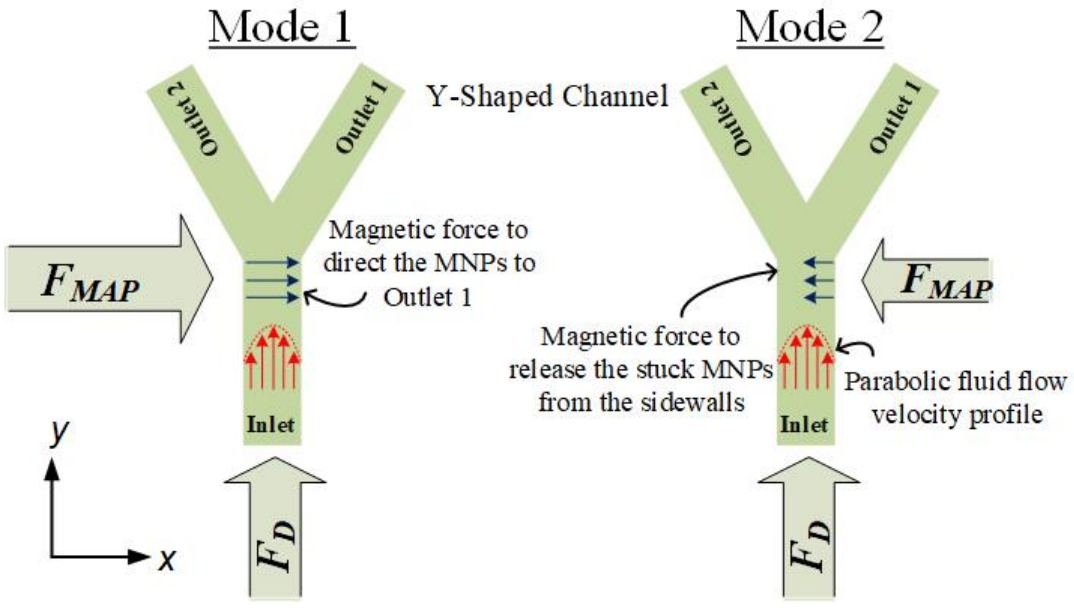

Figure 4.3: XY cross-sectional view of Y-shaped channel in Mode 1 and Mode 2.

The coil parameters are presented in Table 3.2.

4.2.1 Stiction Issue and Aggregation

The EMA system designed using the coil parameters presented in Table 3.2 produces a gradient magnetic field along the x axis, to steer the MNPs to Outlet 1. The MNPs injected into the inlet of the channel are propelled by F_D, they are steered to Outlet 1 by F_{MAP} applied orthogonal to F_D at the bifurcation point. Now, the positive gradient magnetic field produced by our proposed EMA system, results in an increasing F_{MAP} along the x axis (3.7). This, coupled with the parabolic nature of fluid flow, causes dominance of F_{MAP} over F_D i.e., $F_{MAP} >> F_D$, at the inner sidewalls adjacent to Outlet 1. This leads to the stiction of MNPs to the inner sidewalls of the channel, along the direction of magnetic force. Therefore we need a mechanism to ensure that the stuck MNPs are released from the sidewalls and directed to Outlet 1.

The proposed EMA system operates in two modes: (i) Mode 1, where all the four coils operate simultaneously to steer the MNPs to Outlet 1, (ii) Mode 2, where Coil 2 and Coil 3 are powered OFF and only Coil 1 and Coil 4 are active as described in Section 3.4.2. This results in a magnetic force (F_{MAP}) in opposite direction as compared to Mode 1 as shown in Fig. 4.3 (arrow lines). While F_{MAP} dominates over F_D in Mode 1, F_{MAP} produced in Mode 2 is much lower in magnitude than that in Mode 1. This results in dominance of F_D over F_{MAP} in Mode 2, which, in turn, helps to detach the stuck MNPs from the side-walls and also minimizes the aggregation of MNPs under the influence of dominant fluidic force [89]. Fig. 3.10d illustrates a scenario where the magnetic field strength is positive and monotonically decreasing in the region of interest. Thus, it follows that the gradient of the magnetic field strength is negative. Therefore, a negative F_{MAP} is produced along $-x$ axis, which facilitates to pull back the MNPs from the sidewalls. It is important to note that the magnitude of F_{MAP} produced in this case should be small, so that the MNPs are not steered to Outlet 2. Now, using the values of coil parameters presented in Table 3.2, it is seen from (3.17) that the number of turns for the outer coil is approximately three times lower than that of the inner coils. Therefore, the magnetic field produced by the outer coils when used in a standalone fashion, is much lower than that when both inner and outer coils are simultaneously active. Hence, the outer coils facilitate to demagnetize the MNPs at the sidewalls. Furthermore, the gradient of H is negative when only the outer coils operate, as shown in Fig. 3.10d. Thus, by switching OFF the inner coils for a certain period of time, the proposed EMA system can separate the MNPs stuck to the sidewalls with a very small F_{MAP}. The operation of the complete

system combining both steering and demagnetization of MNPs is described in the next subsection.

4.2.2 Working Principle

The proposed EMA system in Fig. 4.1, operates by switching between two modes of operation as follows: (i) Mode 1 for steering of MNPs and (ii) Mode 2 for demagnetization of the stuck MNPs.

- *Mode 1*: In this mode, all the four coils of the EMA system are powered ON to steer the MNPs to Outlet 1, as shown in Fig. 4.2. It produces a monotonically increasing magnetic field strength along the positive x axis, which results in a positive F_{MAP} with respect to x and orthogonal to the direction of F_D at the bifurcation point of the Y-channel. Thus, in this mode

$$H > 0,\ \nabla H > 0,\ F_{MAP} > 0,\ F_{MAP} > F_D.$$

  In this process, some of the MNPs flowing in the channel adhere to the sidewalls.

- *Mode 2*: In this mode, the inner coils are powered OFF and only the outer coils are active. The outer coils produce a positive magnetic field strength and a negative field gradient, which results in a negative F_{MAP}. Moreover, the magnitude of the magnetic force in Mode 2 (F_{MAP}^{Mode2}) is much lower than that in Mode 1 (F_{MAP}^{Mode1}), which ensures that the demagnetized MNPs move forward with the drag force and do not get steered to the undesired outlet. Thus, in this mode

$$H > 0,\ \nabla H < 0,\ F_{MAP} < 0,\ F_{MAP}^{Mode2} << F_{MAP}^{Mode1}.$$

This cycle is being repeated throughout the actuation mechanism. Thus, by adopting a switching mechanism to modulate the magnetophoretic force, the proposed EMA system can efficiently resolve the stiction issue.

To address the aggregation issue of MNPs in the microfluidic channel, we propose a time-varying magnetic field (TVMF) for effective steering of MNPs to the correct outlet of the bifurcated channel, while taking into account the stiction and aggregation of MNPs during navigation operation. Specifically, we put emphasis on the fact that, in contrast to [89], the stiction removal and disaggregation of MNPs can be achieved in a single time slot by adjusting both the magnetic force as well as the slot duration.

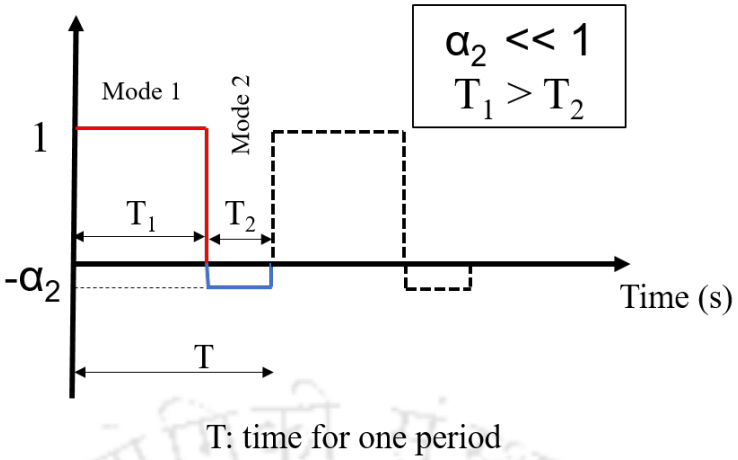

Figure 4.4: Qualitative illustration of the nature of magnetophoretic force vs time.

Fig 4.4 shows a qualitative illustration of the nature of magnetophoretic force resulting from the proposed TVMF. Our proposed TVMF operates by switching between two modes of operation viz, (i) Mode 1 and (ii) Mode 2, as shown in Fig 4.4. Here, T_{ON} and T_{OFF} are the ON and OFF time of the switch operated in Mode 1 and Mode 2 respectively. In Mode 1, the TVMF is applied for a certain duration so as to facilitate the steering of the MNPs towards the target outlet. During this process, some MNPs which aggregate and get stuck to the side-walls are released by applying the TVMF in the reverse direction to that in Mode 1. The magnetic force resulting from the TVMF in Mode 2 has a small magnitude, which can release the stuck MNPs at side-walls but cannot steer them into incorrect outlet. Furthermore, the fluidic force dominates over this small magnetic force as the MNPs are pulled back from the side walls (due to the former's parabolic nature), thereby minimizing the aggregation of MNPs. However, the influence of fluid force could result in random flow of MNPs in the channel. Hence, the duration for applying TVMF in Mode 2 has to be adjusted in such a way that the MNPs are confined within the desired region of interest. This work aims to analyse the coupling of applied magnetic field and switching time for effective navigation of MNPs in the channel. Extensive simulations are performed to find the optimal switching time with respect to the applied magnetic field, such that desired particle trajectory is achieved. Precisely, the optimal duration of ON time and OFF time required for effective navigation as well as minimization of stiction and aggregation of MNPs is found to be $T_{ON} = 3T_{OFF}$.

From the above discussion, it is clear that the entire navigation process in our work is performed by adjusting an external magnetic field, thereby avoiding any random propulsion of MNPs. Hence, we believe that our approach can achieve better navigation efficiency by minimizing the steering of MNPs to undesired outlet,

as compared to that in [89].

4.3 Simulation Framework

COMSOL Multiphysics employs finite element method (FEM) to numerically approximate solutions of partial differential equations (PDEs) with known boundary conditions. The Magnetic Fields interface from AC/DC module is used to compute magnetic field in and around the electromagnetic coils. The Magnetic Fields interface solves Maxwell's equations formulated using the magnetic vector potential. The variables that describe the current direction in coils are solved using Coil Geometry Analysis. The Magnetic Field interface used to compute the magnetic field may not be able to evaluate the spatial derivative of the magnetic field components, as the degrees of freedom correspond to components of the magnetic vector potential. Therefore, Coefficient Form PDE interface is used to evaluate the derivatives of the magnetic field components using scalar basis functions [110]. A steady state Laminar Flow interface from Computational Fluid Dynamics (CFD) module is used to compute the velocity profile of the fluid flow inside the Y-shaped channel. The fluid flow drag force is considered in the simulation. The fluid modeling parameters are selected to reflect blood behavior. The Particle Tracing for Fluid Flow interface from Particle Tracing Module is used to compute the motion of particles in the Y-shaped channel. Particle movement can be driven by drag and magnetic forces. Steady state solver is used for fluid flow and time-dependent solver is used to compute particle trajectory. Unidirectional or one-way coupling is used from the magnetic fields and laminar flow module to the particle trajectories. In other words, first the fields with gradients and velocity profile are computed, and then these fields, gradients and flow velocity are used to exert forces on the particles.

4.4 Results and Discussions

In this analysis, we consider the motion of MNPs in a viscous carrier fluid under the influence of an applied magnetic field. We restrict our attention to slow flow regimes where the magnetic and viscous drag forces dominate, and we neglect the rotational couplings to predict the motion of submicron or larger sized particles. We use classical Newtonian dynamics to study particle motion. The MNPs are injected at the inlet of a Y-shaped microchannel, with an incompressible fluid flowing through it, as shown in Fig. 4.3. The simulation parameters are presented in Table 3.1.

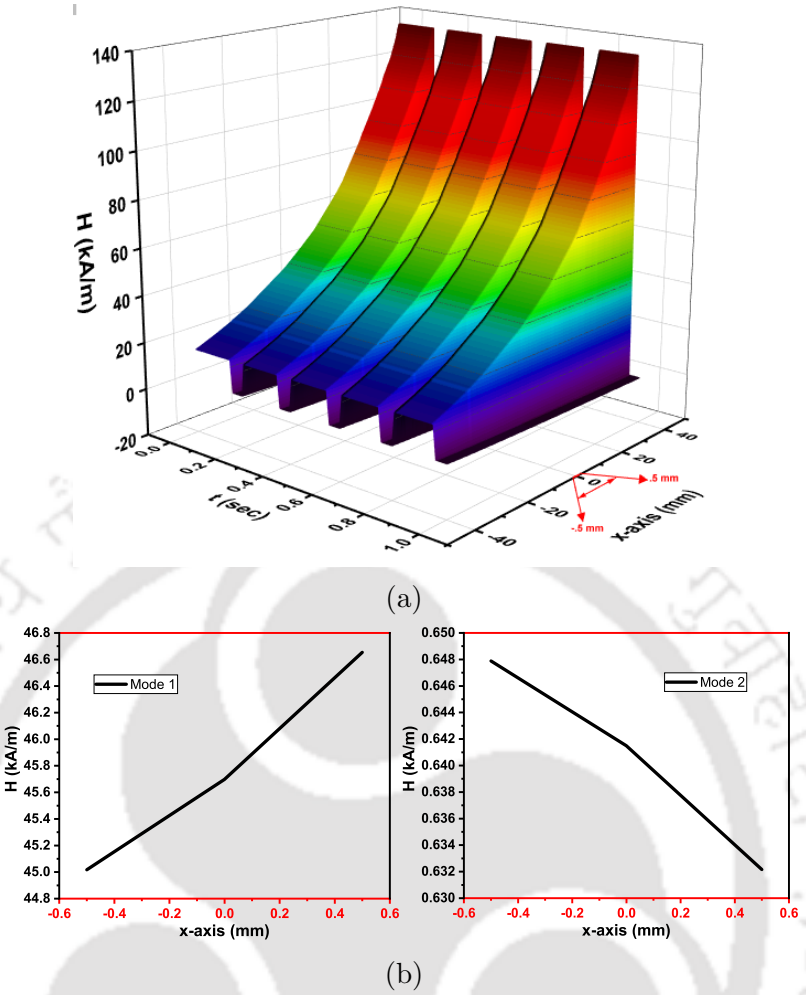

Figure 4.5: (a) Magnetic field intensity with respect to position and time along the space available in between the symmetrical coils, and (b) magnetic field intensity along the channel diameter for Mode 1 and Mode 2 respectively.

Fig. 4.5 shows the variation of magnetic field intensity (H) operating alternately throughout the navigation process in the following two modes: (i) Mode 1 for steering the MNPs to Outlet 1 and (ii) Mode 2 for releasing the stuck MNPs from the sidewalls of the channel. Fig. 4.5a represents the variation of H with respect to both time and position. The plot depicts the overall behaviour of H along the space available in between the coils (-40 mm to 40 mm). Note that the region of interest lies along the channel diameter (-0.5 mm to 0.5 mm). Fig 4.5b shows the 2D behaviour of H with respect to position for both the modes of operation, specific to the region of interest i.e, (-0.5 mm to 0.5 mm). Without any loss of brevity, we present an analysis of TVMF at the center of the Y-shaped channel ($x = 0$), as shown in Fig. 4.6. Here, T_{ON} and T_{OFF} are the ON and OFF time of the switch operated in Mode 1 and Mode 2 respectively. From extensive simulation analysis, the optimal duration of ON time and OFF time required for effective

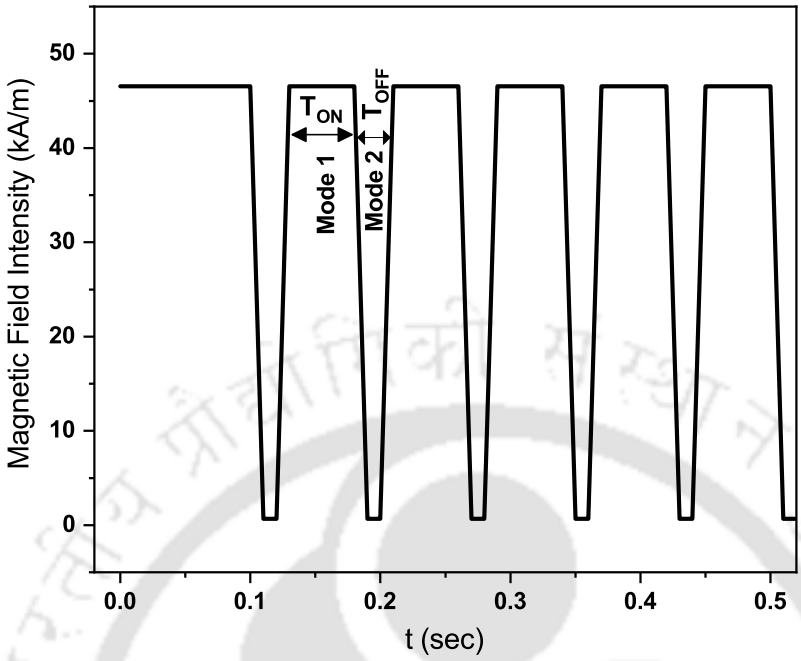

Figure 4.6: Magnetic field intensity with respect to time.

navigation as well as minimization of stiction and aggregation of MNPs is found to be $T_{ON} = 3T_{OFF}$. During the ON time (Mode 1) of the switching operation, the MNPs are steered to Outlet 1, which results in aggregation and stiction of MNPs at the sidewalls. During OFF time (Mode 2) of the switching operation, the stuck MNPs are released from the sidewalls and disaggregated under the influence of dominant fluidic force. The switching operation of the H takes place in this

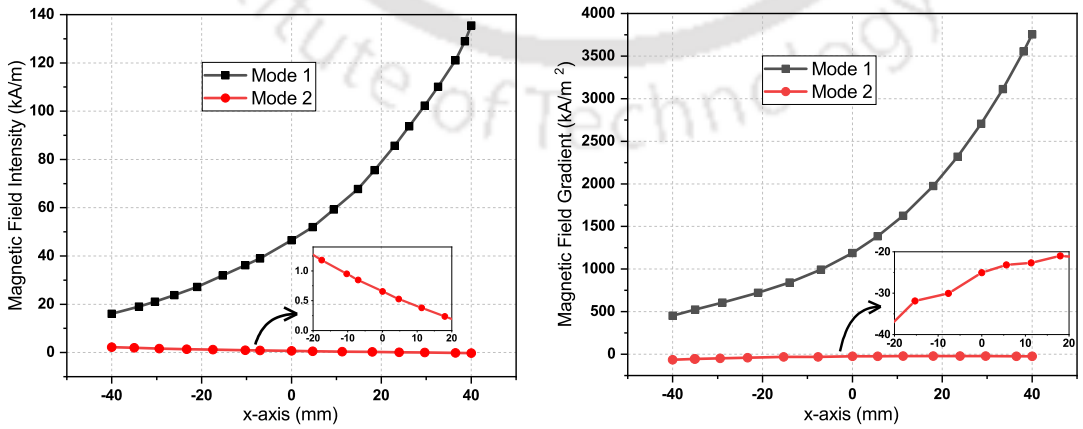

(a) (b)

Figure 4.7: (a) Magnetic field intensity, (b) Magnetic field gradient along the x-axis for both Mode 1 and Mode 2.

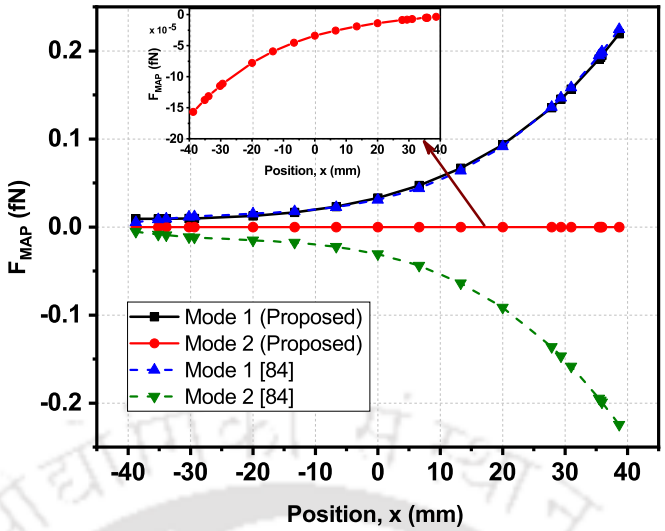

Figure 4.8: Magnetophoretic force for both Mode 1 and Mode 2.

fashion at all positions throughout the region of interest (along x-axis), as shown in Fig. 4.5a.

In Fig. 4.7, the variation of H and field gradient (∇H) are plotted. It may be observed from Fig. 4.7a & 4.7b that H and ∇H are positive in Mode 1. Clearly, a positive F_{MAP} is produced in Mode 1 to steer the MNPs to Outlet 1, following (3.9). However, Mode 2 produces a monotonically decreasing positive magnetic field intensity along the positive x-axis, as shown in Fig. 4.7a, which implies a negative magnetic field gradient as shown in 4.7b. Consequently, F_{MAP} is negative following (3.9) and the magnitude is small enough to ensure that the MNPs get demagnetized and detached from the sidewalls and move forward with drag force. The dominance of F_D over F_{MAP} facilitates the disaggregation of MNPs in Mode 2.

In Fig. 4.8, the variation of magnetophoretic forces (F_{MAP}) for both Mode 1 and Mode 2 are simulated and plotted. It may be noted that F_{MAP} experienced by the MNPs in a fluidic channel is proportional to the particle volume [93]. It may be observed from Fig. 4.7 that H and ∇H is positive in Mode 1. Consequently, a positive F_{MAP} is produced (3.9) in Mode 1, which steers the MNPs to Outlet 1. However, Mode 2 produces a monotonically decreasing positive magnetic field along the positive x-axis, as shown in Fig. 4.7, which implies a negative magnetic field gradient. Consequently, F_{MAP} is negative following (3.9) and the magnitude is small enough to ensure that the MNPs get demagnetized and detached from the sidewalls. Fig. 4.8 shows the simulation based performance comparison of our proposed system with that in [87]. In [87], two coils are configured such that a positive magnetic field is produced for steering (labeled as Mode 1) and an equal and oppositely directed magnetic field is produced to detach (labeled as Mode 2)

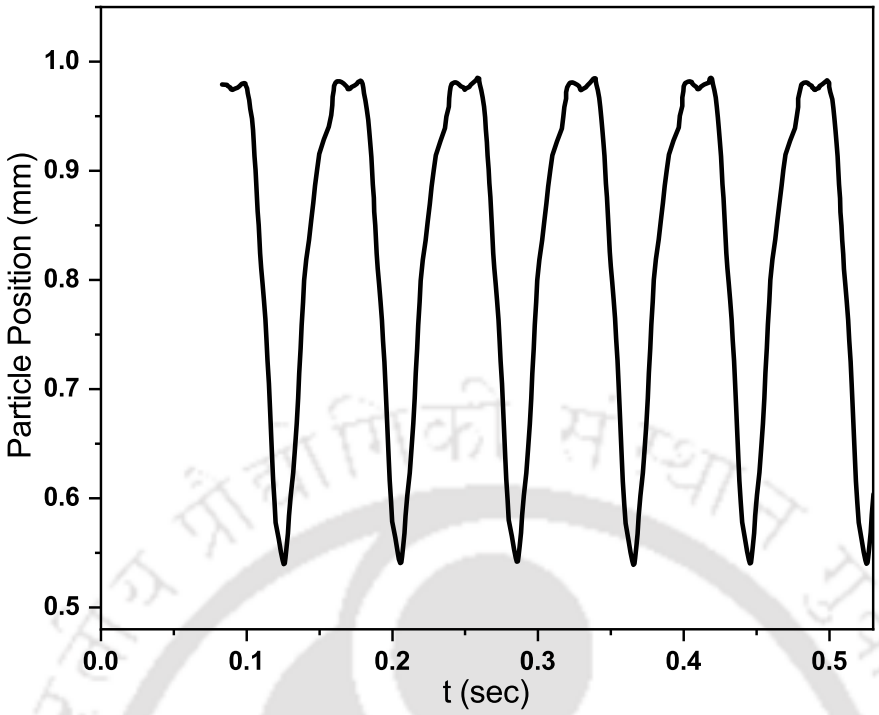

Figure 4.9: MNP trajectory inside the channel.

the MNPs from the vessel wall. Consequently, the magnitude of F_{MAP} remains same for both Mode 1 and Mode 2, while acting in opposite direction. It can be clearly seen that the F_{MAP} for steering the MNPs in both the systems using Mode 1 follows the same profile with comparable magnitude. The justification lies in the fact that both the systems show a similar magnetic field strength profile during Mode 1. However, in Mode 2, F_{MAP} produced in our system is much lower than that in [87]. Comparing the values of F_{MAP} at three different points in the region of interest, i.e., $x = -20$mm, $x = 0$mm and $x = 20$mm, we observe that the force exerted to release the MNPs are respectively 99.48%, 99.8% and 99.9% lower in our system than that in [87]. This highlights that the force used to mitigate the stiction issue in our system does not have adverse affect of guiding the MNPs to the undesired outlet.

Fig. 4.9 represents the analysis of trajectory of MNPs with the switching operation. The movement of MNPs are tracked inside the Y-shaped channel having radius 0.5 mm. In Mode 1, the MNPs are steered along the positive x direction, which results in a net displacement along the sidewalls of the channel. Subsequently, in Mode 2, the MNPs are pulled back from the sidewalls in the opposite direction, to avoid stiction and aggregation of MNPs at the sidewalls. From simulation analysis, we find that the optimal time duration required to pull back the MNPs at the center of the channel is given by $T_{OFF} = 20\ ms$. If the switching time in Mode 2 exceeds the optimal value, the resultant magnetic field intensity

will pull back the MNPs beyond the center of channel, which would lead to wrong navigation at the bifurcation point. This ON & OFF cycle is repeated throughout the navigation process to ensure that the MNPs trajectory is confined within the center and the sidewall of the channel leading towards the correct outlet (Outlet 1).

4.5 Chapter Summary

This chapter addresses the stiction and aggregation issue of MNPs in TDDS. In a magnetically actuated TDDS, the MNPs are guided to the desired blood vessel by steering them from the bifurcation points, using an external EMA system. During the steering process, some of the MNPs aggregate and stick to the vessel wall, thus reducing the efficacy of the navigation process. To mitigate this problem, a time-varying magnetic field (TVMF) is applied for efficient navigation of the MNPs in the channel. The TVMF alternately switches between two modes of operation described as follows. In the first mode of operation, the TVMF is applied for a certain time duration to generate the magnetic force required for steering the MNPs to the desired outlet. The second mode of operation facilitates mitigation of the stiction and aggregation of MNPs by modulating the TVMF and time duration of operation, so as to yield a lower magnetic force in the reverse direction to that in the first mode. Extensive simulations are performed to analyze the switching time for effective steering of the MNPs using COMSOL Multiphysics. Results illustrate that the time duration between the two modes of operation should be set using a ratio of $3:1$ for effective guidance of the MNPs to the correct outlet. The MNPs that are separated from the sidewalls move ahead with the fluid flow to the desired channel and this guidance mechanism is repeated till the MNPs reach the target point. Results demonstrate that the magnetophoretic force produced to release the adhered particles in our system is around 99.5% lower than that of an existing EMA system, which aims to address the same issue. Thus, our system provides enhanced efficacy in mitigating the stiction issue by alleviating the detrimental effect of the MNPs getting steered to the undesired outlet.

Chapter 5

Experimental Validation of TDDS

Contents

5.1 Introduction 66
5.2 Magnetic Nanoparticles 66
5.3 Experimental Setup 68
5.4 Results and Discussions 72
5.5 Chapter Summary 75

5.1 Introduction

In this chapter, we aim to implement the navigation system for MNPs using the proposed EMA system. To achieve the realistic MNP guidance in *in vivo* trials, each patient's precise 3-D blood map should be retrieved using imaging technologies such as MRI. The MNPs are injected into the blood vessels obtained from the imaging technique and propelled by the blood flow velocity. The proposed EMA system is used to navigate the MNPs from the point of injection to the target location.

5.2 Magnetic Nanoparticles

5.2.1 Synthesis

Iron oxide nanoparticles are widely used as magnetic particles for biotechnology and medical applications, including contrast agents for MRI, cell recognition and separation and drug delivery, due to their high saturation magnetization and high magnetic susceptibility. We consider Fe_3O_4 as drug carriers for TDDS. The superparamagnetic properties exhibited by Fe_3O_4 ensures better control of the MNPs, when subjected to an external gradient magnetic field in TDDS [111]. The particles need to be stabilized in the carrier liquid because they tend to agglomerate due to Van der Waals forces. In addition, the magnetite nanoparticles are very much susceptible to air oxidation. The synthesis of Fe_3O_4 is done by mixing aqueous Fe^{2+} and Fe^{3+} salt solutions, which is followed by the addition of NH_4OH base in the air environment, at an elevated temperature of 80°C using co-precipitation technique [112]. The iron oxide nanoparticles are prepared using analytical grade ferric chloride ($FeCl_3 \cdot 6H_2O$), ferrous chloride ($FeCl_2 \cdot 4H_2O$), ammonium hydroxide (NH_4OH). Initial molar ratios of $Fe^{3+} : Fe^{2+} = 1.5 : 1$ are used. Required amounts of $FeCl_3 \cdot 6H_2O$ and $FeCl_2 \cdot 4H_2O$ are dissolved in 40 ml of deionized water. The solution is heated at $80°C$ for 1 hour while being stirred. $Fe^{3+} : Fe^{2+} = 1.5 : 1$ are stabilized in water media. A black suspension is formed upon the addition of NH_4OH. The crystal growth is allowed to proceed for 30 min at $80°C$ with constant stirring. The suspension is then cooled to room temperature. In our simulation model, we consider that the particles are stable, thus ignoring the intra-particle aggregation.

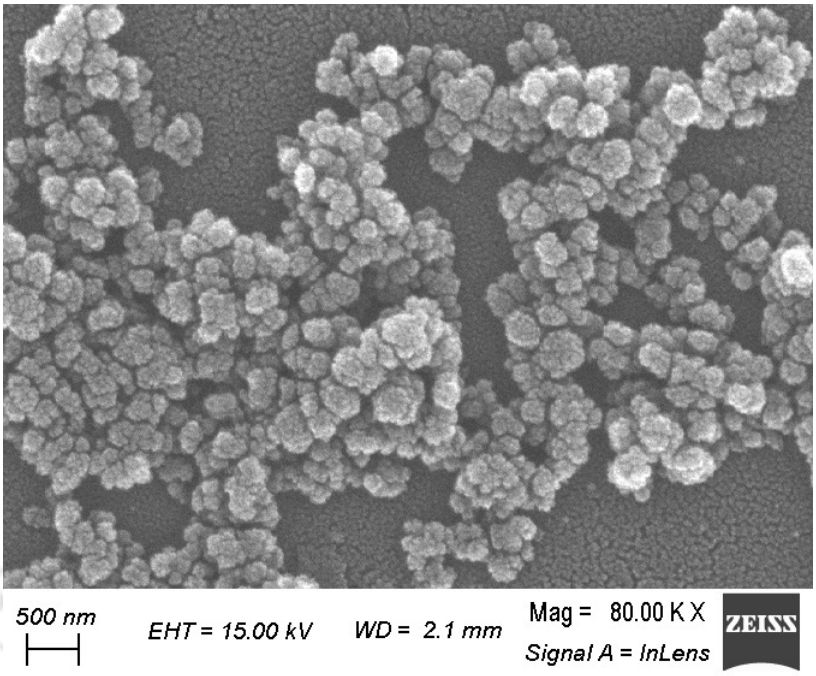

Figure 5.1: FESEM image of Fe_3O_4

5.2.2 Characterization

Fig. 5.1 shows the FESEM image of synthesized Fe_3O_4. The particle size analyzer determines particle size by measuring the rate of fluctuations in laser light

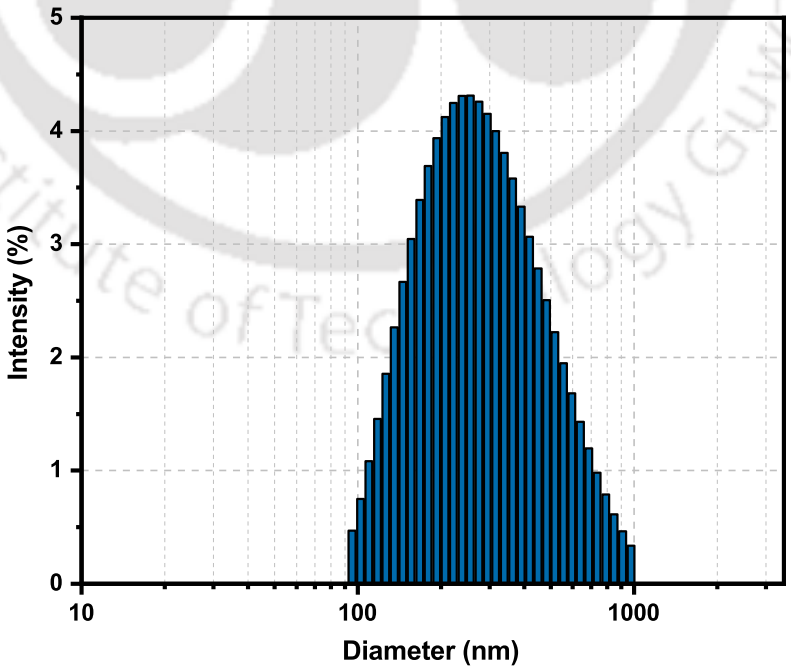

Figure 5.2: Size distribution of Fe_3O_4 using particle size analyzer (Beckman Coulter Delsa Nano).

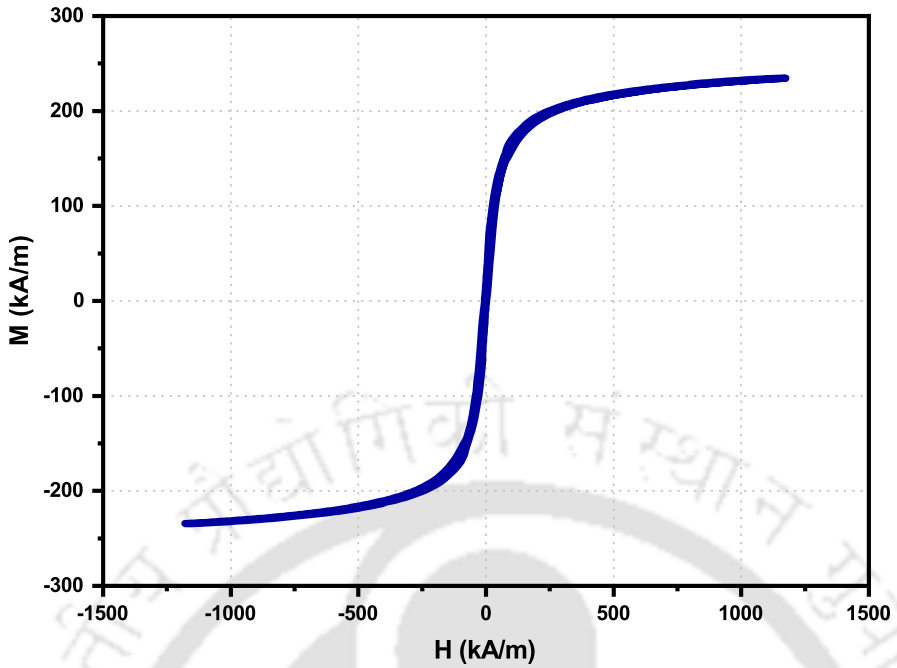

Figure 5.3: Vibrating Sample Magnetometer (VSM) magnetization curve showing saturation.

intensity scattered by particles as they diffuse through a fluid. Fig. 5.2 shows the size distribution of synthesized Fe_3O_4 using Beckman Coulter Delsa Nano and the average diameter of the particles is approximately 250 nm. Fig. 5.3 shows the magnetization characteristics exhibited by the synthesized Fe_3O_4, indicating that magnetic field strength of about $H_{sat} = 1172.575kA/m$ is required for saturation magnetization of MNPs, denoted as $M_{sat} = 234.42kA/m$. In the region of saturation, all the domains of magnetizable particles are aligned along the direction of the magnetic field. Since the graph shows nonlinear characteristics, the MNPs are magnetized to 75% of M_{sat}, $M = 172.82kA/m$ even when a low magnetic field strength of $H = 136.4kA/m$ is applied, which is only 11.6% of H_{sat}. This means that the particles can be magnetized to a sufficient level by generating a magnetic field in the middle range. Thus, application of a strong magnetic field may not be required, as better efficiency can be achieved rather by a high gradient [85].

5.3 Experimental Setup

The synthesized Fe_3O_4 nanoparticles suspended in fluid are injected into the Y-shaped microchannel using a syringe pump and the flow rate is adjusted. For *in vivo* application, the nanoparticles injected into the blood vessel are propelled by fluid flow. Y-shaped microchannel is fabricated on the poly(dimethylsiloxane)

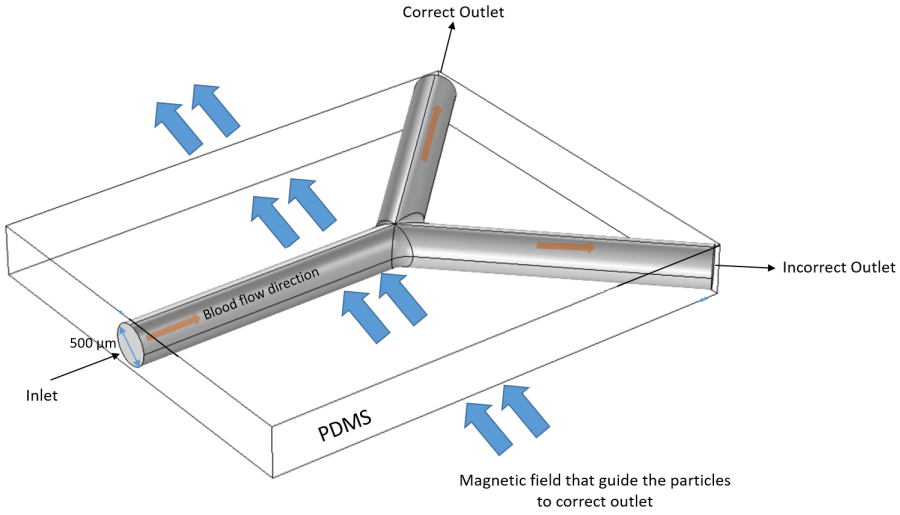

Figure 5.4: Y-shaped microchannel fabricated on the PDMS substrate by replica molding from the master mold.

(PDMS) substrate by replica molding from the master mold as shown in Fig 5.4. Deionized (DI) water is used as suspension fluid in our experimental setup, since it resembles the magnetic properties of blood (relative permeability is 1 for both). However, the magnitude of viscosity of DI water and blood are different, 0.001 Pa s and 0.004 Pa s respectively. Note that the value of fluidic force depends on viscosity of the fluid. Therefore, to replicate the *in vivo* application, we have reduced the flow rate of DI water, such that similar fluidic force as that of blood is obtained in our experimental framework. Thus, the nanoparticles suspended in DI water are injected into the Y-shaped microchannel using a syringe pump and the flow rate is adjusted to yield similar fluidic force as that of blood.

5.3.1 3D Printing of Mold

3D printing has emerged as a potential method for creating 3D microchannels. A computer-aided design (CAD) model of a 3D object decomposed into a series of 2D slices, is used in 3D printing to fabricate the physical object layer by layer.The procedure is fully automated and may be used to create any 3D object. Through the creation of molds for replication, 3D printing makes a significant contribution to microfluidics. Y-shaped microfluidic device is fabricated using a mold produced by a dual extrusion FDM 3D printer (Ultimaker S3). Briefly, the mold is designed using CAD software and the resulting data was transferred to the 3D printer's software (Ultimaker Cura). Finally, thermoplastics are printed and cured for mold fabrication.

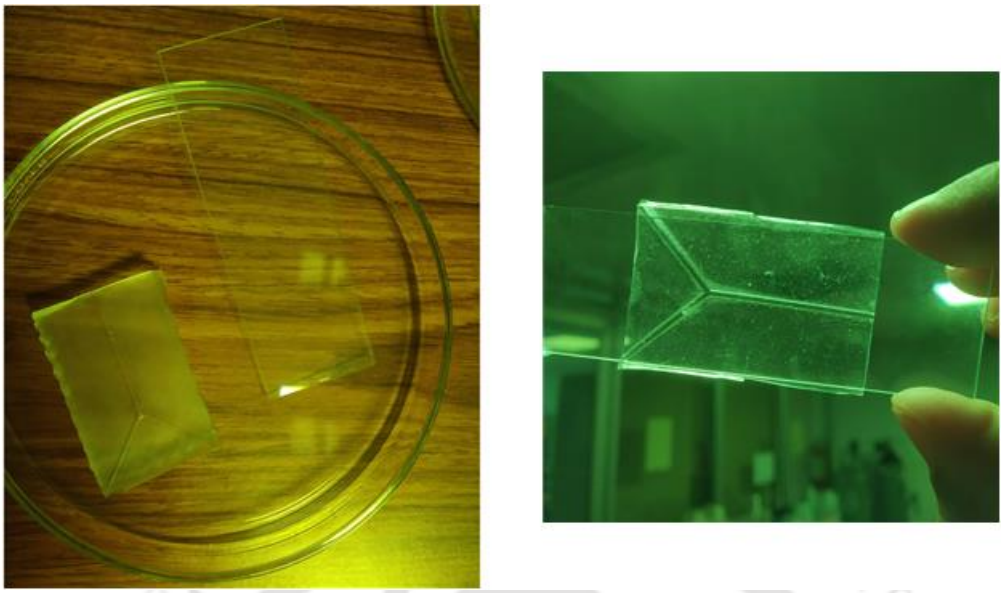

Figure 5.5: PDMS based Y-shaped microfluidic channel.

5.3.2 Fabrication of Y-shaped Microchannel

PDMS is a silcone-based organic polymer used extensively in professional and academic research laboratories for its low cost and high versatility. PDMS is inert, transparent and easily customized via soft lithography, a technique used to mold PDMS and imprint nano-scale features and microchannels into its surface. A well-mixed PDMS was poured into a 3D-printed mold to fabricate a PDMS layer. The PDMS layer is cured in an oven at 65°C for 48 h. After curing, the PDMS layer was peeled off from the mold. Harrick Plasma Cleaner is used to remove organic contamination and activate the PDMS surface in preparation for bonding with other simillarly treated PDMS surfaces. After patterning a PDMS substrate by replica molding from a master mold, the PDMS is oxidized in air plasma. An air plasma

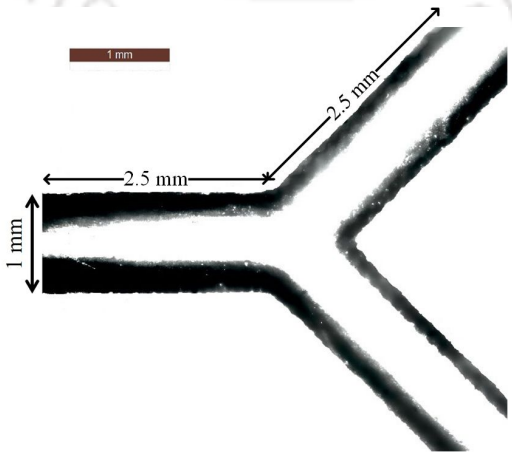

Figure 5.6: Microscopic view of the Y-shaped channel.

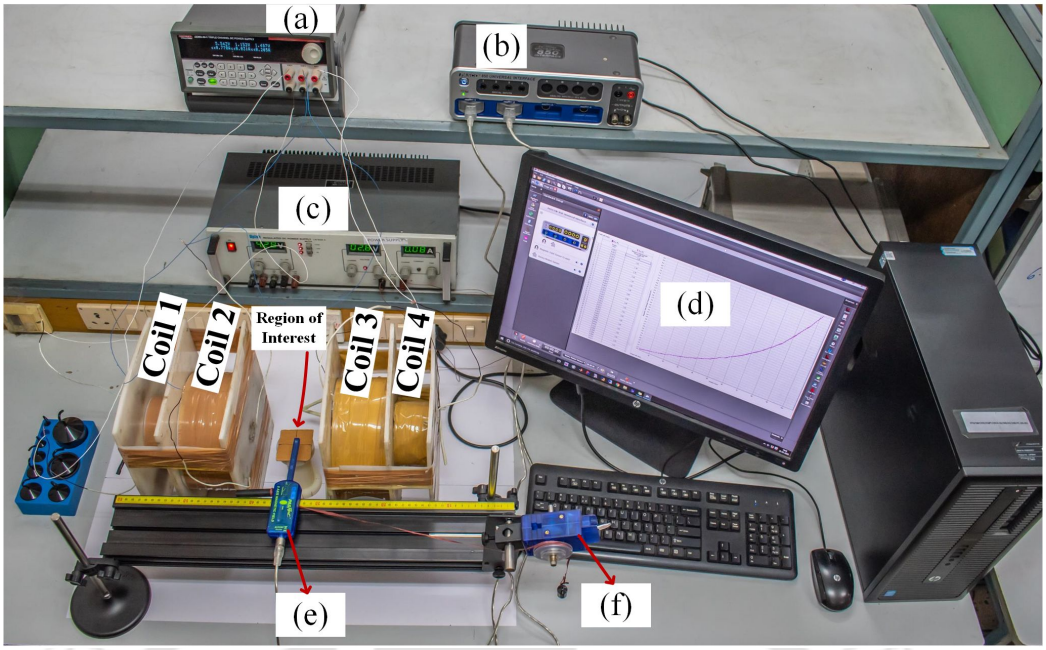

Figure 5.7: Experimental Setup. Coil 1 & Coil 4 represent the outer coils and Coil 2 & Coil 3 represent the inner coils. (a) Keithley 2230G-30-1, (b) PASCO 850 Universal Interface (UI-5000), (c) Aplab LQ6324S, (d) PASCO Capstone Control Panel, (e) PASPORT 2-Axis Magnetic Field Sensor (PS-2162) and (f) PASPORT Rotary Motion Sensor (PS-2120A).

removes organic, hydrocarbon material by chemical reaction with highly reactive oxygen radicals and ablation by energetic oxygen ions. This leaves silanol (SiOH) groups on the surface, rendering the surface more hydrophilic and increasing surface wettability. Following plasma activation, the PDMS is immediately placed in contact with another oxidized PDMS surface to form bridging Si-O-Si bond at the interface, creating an irreversible seal. This water-tight covalent bond results in the formation of Y-shaped microchannel as shown in Fig 5.5. The microscopic view of the fabricated Y-shaped channel is shown in Fig 5.6.

5.3.3 Electromagnetic Actuation System

The experimental setup of the EMA system is designed by using the geometrical parameters of the coils given in Table 3.2, as shown in Fig. 5.7. Subsequently, the number of wire turns in the outer and the inner coils are evaluated as 4986 and 1544 respectively, following (3.17). PASPORT 2-Axis Magnetic Field Sensor (PS-2162) in conjunction with PASPORT Rotary Motion Sensor (PS-2120A) interface is used to measure magnetic field strength along the x-axis, as represented in Fig. 5.7. PASCO 850 Universal Interface (UI-5000) in combination with PASCO Capstone software are used to record, display and analyze the data measured by

the sensors. The electromagnetic coils are powered by programmable DC power supplies (Keithley 2230G-30-1 and Aplab LQ6324S). Due to the limitations of our resources, we use the DC power supplies which support a maximum current of 5A. Hence, we scale down the magnitude of current, given in Table 3.2, in equal proportion, since H is linearly proportional to the currents I_{oL}, I_{iL}, I_{iR} and I_{oR}.

5.4 Results and Discussions

In this section, we validate the experimental results with that from the Finite Element Analysis (FEA) simulation. The simulation analyses are done using AC/DC and Partial Differential Equation (PDE) interfaces module of COMSOL in steady state, to evaluate the magnetic field strength and gradient produced by the coils.

Fig. 5.8 and 5.9 shows the experimental validation of the performance of the proposed EMA system in terms of magnetic field strength. It depicts the variation of magnetic field strength along the x axis of the system, operating in both Mode 1 and Mode 2 for steering and demagnetizing of MNPs respectively. It may be observed from Fig. 5.8 that the magnetic field strength in Mode 1 is positive at all points and has an exponentially increasing profile. In contrast, the magnetic field strength in Mode 2 is positive with a monotonically decreasing profile, as shown in Fig. 5.9. Clearly, the experimental results show a close match with the simulation results, thus highlighting the practical feasibility of the proposed system.

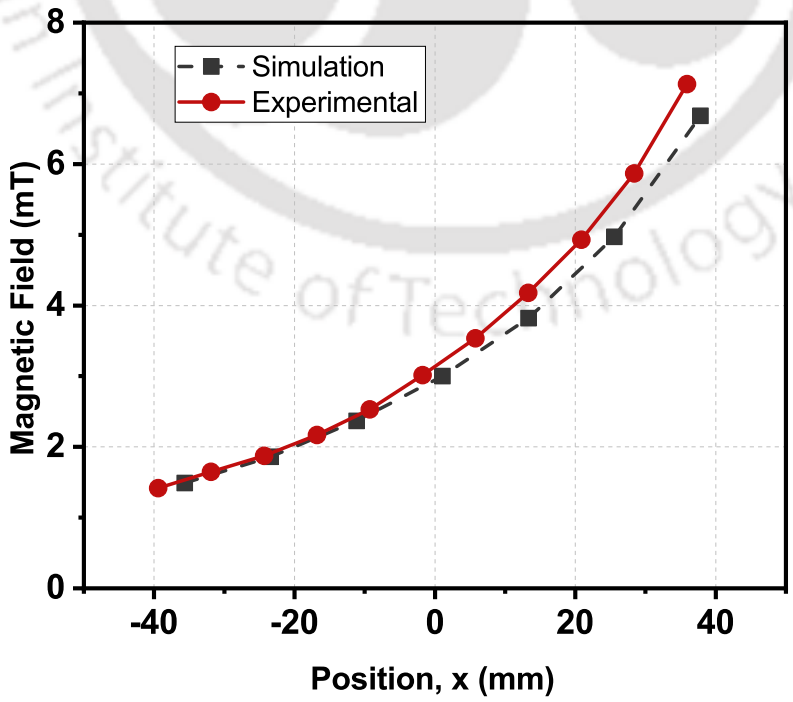

Figure 5.8: Magnetic field produced by Mode 1

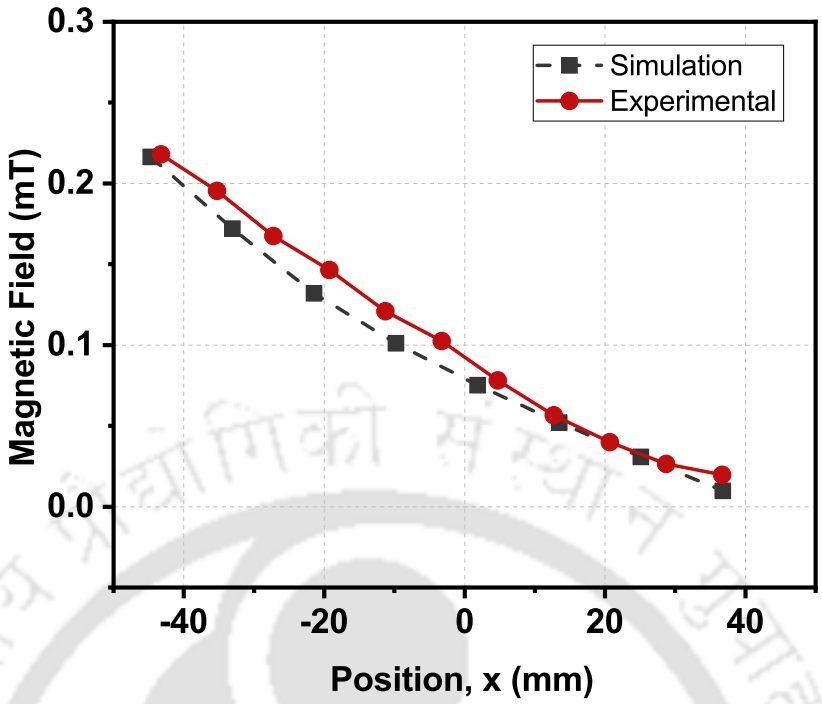

Figure 5.9: Magnetic field produced by Mode 2.

Fig. 5.10 presents the switching characteristics between Mode 1 and Mode 2, in our proposed EMA system. The power supplies of the inner coils are turned

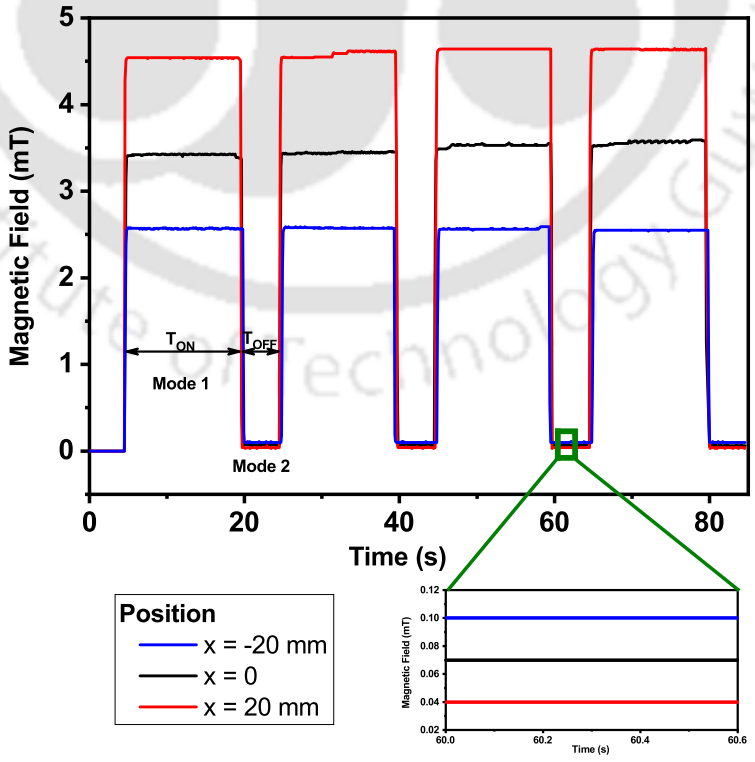

Figure 5.10: Timing Analysis

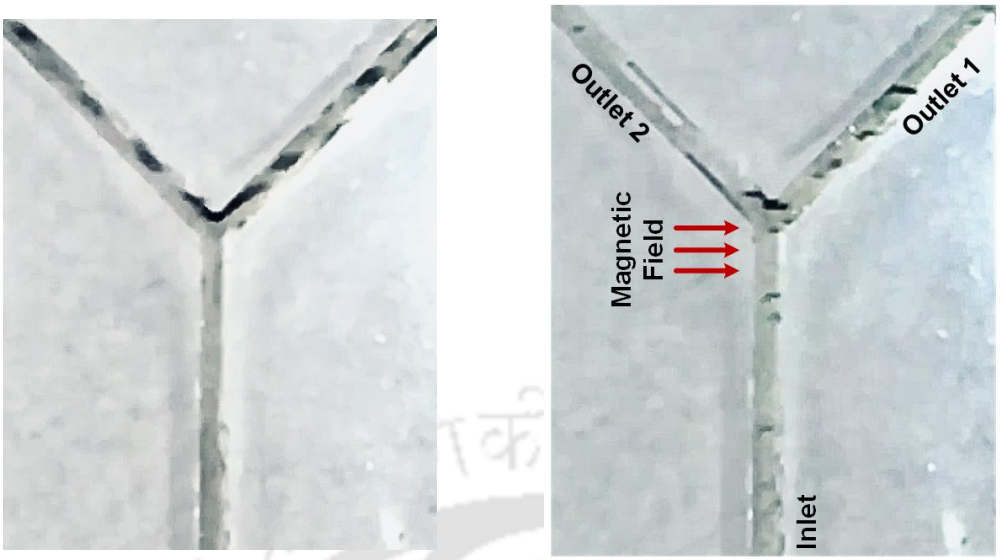

(a) (b)

Figure 5.11: Video image analysis of the steering experimets. (a) Before applying magnetic field and (b) after applying magnetic field around the bifurcation point.

ON/OFF manually in alteration, for a specific period of time. The variation of the magnetic field is plotted at three different points in the region of interest, viz. left edge ($x = -\frac{S_l}{2}$), mid-point ($x = 0$) and right edge ($x = \frac{S_l}{2}$). The ON cycle of the actuator is used to steer the MNPs to Outlet 1 and the OFF cycle is used to release the MNPs adhered to the sidewalls during the OFF cycle. This process is repeated throughout the guidance mechanism.

Fig. 5.11 shows the video image data for experimental validation of steering of MNPs in a Y shaped channel. To record the video data we have used a frame rate of 60 fps. Note that a higher frame rate could result in better visualization of particle trajectory. This plot aims to provide a qualitative understanding of trajectory dynamics of MNPs. The MNPs move under the influence of fluid flowing through the channel and external magnetic field. When no magnetic field is applied, the MNPs flow randomly through both outlets of the channel, as depicted in Fig. 5.11a. Now, the EMA system exerts a magnetic field across the channel directed from left to right, as shown in Fig. 5.11b. In presence of applied magnetic field, it is observed in Fig. 5.11b that majority of the MNPs are steered to Outlet 1.

Fig. 5.12 shows the actual trajectory of MNPs in the channel under influence of magnetic field produced by the EMA system. The particle trajectory analysis is done using ImageJ, an open-source image processing program [113]. For this analysis, we first draw a line of reference at the centre of the channel as shown in Fig. 5.12. The movement of MNPs are tracked in the region of interest around the bifurcation point. We start the analysis from the inlet channel and the MNPs

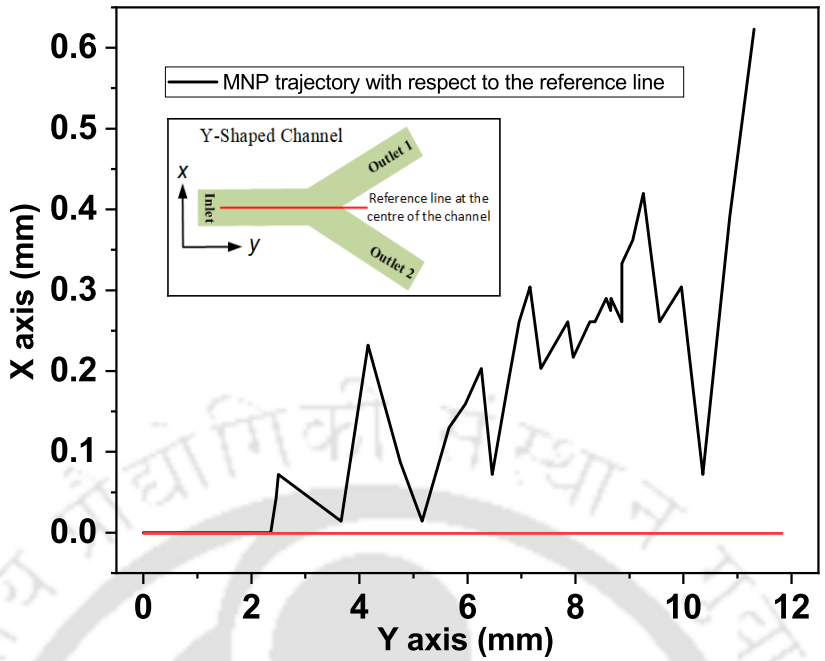

Figure 5.12: Experimental validation of MNP steering to outlet 1 due to magnetophoretic force.

reach bifurcation point at a distance of 11 mm from the initial position in the inlet channel. Radius of the channel is 500 μm. From this analysis, it is clearly seen the MNPs follow a zigzag path, implying steering of the MNPs in Mode 1 (along positive x direction) and pulling them back from the side walls in Mode 2 (along negative x direction) in alteration to avoid stiction issue. Also, it is observed that the force exerted by the system in Mode 2 is so small that the MNPs are not pulled back beyond the reference line at any point. Furthermore, it is seen that after crossing the bifurcation point (11 mm and beyond), the MNPs are steered to a distance of approximately 600μm from the reference line. Since, the MNPs are deflected towards the positive x axis at a distance higher than the radius of the inlet channel (500 μm), it is confirmed that the MNPs are steered to the correct outlet (Outlet 1). From the particle area analysis in ImageJ, the particles reaching Outlet 1 when the inner coils are switched ON and OFF is approximately 81.14%. In contrast, the particles reaching Outlet 1 when all the coils are switched ON is approximately 70.14%.

5.5 Chapter Summary

This chapter validates the proposed EMA system for TDDS. The synthesized Fe_3O_4 magnetic nanoparticles are used as carrier vehicles and the average diameter of the particles are 250 nm. A PDMS based Y-shaped microchannel is

fabricated to mimic the *in vivo* application. The EMA system is designed using the optimized parameters as defined in Table 3.2. We have addressed the stiction issue by designing a novel EMA system. The system comprises of four coils, where all the four coils are operated simultaneously for a certain period of a time cycle, to produce a sufficient magnetophoretic force, which steers the particles at the bifurcation point. During the remaining period, the system operates with only two coils to demagnetize the stuck particles, which are then propelled by the drag force to the desired outlet. Also, the reverse magnetophoretic force produced in this cycle has a low magnitude, which ensures that the particles are not pulled into the undesired outlet. The consistency of the experimental results with the simulation results validates our proposed design in producing a modulated magnetophoretic force. In conclusion, we propose a new design of an electromagnetic actuator for mitigating the stiction issue in a targeted drug delivery system with enhanced accuracy of steering the drug to the desired location, thus ensuring the removal of off-target side effects. We believe that the proposed design is a step towards enhancing the efficacy of the targeted drug delivery system.

Chapter 6

Conclusions and Future Scope

Contents

6.1 Conclusion 78
6.2 Future Scope 80

6.1 Conclusion

This thesis investigated the design of an electromagnetic actuation (EMA) system to steer the magnetic nanoparticles (MNPs) in a Y-shaped microfluidic channel for targeted drug delivery. More precisely, we addressed the stiction and aggregation issue by designing a novel EMA system. The system comprised of four coils, where a time-varying magnetic field (TVMF) was used to navigate the MNPs injected into the Y-shaped microfluidic channel. The proposed TVMF switched between two modes of operation. During the first mode of operation, all the four coils were operated simultaneously for a certain period of a time cycle, to produce sufficient magnetophoretic force, which steered the particles at the bifurcation point. In the second mode of operation, the system operated with only two coils to demagnetize the stuck particles, which were then propelled by the drag force to the desired outlet. The dominance of fluidic force over magnetic force ensured the disaggregation and stiction mitigation of MNPs in the second mode of operation. Also, the reverse magnetophoretic force produced in this cycle had a low magnitude, which ensured that the particles were not pulled into the undesired outlet. Timing analysis of the TVMF was performed to prevent the steering of the MNPs to the undesired outlet. The consistency of the experimental results with the simulation results validated our optimized design in producing a modulated magnetophoretic force. Furthermore, results confirmed that our design was more efficient in mitigating the stiction issue than an already reported work. The specific contribution made are listed below.

- **Design and analysis of EMA systems**: Electromagnetic actuation systems of various coil topologies such as single coil, Helmholtz coil, Maxwell coil, Helmholtz-Maxwell pair and DCC were used to improve the efficiency of the TDDS. To further improve the efficiency of the navigation system, an EMA system was designed using a particular arrangement of four circular electromagnetic coils. The coils were used to produce a magnetic force for steering of MNPs to the correct outlet. We optimized the geometrical parameters and supply current for each coil in the four coils arrangement, to produce a magnetic force along the desired direction of steering. In this process, a few MNPs get stuck to sidewalls.

- **Stiction mitigation and disaggregation of MNPs**: The proposed EMA system alternately operated in two different modes by switching ON and OFF a pair of coils. In the first mode, the system generated a magnetic force responsible for steering the MNPs. In the second mode, it generated a small

magnetic force in the reverse direction, which pulled back the MNPs stuck to the vessel walls, thus mitigating the stiction problem. The MNPs that were separated from the sidewalls moved ahead with the fluid flow to the desired channel and this guidance mechanism was repeated till the MNPs reached the target point. The experimental validation of the proposed EMA system highlighted its practical feasibility to mitigate the stiction issue. Results demonstrated that the magnetophoretic force produced to release the adhered particles in our system was around 99.5% lower than that of an existing EMA system, which aimed to address the same issue. Thus, our system provided enhanced efficacy in mitigating the stiction issue by alleviating the detrimental effect of the MNPs getting steered to the undesired outlet.

- **Enhance the switching performace of EMA system**: To improve the switching efficiency between the two modes of operation, a TVMF was proposed for effective steering of the MMPs to the correct outlet. Extensive simulations were performed to analyze the switching time for effective navigation of the MNPs using COMSOL Multiphysics. Results illustrated that the time duration between the two modes of operation should be set using a ratio of $3:1$ for effective guidance of the MNPs to the correct outlet.

To conclude, we proposed a new design of an electromagnetic actuator for mitigating the stiction and aggregation issue in a targeted drug delivery system with enhanced accuracy of steering the drug to the desired location, thus ensuring removal of off-target side effects. We believe that the proposed design is a step towards enhancing the efficacy of the targeted drug delivery system.

Lastly, it is worth highlighting the use of magnetic fields and field gradients generated by electromagnetic coils. The electromagnet has found applications in many areas such as mining, water purification, biochemistry and medical research. The proposed actuation system may be utilized for the magnetic separation technique by binding selectively the target to the magnetic beads out of a large volume or complex matrix. The actuation system can be used to separate the magnetic bead-bound target. The mining industry extensively uses magnetic separation for ore treatment, material sorting and purification of minerals. The proposed electromagnetic actuation system may be deployed for the separation of erythrocytes from whole blood and to improve the efficiency of the magnetic water treatment process.

6.2 Future Scope

This section presents the potential extension of the problems investigated in this thesis as follows:

- Design of a magnetic particle imaging technique using the proposed EMA system to extract the blood vessel information, which is needed to plan the path from the site of injection to the target location.
- Optimization of the coil parameters considering magnetic field and its gradient $(H\cdot\nabla)H$ with unsaturated nanoparticles or only the gradient magnetic field ∇H with saturated nanoparticles as objective function, to further improve the navigation efficiency.
- Analysis of the EMA system to treat the infected cell *in vivo* using magnetic hyperthermia.
- Functionalization of MNPs to avoid the effect of aggregation in the process of steering them to the target location.
- Development of EMA system towards magnetic separation for biomedical diagnostic.

Bibliography

[1] A. P. Singh, A. Biswas, A. Shukla, and P. Maiti, "Targeted therapy in chronic diseases using nanomaterial-based drug delivery vehicles," *Sig. Transduct. Target. Ther.*, vol. 4, no. 33, 2019.

[2] D. G. Rudmann, "On-target and Off-target-based Toxicologic Effects," *Toxicol. Pathol.*, vol. 41, no. 2, pp. 310–314, 2013.

[3] World Health Organization, "Cancer," 2022. [Online]. Available: https://www.who.int/news-room/fact-sheets/detail/cancer

[4] P. Mathur, K. Sathishkumar, M. Chaturvedi, P. Das, K. L. Sudarshan, S. Santhappan, V. Nallasamy, A. John, S. Narasimhan, and F. S. a. Roselind, "Cancer Statistics, 2020: Report From National Cancer Registry Programme, India," *JCO Global Oncology*, no. 6, pp. 1063–1075, 2020.

[5] V. Schirrmacher, "From chemotherapy to biological therapy: A review of novel concepts to reduce the side effects of systemic cancer treatment (Review)," *Int. J. Oncol.*, vol. 54, no. 2, pp. 407–419, 2019.

[6] K. Nurgali, R. T. Jagoe, and R. Abalo, "Adverse effects of cancer chemotherapy: Anything new to improve tolerance and reduce sequelae?" *Front Pharmacol.*, vol. 9, p. 245, 2018.

[7] K.-H. Altmann, "Cancer Chemotherapy: Basic Science to the Clinic. By Rachel Airley." *ChemMedChem*, vol. 4, no. 12, pp. 2123–2124, 2009.

[8] A. K. Nayak, S. A. Ahmad, S. Beg, T. J. Ara, and M. S. Hasnain, "12 - Drug delivery: Present, past, and future of medicine," in *Applications of Nanocomposite Materials in Drug Delivery*, ser. Woodhead Publishing Series in Biomaterials, Inamuddin, A. M. Asiri, and A. Mohammad, Eds. Woodhead Publishing, 2018, pp. 255–282.

[9] A. Tewabe, A. Abate, M. Tamrie, A. Seyfu, and E. A. Siraj, "Targeted drug delivery—from magic bullet to nanomedicine: principles, challenges,

and future perspectives," *Journal of Multidisciplinary Healthcare*, vol. 14, p. 1711, 2021.

[10] J. K. Patra, G. Das, L. F. Fraceto, E. V. R. Campos, M. d. P. Rodriguez-Torres, L. S. Acosta-Torres, L. A. Diaz-Torres, R. Grillo, M. K. Swamy, S. Sharma *et al.*, "Nano based drug delivery systems: recent developments and future prospects," *Journal of Nanobiotechnology*, vol. 16, no. 1, pp. 1–33, 2018.

[11] Z. Mohammad, A. Zeeshan, S. Faisal, A. Suhail, I. Sahar, S. Mohd, K. Nazma *et al.*, "Vesicular drug delivery system used for liver diseases," *World Journal of Pharmaceutical Sciences*, pp. 28–35, 2017.

[12] A. S. Hoffman, "The origins and evolution of "controlled" drug delivery systems," *Journal of Controlled Release*, vol. 132, no. 3, pp. 153–163, 2008.

[13] Y. H. Bae and K. Park, "Targeted drug delivery to tumors: myths, reality and possibility," *Journal of controlled release*, vol. 153, no. 3, p. 198, 2011.

[14] V. Chandrakala, V. Aruna, and G. Angajala, "Review on metal nanoparticles as nanocarriers: current challenges and perspectives in drug delivery systems," *Emergent Materials*, pp. 1–23, 2022.

[15] K. Ibrahim, S. Khalid, and K. Idrees, "Nanoparticles: properties, applications and toxicities. arab j chem 12 (7): 908–931," 2019.

[16] O. V. Salata, "Applications of nanoparticles in biology and medicine," *Journal of nanobiotechnology*, vol. 2, no. 1, pp. 1–6, 2004.

[17] M. A. Obeid, M. M. Al Qaraghuli, M. Alsaadi, A. R. Alzahrani, K. Niwasabutra, and V. A. Ferro, "Delivering natural products and biotherapeutics to improve drug efficacy," *Therapeutic Delivery*, vol. 8, no. 11, pp. 947–956, 2017.

[18] E. Miele, G. P. Spinelli, E. Miele, E. Di Fabrizio, E. Ferretti, S. Tomao, and A. Gulino, "Nanoparticle-based delivery of small interfering rna: challenges for cancer therapy," *International Journal of Nanomedicine*, vol. 7, p. 3637, 2012.

[19] I. K. Kwon, S. C. Lee, B. Han, and K. Park, "Analysis on the current status of targeted drug delivery to tumors," *Journal of Controlled Release*, vol. 164, no. 2, pp. 108–114, 2012.

[20] J. Yoo, C. Park, G. Yi, D. Lee, and H. Koo, "Active targeting strategies using biological ligands for nanoparticle drug delivery systems," *Cancers*, vol. 11, no. 5, p. 640, 2019.

[21] G. Manish and S. Vimukta, "Targeted Drug Delivery System: A Review," *Res J Chem Sci*, vol. 1, no. 2, pp. 135–138, 2011.

[22] S. Gujral and S. Khatri, "A Review on Basic Concept of Drug Targeting and Drug Carrier System," *Int. J. Adv. Pharm. Biol. Chem*, vol. 2, no. 1, 2013.

[23] A. Kumar, U. Nautiyal, C. Kaur, V. Goel, and N. Piarchand, "Targeted drug delivery system: current and novel approach," *Int J Pharm Med Res*, vol. 5, no. 2, pp. 448–454, 2017.

[24] Y. Matsumura and H. Maeda, "A new concept for macromolecular therapeutics in cancer chemotherapy: mechanism of tumoritropic accumulation of proteins and the antitumor agent smancs," *Cancer research*, vol. 46, no. 12 Part 1, pp. 6387–6392, 1986.

[25] A. Albanese, P. S. Tang, and W. C. Chan, "The effect of nanoparticle size, shape, and surface chemistry on biological systems," *Annual review of biomedical engineering*, vol. 14, pp. 1–16, 2012.

[26] K. Rani and S. Paliwal, "A review on targeted drug delivery: Its entire focus on advanced therapeutics and diagnostics," *Sch. J. App. Med. Sci*, vol. 2, no. 1C, pp. 328–31, 2014.

[27] E. Stimphil, A. Nagesetti, R. Guduru, T. Stewart, A. Rodzinski, P. Liang, and S. Khizroev, "Physics considerations in targeted anticancer drug delivery by magnetoelectric nanoparticles," *Appl. Phys. Rev.*, vol. 4, no. 2, p. 021101, 2017.

[28] J. K. Mills and D. Needham, "Targeted drug delivery," *Expert Opinion on Therapeutic Patents*, vol. 9, no. 11, pp. 1499–1513, 1999.

[29] G. Poste and R. Kirsh, "Site–specific (targeted) drug delivery in cancer therapy," *Bio/Technology*, vol. 1, no. 10, pp. 869–878, 1983.

[30] P. Martins, D. Rosa, A. R. Fernandes, and P. V. Baptista, "Nanoparticle Drug Delivery Systems: Recent Patents and Applications in Nanomedicine," *Recent Pat. Nanomed.*, vol. 3, no. 2, pp. 105–118, 2013.

[31] K. Öztürk-Atar, H. Eroğlu, and S. Çalış, "Novel advances in targeted drug delivery," *Journal of drug targeting*, vol. 26, no. 8, pp. 633–642, 2018.

[32] R. C. Scott, D. Crabbe, B. Krynska, R. Ansari, and M. F. Kiani, "Aiming for the heart: targeted delivery of drugs to diseased cardiac tissue," *Expert opinion on drug delivery*, vol. 5, no. 4, pp. 459–470, 2008.

[33] J. Huang, Y. Li, A. Orza, Q. Lu, P. Guo, L. Wang, L. Yang, and H. Mao, "Magnetic Nanoparticle Facilitated Drug Delivery for Cancer Therapy with Targeted and Image-Guided Approaches," *Adv. Funct. Mater.*, vol. 26, no. 22, pp. 3818–3836, 2016.

[34] K. El-Boubbou, "Magnetic iron oxide nanoparticles as drug carriers: preparation, conjugation and delivery," *Nanomedicine*, vol. 13, no. 8, pp. 929–952, 2018.

[35] K. E. Albinali, M. M. Zagho, Y. Deng, and A. A. Elzatahry, "A perspective on magnetic core-shell carriers for responsive and targeted drug delivery systems," *Int. J. Nanomedicine*, vol. 14, no. 6, pp. 1707–1723, 2019.

[36] N. A. Ochekpe, P. O. Olorunfemi, and N. C. Ngwuluka, "Nanotechnology and drug delivery part 1: background and applications," *Tropical journal of pharmaceutical research*, vol. 8, no. 3, 2009.

[37] R. A. Petros and J. M. DeSimone, "Strategies in the design of nanoparticles for therapeutic applications," *Nature reviews Drug discovery*, vol. 9, no. 8, pp. 615–627, 2010.

[38] J. Zhang, H. Sun, and P. X. Ma, "Host- guest interaction mediated polymeric assemblies: multifunctional nanoparticles for drug and gene delivery," *ACS nano*, vol. 4, no. 2, pp. 1049–1059, 2010.

[39] F. B. Bombelli, C. A. Webster, M. Moncrieff, and V. Sherwood, "The scope of nanoparticle therapies for future metastatic melanoma treatment," *The lancet oncology*, vol. 15, no. 1, pp. e22–e32, 2014.

[40] J. Yu, D.-Y. Huang, M. Z. Yousaf, Y.-L. Hou, and S. Gao, "Magnetic nanoparticle-based cancer therapy," *Chin. Phys. B*, vol. 22, no. 2, p. 027506, feb 2013.

[41] C. H. Cunningham, T. Arai, P. C. Yang, M. V. McConnell, J. M. Pauly, and S. M. Conolly, "Positive contrast magnetic resonance imaging of cells labeled with magnetic nanoparticles," *Magnetic Resonance in Medicine*, vol. 53, no. 5, pp. 999–1005, 2005.

[42] M. Johannsen, U. Gneveckow, L. Eckelt, A. Feussner, N. Waldöfner, R. Scholz, S. Deger, P. Wust, S. Loening, and A. Jordan, "Clinical hyperthermia of prostate cancer using magnetic nanoparticles: presentation of a new interstitial technique," *International journal of hyperthermia*, vol. 21, no. 7, pp. 637–647, 2005.

[43] S. D. Anderson, V. V. Gwenin, and C. D. Gwenin, "Magnetic functionalized nanoparticles for biomedical, drug delivery and imaging applications," *Nanoscale research letters*, vol. 14, no. 1, pp. 1–16, 2019.

[44] C. Sun, K. Du, C. Fang, N. Bhattarai, O. Veiseh, F. Kievit, Z. Stephen, D. Lee, R. G. Ellenbogen, B. Ratner *et al.*, "Peg-mediated synthesis of highly dispersive multifunctional superparamagnetic nanoparticles: their physicochemical properties and function in vivo," *ACS nano*, vol. 4, no. 4, pp. 2402–2410, 2010.

[45] F. M. Kievit and M. Zhang, "Surface engineering of iron oxide nanoparticles for targeted cancer therapy," *Accounts of chemical research*, vol. 44, no. 10, pp. 853–862, 2011.

[46] Z. Fang, Y. Shen, and D. Gao, "Stimulus-responsive nanocarriers for targeted drug delivery," *New Journal of Chemistry*, vol. 45, no. 10, pp. 4534–4544, 2021.

[47] B. Chen, B. W. Pogue, and T. Hasan, "Liposomal delivery of photosensitising agents," *Expert opinion on drug delivery*, vol. 2, no. 3, pp. 477–487, 2005.

[48] N. Lee, D. Yoo, D. Ling, M. H. Cho, T. Hyeon, and J. Cheon, "Iron oxide based nanoparticles for multimodal imaging and magnetoresponsive therapy," *Chemical reviews*, vol. 115, no. 19, pp. 10 637–10 689, 2015.

[49] J. Mosayebi, M. Kiyasatfar, and S. Laurent, "Synthesis, functionalization, and design of magnetic nanoparticles for theranostic applications," *Advanced Healthcare Materials*, vol. 6, no. 23, p. 1700306, 2017.

[50] J. Li, B. E.-F. de Ávila, W. Gao, L. Zhang, and J. Wang, "Micro/nanorobots for biomedicine: Delivery, surgery, sensing, and detoxification," *Science Robotics*, 2017.

[51] S. L. McGill, C. L. Cuylear, N. L. Adolphi, M. Osinski, and H. D. Smyth, "Magnetically responsive nanoparticles for drug delivery applications using low magnetic field strengths," *IEEE transactions on nanobioscience*, vol. 8, no. 1, pp. 33–42, 2009.

[52] K. Gitter and S. Odenbach, "Investigations on a branched tube model in magnetic drug targeting—systematic measurements and simulation," *IEEE transactions on magnetics*, vol. 49, no. 1, pp. 343–348, 2012.

[53] A. Senyei, K. Widder, and G. Czerlinski, "Magnetic guidance of drug-carrying microspheres," *Journal of Applied Physics*, vol. 49, no. 6, pp. 3578–3583, 1978.

[54] C. Alexiou, D. Diehl, P. Henninger, H. Iro, R. Rockelein, W. Schmidt, and H. Weber, "A high field gradient magnet for magnetic drug targeting," *IEEE Transactions on applied superconductivity*, vol. 16, no. 2, pp. 1527–1530, 2006.

[55] J. Nam, W. Lee, E. Jung, and G. Jang, "Magnetic navigation system utilizing a closed magnetic circuit to maximize magnetic field and a mapping method to precisely control magnetic field in real time," *IEEE Transactions on Industrial Electronics*, vol. 65, no. 7, pp. 5673–5681, 2017.

[56] S. Martel, "Magnetic navigation control of microagents in the vascular network: Challenges and strategies for endovascular magnetic navigation control of microscale drug delivery carriers," *IEEE Control Systems Magazine*, vol. 33, no. 6, pp. 119–134, 2013.

[57] F. Ongaro, S. Pane, S. Scheggi, and S. Misra, "Design of an electromagnetic setup for independent three-dimensional control of pairs of identical and nonidentical microrobots," *IEEE Transactions on Robotics*, vol. 35, no. 1, pp. 174–183, 2019.

[58] A. S. Lübbe, C. Alexiou, and C. Bergemann, "Clinical applications of magnetic drug targeting," *Journal of Surgical Research*, vol. 95, no. 2, pp. 200–206, 2001.

[59] A. Nacev, A. Komaee, A. Sarwar, R. Probst, S. H. Kim, M. Emmert-Buck, and B. Shapiro, "Towards control of magnetic fluids in patients: directing therapeutic nanoparticles to disease locations," *IEEE Control Systems Magazine*, vol. 32, no. 3, pp. 32–74, 2012.

[60] S. Schuerle, S. Erni, M. Flink, B. E. Kratochvil, and B. J. Nelson, "Three-dimensional magnetic manipulation of micro- and nanostructures for applications in life sciences," *IEEE Transactions on Magnetics*, vol. 49, no. 1, pp. 321–330, 2013.

[61] T. Buzug, T. Sattel, M. Erbe, S. Biederer, D. Finas, K. Diedrich, F. Vogt, J. Barkhausen, J. Borgert, K. Lüdtke-Buzug, and T. Knopp, "Magnetic particle imaging: Principles and clinical application," *Nanomedicine - Basic and Clinical Applications in Diagnostics and Therapy*, vol. 2, pp. 88–95, 09 2011.

[62] P. Martins, D. Rosa, A. R. Fernandes, and P. V. Baptista, "Nanoparticle drug delivery systems: Recent patents and applications in nanomedicine," *Recent Patents on Nanomedicine (Discontinued)*, vol. 3, no. 2, pp. 105–118, 2013.

[63] M. Kaur, P. Bailey, and Y. Qiang, "Collidal study of magnetic nanoparticles using electromagnetic separation device," in *2011 11th IEEE International Conference on Nanotechnology*, Aug 2011, pp. 1257–1260.

[64] P. Tartaj, M. Morales, T. Gonzalez-Carreño, S. Veintemillas-Verdaguer, O. Bomati-Miguel, A. Roca, R. Costo, and C. Serna, "Biomedical applications of magnetic nanoparticles," in *Reference Module in Materials Science and Materials Engineering*. Elsevier, 2016.

[65] S. S. Leong, S. P. Yeap, and J. Lim, "Working principle and application of magnetic separation for biomedical diagnostic at high- and low-field gradients," *Interface Focus*, vol. 6, no. 6, p. 20160048, 2016.

[66] S. ichi Takeda, F. Mishima, S. Fujimoto, Y. Izumi, and S. Nishijima, "Development of magnetically targeted drug delivery system using superconducting magnet," *Journal of Magnetism and Magnetic Materials*, vol. 311, no. 1, pp. 367 – 371, 2007.

[67] X. Han, Q. Cao, and L. Li, "Design and Evaluation of Three-Dimensional Electromagnetic Guide System for Magnetic Drug Delivery," *IEEE Trans. Appl. Supercond.*, vol. 22, no. 3, pp. 4 401 404–4 401 404, June 2012.

[68] K. B. Yesin, K. Vollmers, and B. J. Nelson, "Modeling and control of untethered biomicrorobots in a fluidic environment using electromagnetic fields," *The International Journal of Robotics Research*, vol. 25, no. 5-6, pp. 527–536, 2006.

[69] N. S. Zaidi, J. Sohaili, K. Muda, and M. Sillanpää, "Magnetic Field Application and its Potential in Water and Wastewater Treatment Systems," *Sep. Purif. Rev.*, vol. 43, no. 3, pp. 206–240, 2014.

[70] B. Gleich, N. Hellwig, H. Bridell, R. Jurgons, C. Seliger, C. Alexiou, B. Wolf, and T. Weyh, "Design and Evaluation of Magnetic Fields for Nanoparticle Drug Targeting in Cancer," *IEEE Trans. Nanotechnol.*, vol. 6, no. 2, pp. 164–170, March 2007.

[71] J.-B. Mathieu and S. Martel, "Steering of Aggregating Magnetic Microparticles Using Propulsion Gradients Coils in an MRI Scanner," *Magn. Reson. Med.*, vol. 63, pp. 1336–45, May 2010.

[72] X. Chen, J. Yu, Z. Wu, Y. Meng, and S. Kong, "Toward a Maneuverable Miniature Robotic Fish Equipped With a Novel Magnetic Actuator System," *IEEE Trans. Syst., Man, Cybern. Syst.*, pp. 1–11, 2018.

[73] Q. Cao, Y. Tan, R. Dong, and W. Shen, "A Modeling Method of Electromagnetic Micromirror in Random Noisy Environment," *IEEE Trans. Syst., Man, Cybern. Syst.*, pp. 1–10, 2018.

[74] M. C. Hoang, K. T. Nguyen, V. H. Le, J. Kim, E. Choi, B. Kang, J. Park, and C. Kim, "Independent Electromagnetic Field Control for Practical Approach to Actively Locomotive Wireless Capsule Endoscope," *IEEE Trans. Syst., Man, Cybern. Syst.*, pp. 1–13, 2019.

[75] E. P. Furlani and K. C. Ng, "Analytical model of magnetic nanoparticle transport and capture in the microvasculature," *Phys. Rev. E*, vol. 73, p. 061919, Jun 2006.

[76] S. Jeon, G. Jang, H. Choi, and S. Park, "Magnetic Navigation System With Gradient and Uniform Saddle Coils for the Wireless Manipulation of Micro-Robots in Human Blood Vessels," *IEEE Trans. Magn.*, vol. 46, no. 6, pp. 1943–1946, June 2010.

[77] Q. Cao, X. Han, and L. Li, "Numerical analysis of magnetic nanoparticle transport in microfluidic systems under the influence of permanent magnets," *J. Phys. D: Appl. Phys.*, vol. 45, no. 46, p. 465001, oct 2012.

[78] K. Belharet, D. Folio, and A. Ferreira, "Simulation and Planning of a Magnetically Actuated Microrobot Navigating in the Arteries," *IEEE Trans. Biomed. Eng.*, vol. 60, no. 4, pp. 994–1001, April 2013.

[79] F. Mishima, S. Takeda, Y. Izumi, and S. Nishijima, "Three Dimensional Motion Control System of Ferromagnetic Particles for Magnetically Targeted Drug Delivery Systems," *IEEE Trans. Appl. Supercond.*, vol. 16, no. 2, pp. 1539–1542, June 2006.

[80] S. . Takeda, F. Mishima, B. Terazono, Y. Izumi, and S. Nishijima, "Development of Magnetic Force-Assisted New Gene Transfer System Using Biopolymer-Coated Ferromagnetic Nanoparticles," *IEEE Trans. Appl. Supercond.*, vol. 16, no. 2, pp. 1543–1546, June 2006.

[81] J.-B. Mathieu and S. Martel, "Magnetic microparticle steering within the constraints of an MRI system: proof of concept of a novel targeting approach," *Biomed. Microdevices*, vol. 9, no. 6, pp. 801–808, Dec 2007.

[82] S. Martel, J.-B. Mathieu, O. Felfoul, A. Chanu, E. Aboussouan, S. Tamaz, P. Pouponneau, L. Yahia, G. Beaudoin, G. Soulez, and M. Mankiewicz, "Automatic navigation of an untethered device in the artery of a living animal using a conventional clinical magnetic resonance imaging system," *Applied Physics Letters*, vol. 90, no. 11, p. 114105, 2007.

[83] A. Chanu, O. Felfoul, G. Beaudoin, and S. Martel, "Adapting the clinical mri software environment for real-time navigation of an endovascular untethered ferromagnetic bead for future endovascular interventions," *Magnetic Resonance in Medicine: An Official Journal of the International Society for Magnetic Resonance in Medicine*, vol. 59, no. 6, pp. 1287–1297, 2008.

[84] Q. Cao, X. Han, B. Zhang, and L. Li, "Analysis and Optimal Design of Magnetic Navigation System Using Helmholtz and Maxwell Coils," *IEEE Trans. Appl. Supercond.*, vol. 22, no. 3, pp. 4 401 504–4 401 504, June 2012.

[85] M. D. Tehrani, M. O. Kim, and J. Yoon, "A Novel Electromagnetic Actuation System for Magnetic Nanoparticle Guidance in Blood Vessels," *IEEE Trans. Magn.*, vol. 50, no. 7, pp. 1–12, July 2014.

[86] B. Chertok, A. E. David, and V. C. Yang, "Brain tumor targeting of magnetic nanoparticles for potential drug delivery: effect of administration route and magnetic field topography," *Journal of controlled release*, vol. 155, no. 3, pp. 393–399, 2011.

[87] M. D. Tehrani, J. Yoon, M. O. Kim, and J. Yoon, "A Novel Scheme for Nanoparticle Steering in Blood Vessels Using a Functionalized Magnetic Field," *IEEE Trans. Biomed. Eng.*, vol. 62, no. 1, pp. 303–313, 2015.

[88] T.-A. Le, A. K. Hoshiar, T. D. Do, and J. Yoon, "A modified functionalized magnetic field for nanoparticle guidance in magnetic drug targeting," in *2016 13th International Conference on Ubiquitous Robots and Ambient Intelligence (URAI)*, 2016, pp. 493–496.

[89] A. K. Hoshiar, T.-A. Le, F. U. Amin, M. O. Kim, and J. Yoon, "A Novel Magnetic Actuation Scheme to Disaggregate Nanoparticles and Enhance Passage across the Blood–Brain Barrier," *Nanomaterials*, vol. 8, no. 1, 2018.

[90] Ya-Li Liu and Da Chen and Peng Shang and Da-Chuan Yin, "A review of magnet systems for targeted drug delivery," *J. Control. Release*, vol. 302, pp. 90–104, 2019.

[91] T.-A. Le, M. P. Bui, and J. Yoon, "Electromagnetic actuation system for focused capturing of magnetic particles with a half of static saddle potential energy configuration," *IEEE Transactions on Biomedical Engineering*, vol. 68, no. 3, pp. 869–880, 2021.

[92] "IEEE Standard for Safety Levels with Respect to Human Exposure to Electric, Magnetic, and Electromagnetic Fields, 0 Hz to 300 GHz," *IEEE Std C95.1-2019 (Revision of IEEE Std C95.1-2005/ Incorporates IEEE Std C95.1-2019/Cor 1-2019)*, pp. 1–312, 2019.

[93] T. B. Jones, *Electromechanics of Particles*. Cambridge University Press, 1995.

[94] S. Hidalgo-Tobon, "Theory of gradient coil design methods for magnetic resonance imaging," *Concepts in Magnetic Resonance Part A*, vol. 36A, no. 4, pp. 223–242, 2010.

[95] Northeastern University. [Online]. Available: https://ece.northeastern.edu/fac-ece/nian/mom/electromagnets.html

[96] R. Gerber, "Magnetic filtration of ultra-fine particles," *IEEE Transactions on Magnetics*, vol. 20, no. 5, pp. 1159–1164, 1984.

[97] E. P. Furlani, "Analysis of particle transport in a magnetophoretic microsystem," *Journal of Applied Physics*, vol. 99, no. 2, p. 024912, 2006.

[98] E. J. Furlani and E. P. Furlani, "A model for predicting magnetic targeting of multifunctional particles in the microvasculature," *J. Magn. Magn. Mater.*, vol. 312, no. 1, pp. 187 – 193, 2007.

[99] B. Sebastian and P. S. Dittrich, "Microfluidics to Mimic Blood Flow in Health and Disease," *Annu. Rev. Fluid Mech.*, vol. 50, no. 1, pp. 483–504, 2018.

[100] M. Larimi, A. Ramiar, and A. Ranjbar, "Numerical simulation of magnetic nanoparticles targeting in a bifurcation vessel," *J. Magn. Magn. Mater.*, vol. 362, pp. 58 – 71, 2014.

[101] "Motion of Particles in a Fluid," in *Coulson and Richardson's Chemical Engineering (Sixth Edition)*, sixth edition ed., R. Chhabra and M. G. Basavaraj, Eds. Butterworth-Heinemann, 2019, pp. 281 – 334.

[102] T. Lunnoo and T. Puangmali, "Capture Efficiency of Biocompatible Magnetic Nanoparticles in Arterial Flow: A Computer Simulation for Magnetic Drug Targeting," *Nanoscale Res Lett.*, vol. 10, 2015.

[103] L. Shen, , P. E. Laibinis, and T. A. Hatton, "Bilayer Surfactant Stabilized Magnetic Fluids: Synthesis and Interactions at Interfaces," *Langmuir*, vol. 15, pp. 447–453, 1999.

[104] J. Rivas, J. Zamarro, E. Martin, and C. Pereira, "Simple approximation for magnetization curves and hysteresis loops," *IEEE Trans. Magn.*, vol. 17, no. 4, pp. 1498–1502, 1981.

[105] E. P. Furlani, "Chapter 1 - Materials," in *Permanent Magnet and Electromechanical Devices*, ser. Electromagnetism, E. P. Furlani, Ed. San Diego: Academic Press, 2001, pp. 1–72.

[106] E. P. Furlani, "Analysis of Particle Transport in a Magnetophoretic Microsystem," *J. Appl. Phys.*, vol. 99, no. 2, p. 024912, 2006.

[107] A. R. Conn, K. Scheinberg, and L. N. Vicente, *Introduction to Derivative-Free Optimization*. MPS-SIAM Series on Optimization, SIAM, 2009.

[108] M. Feychting, "Health effects of static magnetic fields—a review of the epidemiological evidence," *Progress in biophysics and molecular biology*, vol. 87, no. 2-3, pp. 241–246, 2005.

[109] T. D. Do, F. U. Amin, Y. Noh, M. O. Kim, and J. Yoon, "Functionalized Magnetic Force Enhances Magnetic Nanoparticle Guidance: From Simulation to Crossing of the Blood–Brain Barrier In Vivo," *IEEE Trans. Magn.*, vol. 52, no. 7, pp. 1–4, July 2016.

[110] COMSOL Multiphysics, "Particle tracing module user's guide," *COMSOL*, vol. 4, 2015.

[111] Q. A. Pankhurst, J. Connolly, S. K. Jones, and J. Dobson, "Applications of magnetic nanoparticles in biomedicine," *J. Phys. D*, vol. 36, no. 13, pp. R167–R181, jun 2003.

[112] D. Maity and D. Agrawal, "Synthesis of iron oxide nanoparticles under oxidizing environment and their stabilization in aqueous and non-aqueous media," *J. Magn. Magn. Mater.*, vol. 308, no. 1, pp. 46 – 55, 2007.

[113] J. Sheffield, "ImageJ, A Useful Tool for Biological Image Processing and Analysis," *Microscopy and Microanalysis*, vol. 13, no. S02, p. 200–201, 2007.

Author's Statements

Journals

1. P. Chakrabarty, S. Roy and R. P. Paily, "Stiction Mitigation of Nanoparticles in Magnetically Targeted Drug Delivery System," in *IEEE Transactions on Magnetics*, vol. 58, no. 3, pp. 1-10, March 2022.

2. P. Chakrabarty and R. P. Paily, "A Time-Varying Magnetic Field to Enhance the Navigation of Magnetic Microparticles in Bifurcated Channel," in *IEEE Magnetics Letters*, vol. 13, pp. 1-5, 2022.

Conferences

1. P. Chakrabarty, S. Roy and R. Paily, "Analysis of Electromagnetic Actuation System for Different Coil Topologies," *TENCON 2019 - 2019 IEEE Region 10 Conference (TENCON)*, pp. 679-683, 2019.

Awards/Honor/Talks

- Visvesvaraya PhD Fellowship for Electronics & Information Technology (Awardee Number: VISPHD-MEITY-1224) from Ministry of Electronics & IT, Government of India for the period July 2015- July 2020.